

POLITECNICO DI TORINO

Master's Degree in Civil Engineering



Master Thesis

**Correlation between fracto-emission and
statistical seismic precursors in the case
of low-magnitude earthquakes**

Tutors

Prof. Alberto CARPINTERI

Dr. Oscar BORLA

Candidate

Claudio ARCURI

Academic Year 2017-2018

SUMMARY

INTRODUCTION

Chapter 1 : FRACTO-EMISSIONS AS SEISMIC PRECURSORS	1
1.1 Preliminary remarks	1
1.2 Acoustic Emissions (AE)	2
1.3 Electromagnetic Emissions (EME)	4
1.4 Neutron Emissions (NE)	5
Chapter 2 : FRACTO-EMISSIONS AND LUNAR PHASES: REVIEW ON PREVIOUS RESULTS	6
2.1 Description of "San Pietro-Prato Nuovo" gypsum mine	6
2.2 Analysis of previous results (June 2013 - June 2017) : Multimodal statistical analysis of fracto-emissions	8
2.3 Possible correlation between seismic activity and lunar phases	21
2.4 Relation between the phase of the moon and the micro-earthquakes	23
2.5 Correlation between seismicity and lunar periodicity at the "San Pietro-Prato Nuovo" gypsum mine (July 2013 - June 2017)	24
Chapter 3 : NEW EXPERIMENTAL EVIDENCE FROM "SAN PIETRO-PRATO NUOVO" GYPSUM MINE	29
3.1 The recent experimental results of fracto-emissions (July 2017 - December 2017) ...	29
3.2 The recent analysis of lunar phases (July 2017 - December 2017)	36
Chapter 4 : <i>b</i>-VALUE STATISTICAL SEISMIC PRECURSOR OF LOW-MAGNITUDE EARTHQUAKES	38
4.1 <i>b</i> -value as statistical seismic precursor	38
4.2 Maximum Likelihood technique (MLE)	40
4.3 Ordinary Least Squares	40
4.4 Magnitude of completeness (M_c)	41

4.5 <i>b</i> -value analysis for the seismic swarms at the "San Pietro-Prato Nuovo" gypsum mine (July 2013 - December 2017)	45
Concluding remarks	67
References	69

Summary

Several mechanical tests carried out on rock samples have demonstrated that different forms of energy were released at brittle failure occurrence.

In particular, the crack propagation is accompanied by the emission of pressure waves with a very specific frequency: from TeraHertz for crack at the nanoscale up to Hertz at the kilometre scale. Depending on their frequency, these pressure waves are able to trigger the production of: acoustic (AE), electromagnetic (EME), and neutron (NE) emissions.

The same phenomenon can take place during the early stages of an earthquake. As a matter of fact, at the tectonic scale cracking is a multi-scale phenomenon, as well as the frequencies of pressure waves cover a broad spectrum, from THz up to the simple Hz, which is the typical frequency of seismic oscillations.

As well as at the laboratory scale fracto-emissions (AE, EME, and NE) provide important information in terms of fracture precursor, these parameters can be also used as a promising tool for seismic risk forecasting at the Earth's crust scale.

Besides fracto-emissions, another important parameter for seismic prevention is represented by the temporal variation of b -value, a statistical precursor deriving from the Gutenberg-Richter's law for the magnitude-frequency distribution.

The aim of this thesis is to confirm the precursive potentialities of the fracto-emissions and also to investigate the possibility of using the b -value as a further seismic precursor applied to low-magnitude earthquakes.

Hence, from the experimental point of view, the seismic swarms detected in the surroundings of the "San Pietro-Prato Nuovo" gypsum mine, a site located in Murisengo, Alessandria, Italy, have been analyzed.

A specific monitoring system able to detect the fracto-emissions has been installed in the mine at about one hundred metres below the ground level.

After summarizing the experimental results already obtained during the first eight semesters of monitoring (July 2013 - June 2017), the new experimental evidences related to a new semester (June 2017 - December 2017) are discussed reinforcing the idea of the great forecasting potentiality of fracto-emissions. In addition a new indication about the possible correlation between seismic swarms and lunar phases has been observed for the same period.

In addition, important results have been also obtained by the analysis of the temporal variation of the b -value applied to all the seismic swarms occurred in the nine semester of experimentation.

Therefore, the combined use of these parameters (fracto-emissions and b -value) could lead to significant step forwards in the field of Civil Engineering and Seismology in terms of protection against seismic risk.

Introduction

Some recent studies (Carpinteri A., Lacidogna G., Manuello A., 2015) have noticed that during laboratory tests on rock samples, different forms of energy (acoustic AE, electromagnetic EME, and neutron NE emissions) were released at brittle failure occurrence. These fracto-emissions (AE, EME, and NE), triggered by mechanical instabilities (such as fracture in solids and turbulence in fluids), seem to be similar to the anomalous physical phenomena observed before major earthquakes.

It is well accepted that during the formation or advancement of cracks in solid bodies subjected to brittle failure, the wavelength of pressure waves emitted is of the same order of magnitude of crack size or crack advancement length. Moreover, considering that the average crack propagation velocity of solids has an order of magnitude of about 10^3 m/s, a very specific frequency is associated to the pressure waves (Carpinteri A., Lacidogna G., Manuello A., 2015): from TeraHertz (10^{12} Hertz) for fracture at the nanoscale (10^{-9} m) to Hertz at the kilometer scale (10^3 m) (i.e. scale of the seismic events).

In the particular case of earthquakes, the cracking can be defined as a multi-scale phenomenon: in the first stage, small cracks are produced and so high frequencies are generated, in the last phase instead, large cracks led to low frequencies.

In particular, when the active cracks are still below the metre scale, frequencies in the ultrasonic field are produced; at the intermediate scale, with cracks from micron to millimetre scale pressure waves can generate electromagnetic signals; when cracks are below the micron scale an unexpected phenomenon is held: pressure waves resonate with the crystal lattices, and through a complex cascade of events, nuclear fission reactions may occur (neutron and/or alpha particle emissions) (Bridgman, 1927; Batzel et al., 1951; Carpinteri et al. 2015b; Cook et al. 2010; Fulmer et al. 1967; Lucia and Carpinteri, 2015; Widom et al. 2013, 2015; Hagelstein et al. 2010, 2015 ; Diebner, 1962; Derjaguin et al., 1989; Fujii et al., 2002).

Hence, pressure waves, according to their frequencies, are responsible for the production of three kind of energy: Acoustic Emissions (AE), Electromagnetic Emissions (EME) and Neutron Emissions (NE) which are considered the most reliable seismic precursors.

However, fracto-emissions are not the only seismic precursors, in fact also unusual animal behaviour, hydrochemical precursors, changing in temperature and water level, radon gas, oil wells, increasing of foreshocks were observed before the main shocks. As a matter of the fact, an unusual animal behaviour and the changing in chemical composition in underground water were observed before the destroying earthquake of 7,3 magnitude in the Haicheng region, China, in February 4 of 1975 (Adams R.D.1976).

Thus, the correct monitoring of all those phenomena that take place well in advance than the occurrence of a seismic event can provide the basis for the assessment of three main parameters of an earthquake: place and time of occurrence, as well as the magnitude of the quake. So that, the simultaneous acquisition of different seismic precursors is necessary in order to forecast properly earthquakes because of the complicated physical processes which give them to rise.

As a matter of fact, an earthquake is a sudden movement of the Earth's crust that generates elastic waves. The waves propagate spherically outwards from the source, as a result of a big amount of energy released at the time of this vibration. Moreover, an

earthquake of high magnitude is characterized by a series of clusters which can be divided in three different phenomena: foreshocks, mainshock and aftershock. Foreshocks are clusters of the seismic period that happen in the preparation time and announce the incoming main shock. Aftershocks are associated with stress triggering of a main shock and decay according to the well-known Omori law in time (Utsu et al. 1995). Seismic swarms are not associated with any dominant mainshock and they have other origins, probably due to a-seismic dislocations related to fluid intrusion (Yamashita 1999; Hainzl 2003) or to a-seismic slow-slip events (Holtkamp & Brudzinski 2011).

There may be short or long term forecasting. In subduction regions the sequences foreshock-main shock-aftershock may last for a few weeks or months (Davis & Frohlich 1991), whereas in zones with a low tectonic deformation rate may last for centuries (Ebel et al. 2000). Medium and short range predictions are very useful because they can help in saving the largest population from disaster.

The following study, based on the correlation between the fracto-emissions (Acoustic Emissions (AE) at the tectonic scale, Electro-Magnetic Emissions (EME) at the intermediate scale, Neutron Emission (NE) at the nano-scale) and *b*-value, which is a statistical seismic precursor, starts from the necessity for human being to forecast in time earthquakes to avoid devastating consequences which can derive from an earthquake of high magnitude.

In particular, *b*-value can assume whatever value comprised in 1.5 to 1.0 range (McGarr, 1984), but in some cases also values outside the limits are achieved. Higher values for this parameter have been correlated with the occurrence of earthquakes with small magnitude spread over a wide geographical area, lower values are related to a concentration of earthquakes with higher magnitude localized along a fault (Carpinteri et al. 2009a).

The innovative aspect of this thesis is that the *b*-value, already used for high intensity earthquakes in high-seismicity regions (Ouchi and Uekawa, 1986), is applied, together with the fracto-emissions, even in the case of low-magnitude seismic events in low-seismicity areas.

From the experimental point of view, the data analyzed and discussed in this thesis refer to a monitoring campaign carried out at a gypsum mine located in Northern Italy by means of a dedicated monitoring platform installed at about one hundred metres below the ground level in order to avoid interferences coming from human activities.

This thesis is organized in four chapters:

1. A general description of fracto-emissions with their respective specific frequencies: as fracture at the nanoscale (10^{-9} m) emits pressure waves at the frequency scale of TeraHertz (10^{12} Hertz), so fracture at the intermediate scale between the microscale (10^{-6} m) and millimetre (10^{-3} m) scale emits pressure waves at the frequency scale of GigaHertz (10^9 Hertz) and MegaHertz (10^6 Hertz); at the scale of metre emits pressure waves at the scale of kiloHertz (10^3 Hertz). These pressure waves depending on their frequencies can trigger the emission of NE, EME and AE that can be used as seismic precursors.
2. A review on previous results based on fracto-emissions and the possible correlation between lunar phases and the seismic swarms in the period from July 2013 to

June 2017 (eight semesters). Fracto-emissions are analyzed by means of a multi-modal technique: an iterative procedure that allows to obtain the best fit for the experimental measures in terms of continuous curves similar to Gaussians starting from a discrete distribution of points.

3. The recent experimental evidence of fracto-emissions, and the correlation between lunar phases and main earthquakes for the new semester of monitoring from July 1st, 2017 to December 31, 2017 (second semester of 2017). In particular, by performing the multi-modal analysis for the earthquakes and the fracto-emissions, 4 seismic swarms and an equal number of fracto-emission peaks have been obtained.
4. Analysis of the b -value and its temporal variation for all the period of investigation (July 2013 to December 2017). The first step to compute b -value is to define the Magnitude of Completeness (M_c) that is the lowest magnitude of the seismic catalogue at which all the events are reliably detected (Rydelek and Sacks, 1989) and it is the maximum magnitude of the non-cumulative frequency magnitude distribution. Then, only earthquakes with a magnitude greater than M_c have been taken into account and choosing the correct temporal windows, b -value has been derived from the slope of the regression line of the cumulative frequency-magnitude distribution.

Chapter 1

FRACTO-EMISSIONS AS SEISMIC PRECURSORS

1.1 Preliminary remarks

Some recent studies have noticed that during laboratory tests on rock samples, different forms of energy were released at brittle failure occurrence.

The formation and the advancement length of cracks generate pressure waves with wavelength of the same order of magnitude of the crack-size. These waves, also known as phonons travel with a speed which is function of the medium an equal to about 10^3 m/s in the specific case of solid body. Moreover, according to the relation 1.1, these phonons are characterized by a well precise frequency:

$$f = \frac{v}{\lambda} \quad (1.1)$$

where λ is the wave length, f is the frequency, and v is the wave speed.

Earthquakes are also a multi-scale phenomenon, since the different waves produced by mechanical instabilities are spread over a broad spectrum (fig.1.1). As fracture at the nanoscale (10^{-9} m) emits pressure waves at the frequency scale of TeraHertz (10^{12} Hertz), so fracture at the microscale (10^{-6} m) emits pressure waves at the frequency scale of GigaHertz (10^9 Hertz), at the scale of millimetre emits pressure waves at the scale of MegaHertz (10^6 Hertz), at the scale of metre emits pressure waves at the scale of kiloHertz (10^3 Hertz), faults at the kilometer scale emit pressure waves at the scale of Hertz, which is the typical frequency of earthquakes.

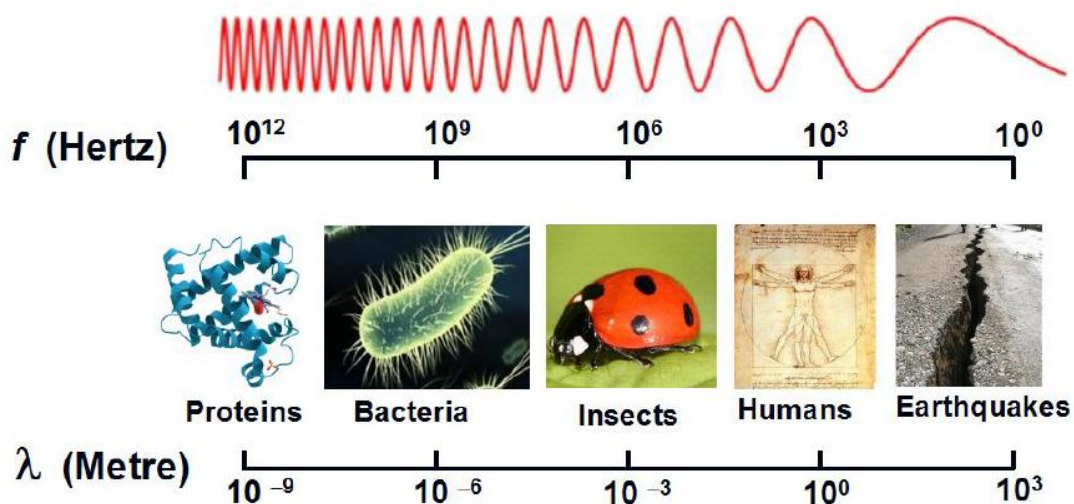


fig. 1.1: Correlation between wavelength scale and frequency by assuming a constant pressure wave speed

When the active cracks are below the metre scale, the frequencies in the ultrasonic field are produced (with frequencies bigger than 20 kiloHertz). At the intermediate scale, with fracture between micron and millimetre, we have frequency between Mega and Giga-Hertz and in this field electro-magnetic waves could be registered. At scale below the micron, TeraHertz pressure waves are produced and fracture experiments on natural rocks have recently demonstrated that these high-frequency waves are able to induce nuclear fission reactions with neutron and/or alpha particle emissions (Carpinteri A., Lacidogna G., Manuello A., 2015b). These reactions, also known as piezonuclear reactions were observed for the first time in fluids subjected to cavitation, afterwards it was also demonstrated for experiments in solids (A. Carpinteri, F. Cardone and G. Lacidogna, 2009b).

By means of these nuclear fission reactions an heavy atom becomes a lighter element and during this process neutrons can be emitted.

The piezonuclear reactions are triggered by phonons that have a frequency close to the frequency of resonance of the crystal lattice and an energy close to that of thermal neutrons.

As a matter of fact, the Debye frequency, which is the fundamental frequency of free vibration of crystal lattices is of the order of magnitude of TeraHertz due to the fact that the inter-atomic distance is just around the nanometre, as exactly the minimum size of the lattice defects.

Pressure waves produce the three fracto-emissions: Acoustic Emissions (AE), Electromagnetic Emissions (EME) and Neutron Emissions (NE) which are used as a strong tool to forecast earthquakes.

The time delay between the three fracto-emissions is related to a different time of generation of the signals due to the cracking of the rocks that anticipate the occurrence of the seismic event. In the first stage of cracking, when the active cracks are very small, high frequencies can be picked up; instead, when the tips of the micro-cracks join together to give origin to the macro-crack in the damaged zone, lower frequencies arrive.

1.2 Acoustic Emissions (AE)

Acoustic emission technique used for non-destructive evaluation of materials can monitor changes in material behaviour, without moving its components (sensors). The main ability of this technique is to detect crack propagation occurring not only on the surface but also inside a material. The ultrasound method is able to detect the geometric shape of a defect in a specimen using an artificially generated source signal and receiver.

Cracking, in fact, is accompanied by the emission of elastic waves which can be received and recorded by transducers applied to the surface of the structural elements. In AE monitoring, piezoelectric (PZT) sensors are generally used to record electric signals emitted by crystals every time they are subjected to a mechanical stress.

Seismology investigates earthquake in distances between hundreds and thousands of kilometers, AE techniques are usually applied for source-receiver distances of up to several tenth meters, but specimen can also be smaller than some millimetres. As we said

before, AE technique deals with frequencies from 20 kHz to 1 MHz. Seismological techniques were adapted for civil engineering by some authors (Ohtsu 1982, 1994; Ouyang et al. 1991; Maji and Sahu 1994). Ono and Ohtsu were probably some of the first scientists transferring earthquake data processing techniques to AE data processing.

The AE method is structured in these following steps:

1. the signal picked up by a transducer is pre-amplified and transformed into electric voltage;
2. it is filtered in order to eliminate unwanted frequencies;
3. the signal is analyzed by a measuring system counting the emissions that exceed a certain voltage threshold measured in volt (V).

We can have two different kinds of sensor: resonant and wideband.

The first type is more sensitive at certain frequencies, which depend on the internal resonant frequency of a piezoelectric (PZT) crystal. Resonant sensors exploit the capacity of these PZT crystals to produce electric signals whenever they are subjected to a mechanical stress.

Wideband sensors, instead, use an energy-absorbing backing material to damp out the predominant frequencies. This allows to cover a wider frequency range but lower sensitivity.

These are based on one-dimensional analysis, but we also can find solution for 3D PZT bodies. PZT element was analyzed by using the finite element model (FEM) (Ohtsu & Ono 1983).

The constitutive laws of PZT are represented as follow (Holland & Eeirnisse 1969) and (Kawabata 1973):

$$\{\varepsilon\} = [C] \{\sigma\} + [d]^T \{E\} \quad (1.2)$$

$$\{D\} = [d] \{\sigma\} + [p] \{E\} \quad (1.3)$$

where $\{\varepsilon\}$ are the elastic strains, $\{\sigma\}$ are the stresses, $\{E\}$ are the electric potentials and $\{D\}$ are the displacements. $[C]$ represents the adiabatic elastic compliance tensor at constant electric field, $[d]$ is the adiabatic piezoelectric tensor and $[p]$ is the adiabatic electric permittivity at constant stress. From these constitutive equations, piezoelectric element generates electric signals due to mechanical motions and vice versa.

The well known Gutenberg Richter law (Richter 1958) can be applied to AE signals as follow:

$$\log(N \geq m) = a - bM \quad (1.4)$$

where N is the cumulative number of shocks that have a magnitude greater than or equal to a given magnitude m , and a and b are empirical constants. In particular, a is a function of the number of earthquakes and of the dimension of the area and it can give a measure of the tax of total seismicity (Pacheco et al. 1992; Lopez Casado et al., 1995; Bayrak et al., 2002); b which is the slope of the line gives information about the density of probability of

some earthquakes to occur in a determined area with a defined magnitude. This parameter which is also known as "b-value" is variable in space and time.

Related to AE statistics we can write:

$$N(\geq m) = 10^{a-bm} \quad (1.5)$$

where N is the number of AE signals with magnitude $\geq m$ in the monitored structural element and a and b are positive coefficients to be determined subjecting collected AE data to a statistical analysis.

1.3 Electromagnetic Emissions (EME)

The EM signals are related to brittle failure, when the fracture propagates suddenly and this is accompanied by the release of a given quantity of energy. It was also observed that the EM signals detected during failure of materials are analogous to the anomalous radiation of geo-electromagnetic waves and changes in geo-electric potential observed before the major earthquakes. Some experiments on rock sample demonstrated that micro and macro-cracking processes are accompanied by emissions of acoustic and electromagnetic signals (Mori, Yasuhiko et al. 2009). In the same way other researchers tried to transfer their knowledge from laboratory test to the Earth's crust scale (Yamada, I.; Masuda, K.; Mizutani, H., 1989) and they arrived at the same conclusion of the researchers cited before. Yamada I. et al. noticed that AE and EME were generated at the same time in laboratory tests on samples as proof that they are indicator of the same micro-cracking process and that efficiency of generating electromagnetic emission seems to be higher in tensile cracks than in shear cracks. If their interpretation is correct, production of new cracks is a necessary condition to produce electromagnetic emissions and earthquakes seem to be the result of a shear faulting which connects pre-existing micro-cracks between them. EME was initially explained as a charge separation occurring across the fracture (Miroshnichenko & Kuksenko 1980; O' Keefe & Thief 1995). Recently a new model was proposed: positive ions on both newly created fracture surfaces oscillate around their equilibrium position in opposite phase to the negative ones (Frid *et al.* 2003, Rabinovitch *et al.* 2007). When a material is strained until to generate an opening crack, electromagnetic emissions (EME) are produced in a range between MHz and GHz and these are called "precursors of general fracture" (Bahat et al., 2005; Eftaxias et al., 2007; Eftaxias et al., 2009, Hayakawa and Fujinawa, 1994; Hayakawa, 1999; Hayakawa and Molchanov, 2002). Kachakhidze et al., 2012 found a correlation between the main frequency of the observed electromagnetic emission and the linear dimension (the length of the fault) in order to predict the possible magnitude of the incoming earthquake and they found that:

$$\omega = \beta \frac{c}{l} \quad (1.6)$$

where β is the characterised coefficient of geological medium and approximately equal to 1.

They applied this formula to some earthquakes like Wenchuan earthquake (May 2008, Magnitude 8.0, depth 19 km). Therefore, applying the formula (1.6) they obtained a fault 300 km length and then using Ulomov's formula (1993) (valid for magnitudes greater than 5.0) they obtained:

$$\log l = 0.6M - 2.5 \quad (1.7)$$

from which $M \approx 8.1$, that is the real magnitude of this earthquake (Xuemin Zhang, 2010).

The stressed rock behaves like a stress EM transformer. One of the most cited prediction of earthquakes is that of Loma Prieta earthquakes thanks to Fraser Smith et al. (1990) and Bernardi et al. (1991). They detected this anomalies with a ground-based sensor located in Corralitos, CA just 7 km from the earthquake epicentre. The same thing happened for an earthquake occurred at Biak Island on 17 February of 1996 with a magnitude of 8.2. Even this case, two stations which were at a distance of 1200 km far, detected some anomalies in the frequency range.

1.4 Neutron Emissions (NE)

Volodichev et al. (2000) observed an anomalous releasing of neutron emissions in the Pamir region (4200 m a.s.l.) exceeding the usual neutron background of about two orders before earthquakes with a magnitude equal or bigger than 4. More recent studies on neutron emissions have been performed for the Sumatra earthquake of December 2004, and also in this case, anomalous neutron emissions were detected before the catastrophic events. Also Carpinteri et al. arrived to the same conclusion with some recent data acquired in the "Testa Grigia" Laboratory of Plateau Rosa, Cervinia (Italy), during an experimental campaign on neutron radiation from cosmic rays. An increasing in neutron radiation was monitored between July 31th and August 1st exceeding six times the usual neutron background. In this period no events related to cosmic events were found. About 20 days after, a discrete earthquake of the 3rd degree in the Richter scale was detected some km far from this place. This fact proves the thesis of Kuzhevskij et al., according which there is a relation between neutron emission and appreciable seismic events.

Another experimental campaign was conducted at Villanova Chiesa, Bettola, at the "Val Trebbia", in the Northern Italy from December 28, 2012 to January 6, 2013 (Borla et al. 2015). Neutron emissions were monitored in a "continuous mode" with an ^3He neutron radiation monitor, that is an high sensitive device with a measuring range comprised in 0.025 eV to 14 MeV with a fast response to radiation field change.

In the period from December 30, 2012 to January 2, 2013, the neutron field reached three point of maximum and an increase by about six times in the neutron dose rate with respect to the average natural background was observed in two cases, stabilizing 3 hours later. In this case, as the previous one, no changes in cosmic rate flux were observed. After seven days, a 5 magnitude earthquake occurred in the surrounding area.

Chapter 2

FRACTO-EMISSIONS AND LUNAR PHASES: REVIEW ON PREVIOUS RESULTS

2.1 Description of "San Pietro-Prato Nuovo" gypsum mine



fig. 2.1: picture downloaded by Google Maps about the geographical location of Murisengo (represented by the red icon)

San Pietro Prato Nuovo is a gypsum quarry located in Murisengo (Alessandria) in Italy (fig. 2.1). A monitoring platform has been installed at about one hundred metres below the ground level to monitor and ensure the stability of the structure and to conduct research activities. The environment of the quarry and the position of the monitoring station within the quarry itself allow to reduce the acoustic and electromagnetic noise of human origin and at the same time the neutron background is about between one and two orders of magnitude lower than on the Earth.

In the quarry, gypsum layers which describes the evolution of the seabed that occupied the Monferrato during the Messiniano can be observed. Then, a collapse involved the rocks, mixing them and creating a new kind of storage called "caotic".

Gypsum is a soft sulfate mineral composed of calcium sulfate dihydrate, with the chemical formula $\text{CaSO}_4 \cdot 2\text{H}_2\text{O}$. This gypsum mine is currently structured in five levels of underground and from there a big quantity of gypsum is extracted every day.

The stability of the structure is ensured by the coaxial archway pillar system 4 m thick which avoid any dangerous eccentricity loads. An hyperstatic structure is created since

there are vertical and horizontal elements that are fully restrained and for this reason any other technical supports are not necessary. Since June 2013 the quarry is subjected to a multiparameter monitoring to evaluate the seismic risk of the surrounding area with the detection of the environmental neutron field fluctuations.

Experimental set up



fig. 2.2: Experimental set-up of the monitoring station

In the first phase of the experimental campaign carried out at the San Pietro-Prato Nuovo gypsum mine, only acoustic and neutron emissions were detected, subsequently also electromagnetic emissions were recorded (February 2015).

The six piezoelectric acoustic sensors were placed into a cavity, realized inside a pillar whose dimensions are 8x8x6 m (fig. 2.2). The first aim of the platform monitoring was to exclude frequencies coming from blasting, used for the excavation of the mine. After different assessments, it was demonstrated that blasting frequencies (comprised in 20 Hz to 20 kHz) were outside the range frequencies of acoustic emissions (between 50 and 800 kHz). The AE signals are preamplified, filtered through a bandpass filter in order to have a high signal to noise ratio and a flat frequency response over a broad range. As regards electromagnetic emissions, a telescopic antenna 125 cm long connected with an

oscilloscope (Agilent DSO1052B) via low impedance coaxial cable with a termination of 50 ohms was placed in the nearby cavity. Telescopic antenna is wide band because its length can be modified in function of the frequencies/wavelength that the operator wants to detect. The oscilloscope has a maximum data acquisition frequency of 300 MHz (2 channels) and so allows the monitoring of EM signals with frequencies up to tens of MHz. As regards neutrons, it is well known that they are electrically neutral particles, so they cannot directly produce ionization in a detector. For this reason, a conversion process it's exploited by neutron detectors: an incident neutron interacts with a nucleus to produce a secondary charged particle. The device used is AT1117M (ATOMTEX, Minsk, Republic of Belarus) and it provides a high sensitivity and wide measuring ranges (neutron energy range 0.025 eV–14 MeV), with a fast response to radiation field change ideal for any environmental monitoring purpose.

2.2 Analysis of previous results (June 2013 - June 2017) : Multimodal statistical analysis of fracto-emissions

Studies on the correlation between fracto-emissions and seismic activity were performed and are still carried out by Polytechnic of Turin at San Pietro-Prato Nuovo gypsum mine. Initially, only acoustic and neutron emissions were recorded, subsequently also electromagnetic emissions were recorded (February 15, 2015). For this scope the data of the three kind of energies and the information coming from seismic activities are required. The first information are extrapolated by sensors in situ month by month, the second one are taken by the italian site ISIde (Italian Seismological Instrumental and parametric database) based on the data coming from INGV (National Institute of Geophysics and Volcanology). As regard for the seismic data, a radius of about 100 km from Murisengo has been considered and earthquakes whose magnitude was greater than 1,8 in the Richter scale, because under this seismic threshold no significant change in neutron flux was observed. Seismic data as long as fracto-emissions, were analysed by a multi-modal approach that is a statistical evaluation that makes use of a suitable multi-peak distribution curve. Starting from a discrete number of points, corresponding to the data of the fracto-emissions and seismic events, the relative maxima of the distribution and the best Gaussian fit are evaluated by an iterative method with the software Microcal Origin. The computation is based on the variation of some parameters as shown in the figure 2.3 below:

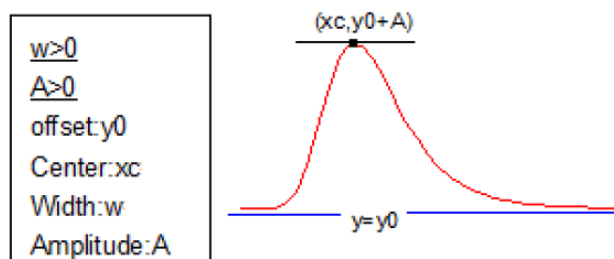


fig. 2.3: Example of curve of Extreme Function

where w is the width, A is the amplitude, y_0 is the offset and x_c is the center of the distribution of the Extreme Function that can be described by this analytical equation:

$$y = y_0 + Ae^{(-e^{-z-z_c+1})} \quad (2.1)$$

$$\text{where } z = \frac{z-z_c}{w} \quad (2.2)$$

Analysis on fracto-emissions were carried out in the period from June 2013 to December 2017 and divided in different steps of time:

- 1) the first phase of the experimental campaign concerns five semesters in the period from June 2013 to December 2015 (Carpinteri A., Borla O., 2017);
- 2) the second phase is relative to three semesters and comprised in the period from December 2015 to June 2017 (Barone E., 2017);
- 3) the third phase is relative to one semester from June 2017 to December 2017, whose discussion is dedicated to Chapter 3.

In the first five semesters of monitoring, 242 earthquakes with a magnitude comprised in the range 2,5 to 4,7 were detected, and among these 31 seismic swarms emerged, after having performed the multi-modal analysis. According to the acoustic emissions, it was considered the discrete distribution of the total daily number of observed acoustic events. Over a number of 921 days of monitoring, 31 main AE were identified, with monitored frequencies comprised in the range 53,76 kHz to 684,21 kHz and an average frequency of about 124 kHz.

In addition, also EME were analyzed by multi-modal approach considering the total daily number of anomalous electromagnetic events. On a monitoring period of 320 days, 9 electromagnetic peaks emerged.

In this case, the data analysis is limited to 2015 because the acquisition of electromagnetic signals is started on 15 February 2015 and so only two semesters of monitoring are available.

Finally, also for neutron radiations the multi-peak Gaussian analysis was performed and 31 main neutron emission peaks were identified. Even in this case, the values shown in the diagrams refer to the total daily measured flux.

In the second phase of monitoring, the same approach of the first experimental campaign was used. Starting from the temporal distribution of 154 earthquakes, 17 seismic swarms were identified. As concern for fracto-emissions was found the same number of peaks of earthquakes.

In addition to that, a new semester has been analyzed in the following chapter, from July 1st, 2017 to December 31, 2017 revisiting the same studies performed for the previous seismic swarms.

In the next figures (figs. 2.4-2.24) we can observe the superposition of the multi-peaks distribution curve between the fracto-emissions and the seismic events (for the period from July 2013 to June 2017). The earthquakes distribution is represented by a black line, a red

line is used for acoustic emission, a blue line is used for electromagnetic emissions and a violet line is used for neutron emissions.

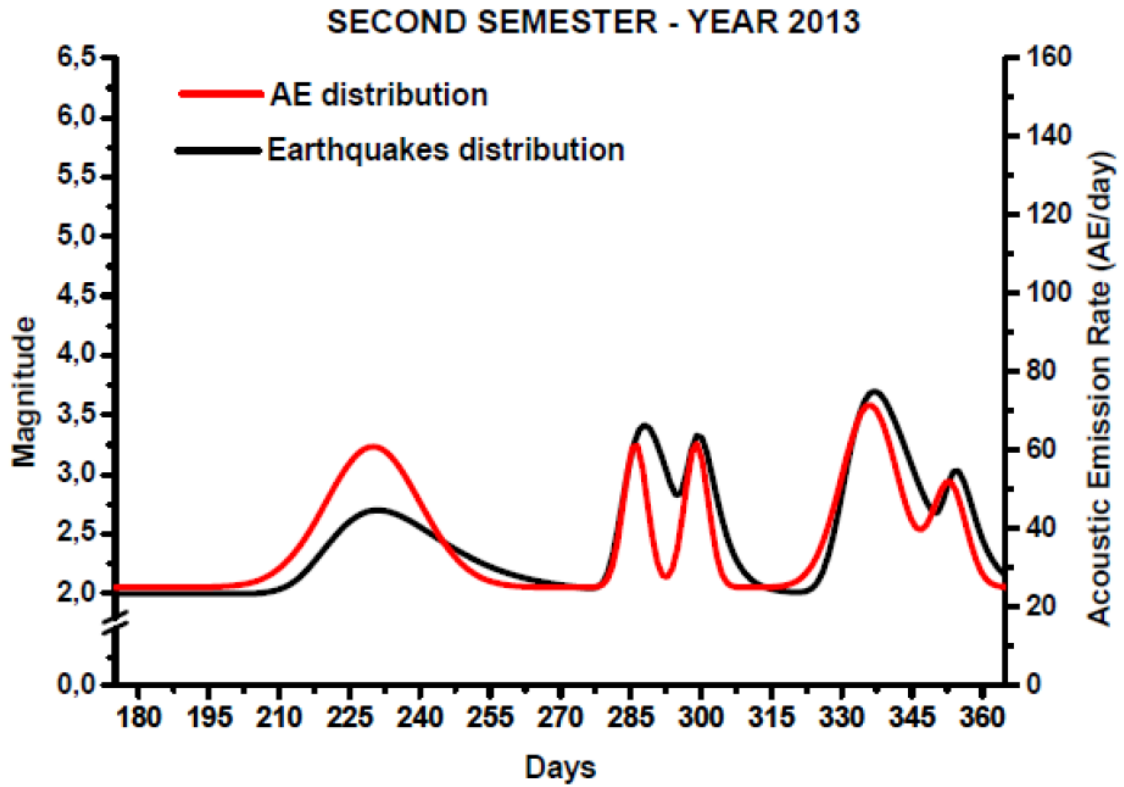


fig. 2.4: Multi-peak distribution of AE events and earthquakes for the second semester 2013

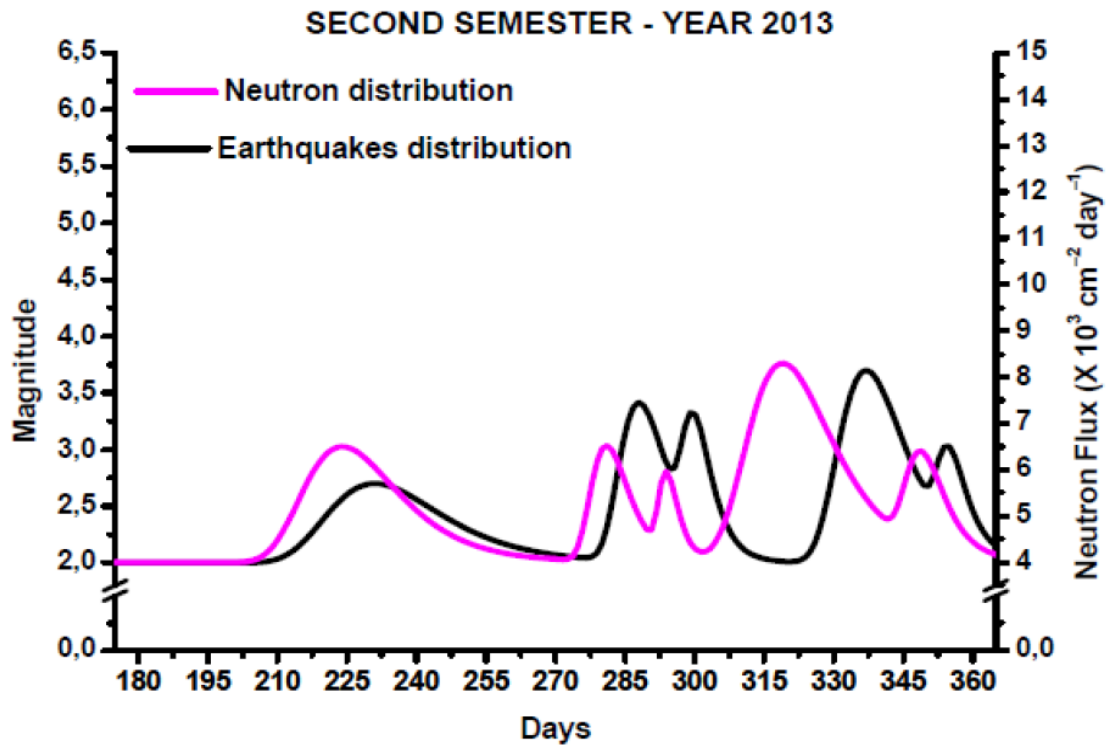


fig. 2.5: Multi-peak distribution of NE events and earthquakes for the second semester 2013

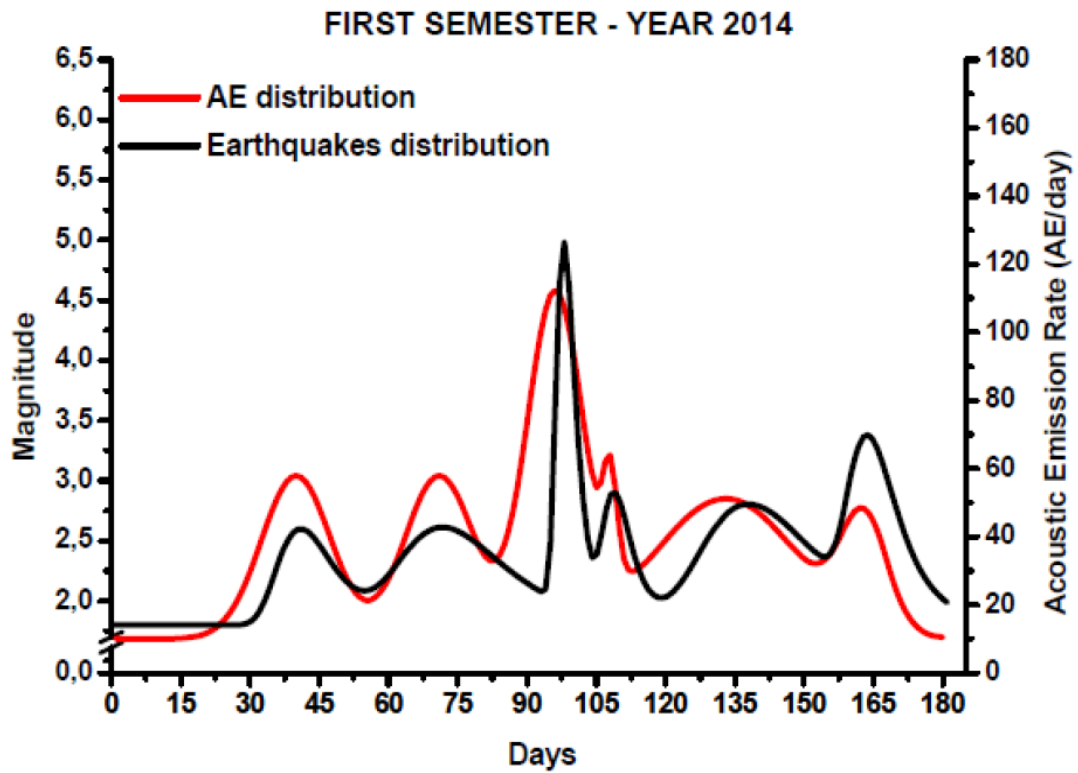


fig. 2.6: Multi-peak distribution of AE events and earthquakes for the first semester 2014

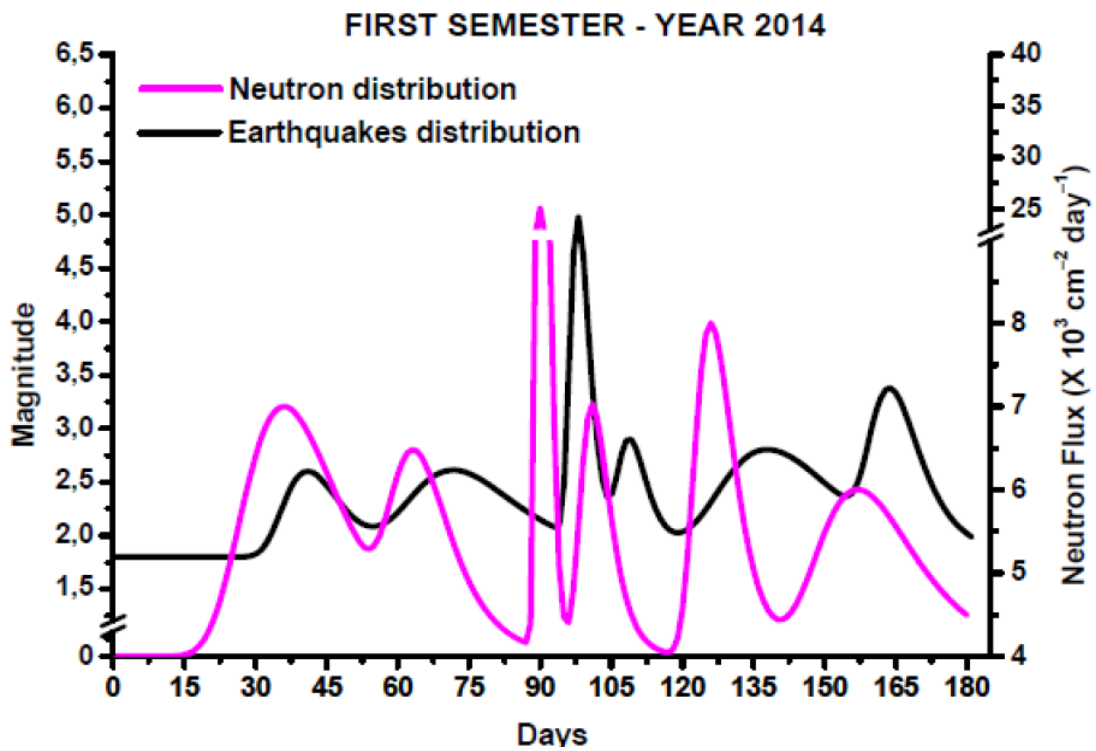


fig. 2.7: Multi-peak distribution of NE events and earthquakes for the first semester 2014

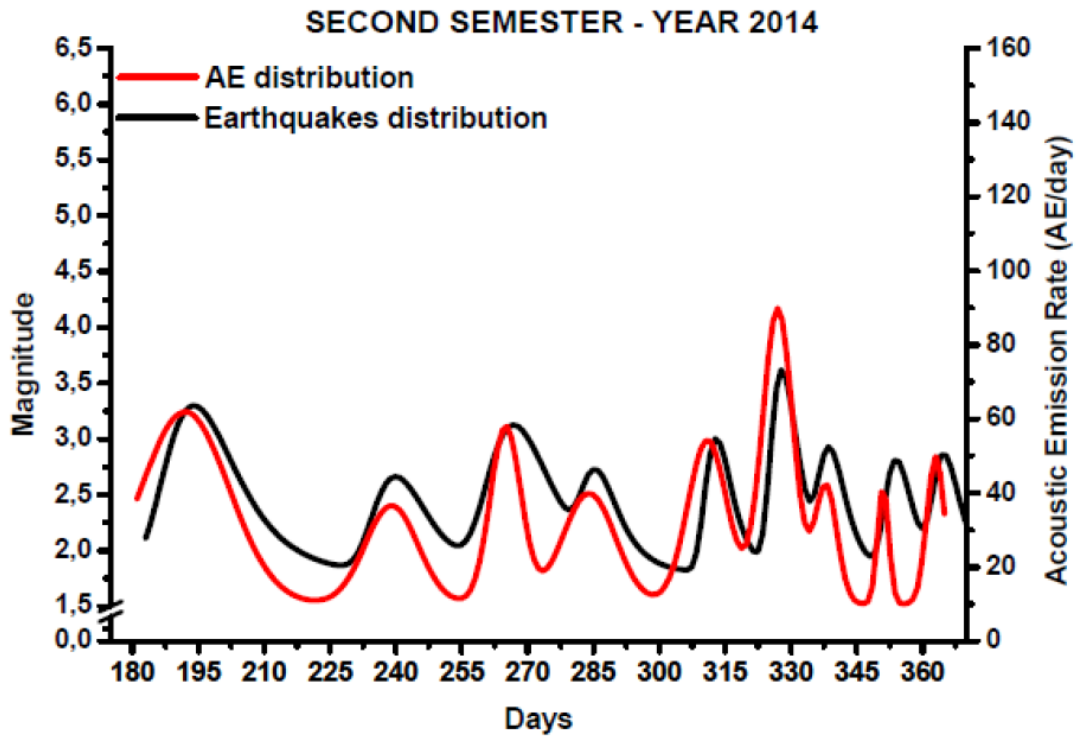


fig. 2.8: Multi-peak distribution of AE events and earthquakes for the second semester 2014

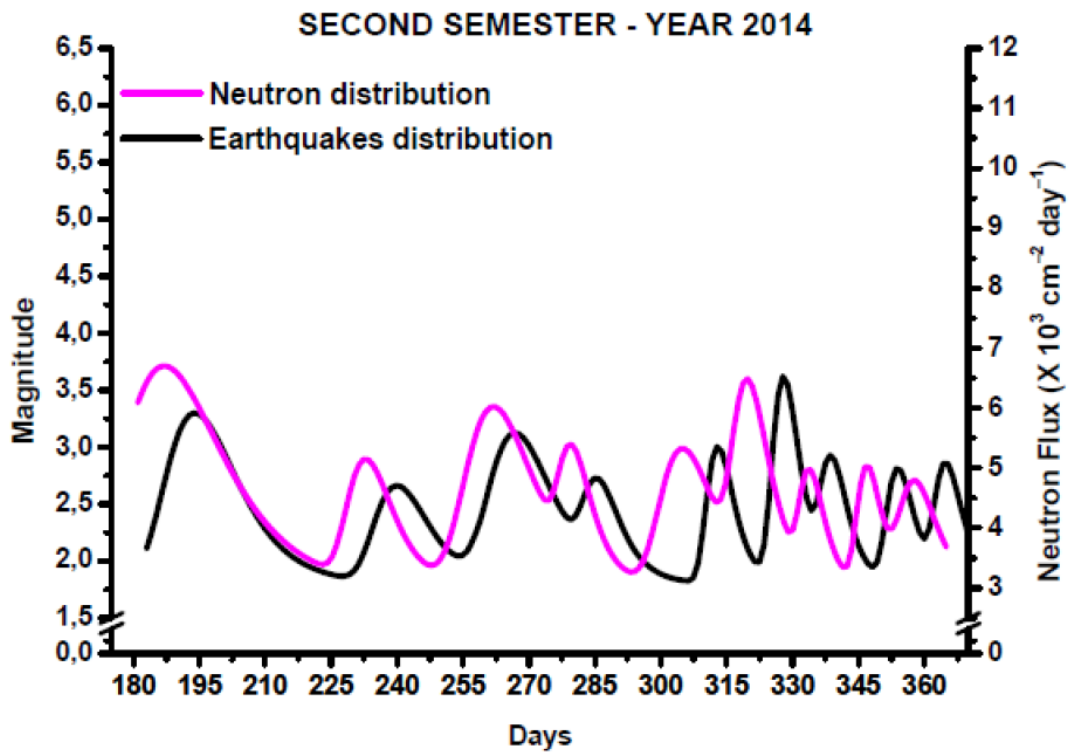


fig. 2.9: Multi-peak distribution of NE events and earthquakes for the second semester 2014

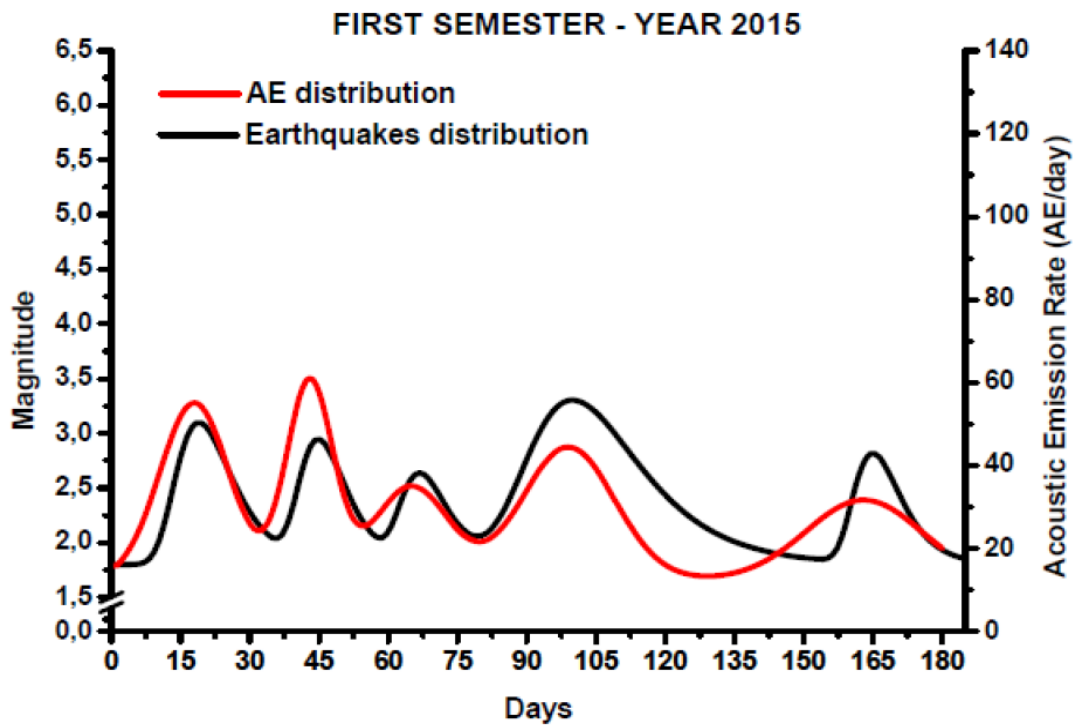


fig. 2.10: Multi-peak distribution of AE events and earthquakes for the first semester 2015

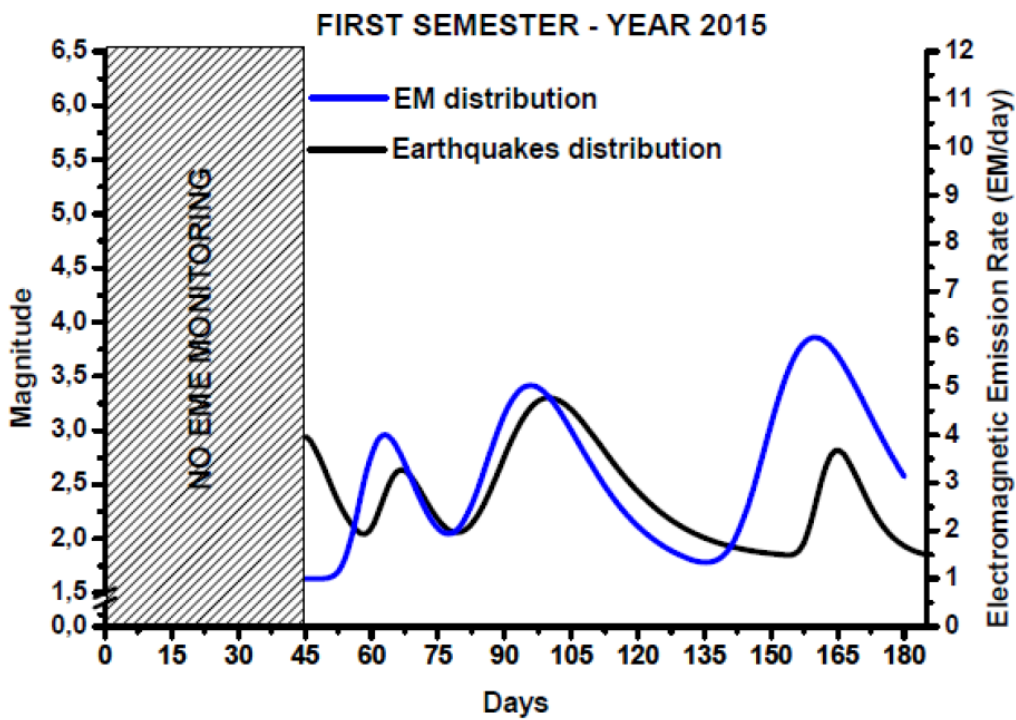


fig. 2.11: Multi-peak distribution of EME events and earthquakes for the first semester 2015

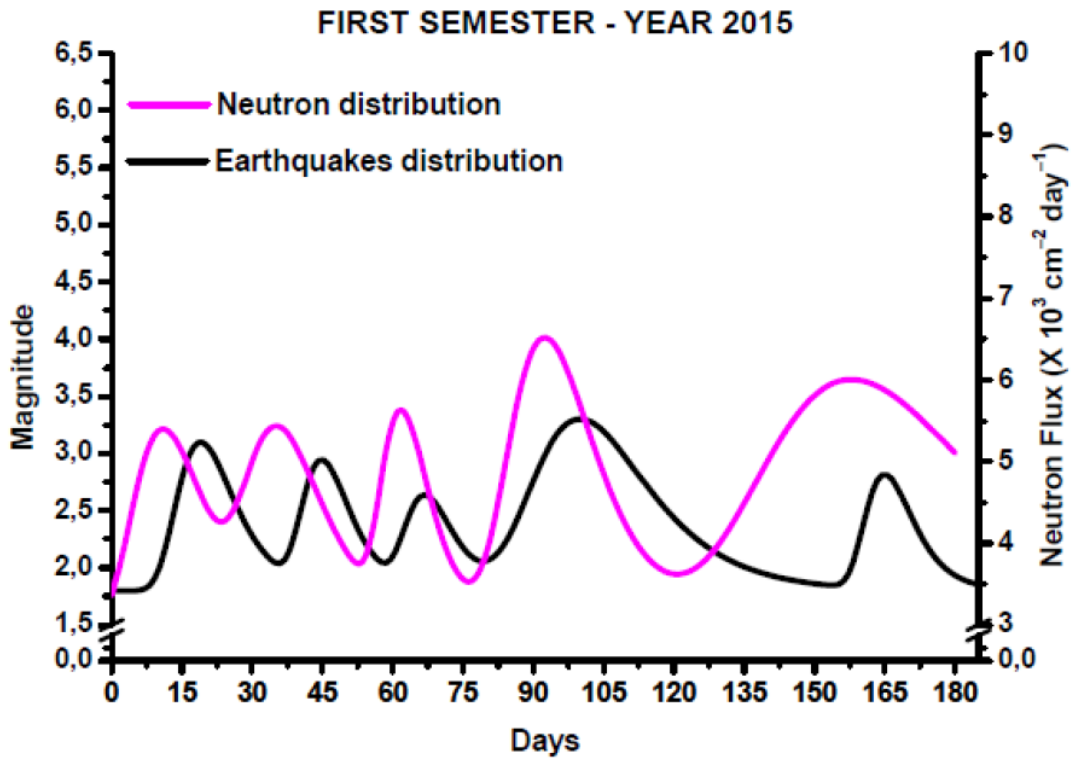


fig. 2.12: Multi-peak distribution of NE events and earthquakes for the first semester 2015

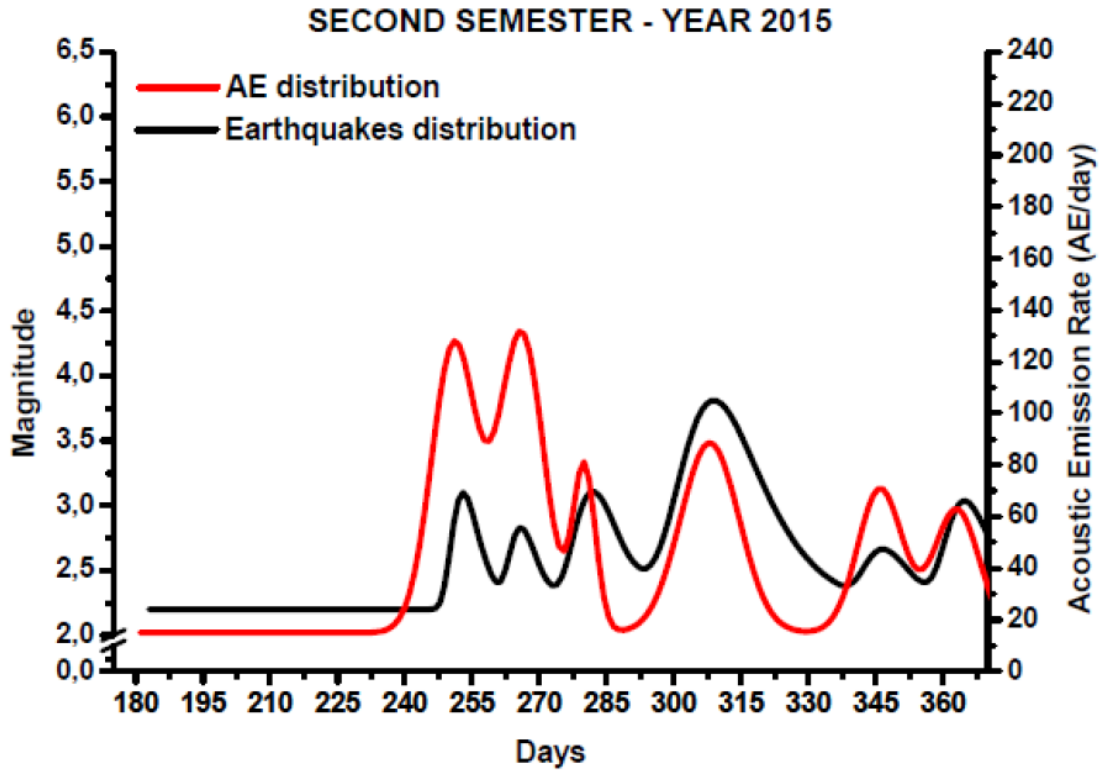


fig. 2.13: Multi-peak distribution of AE events and earthquakes for the second semester 2015

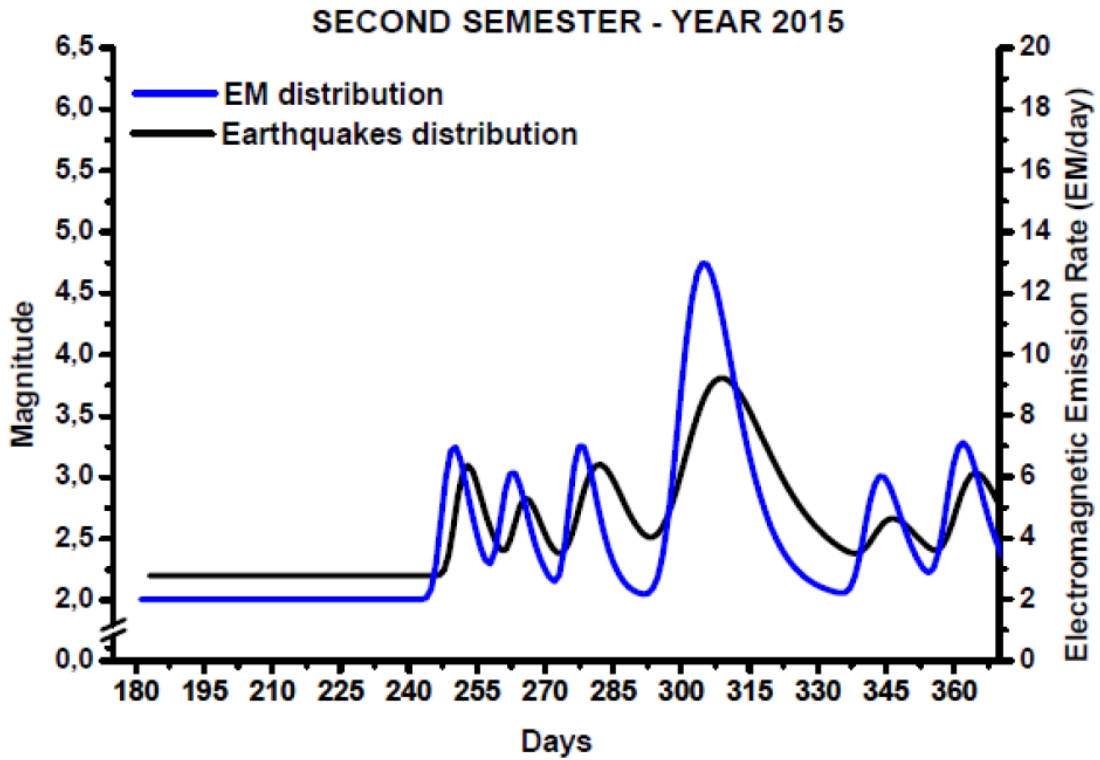


fig. 2.14: Multi-peak distribution of EME events and earthquakes for the second semester 2015

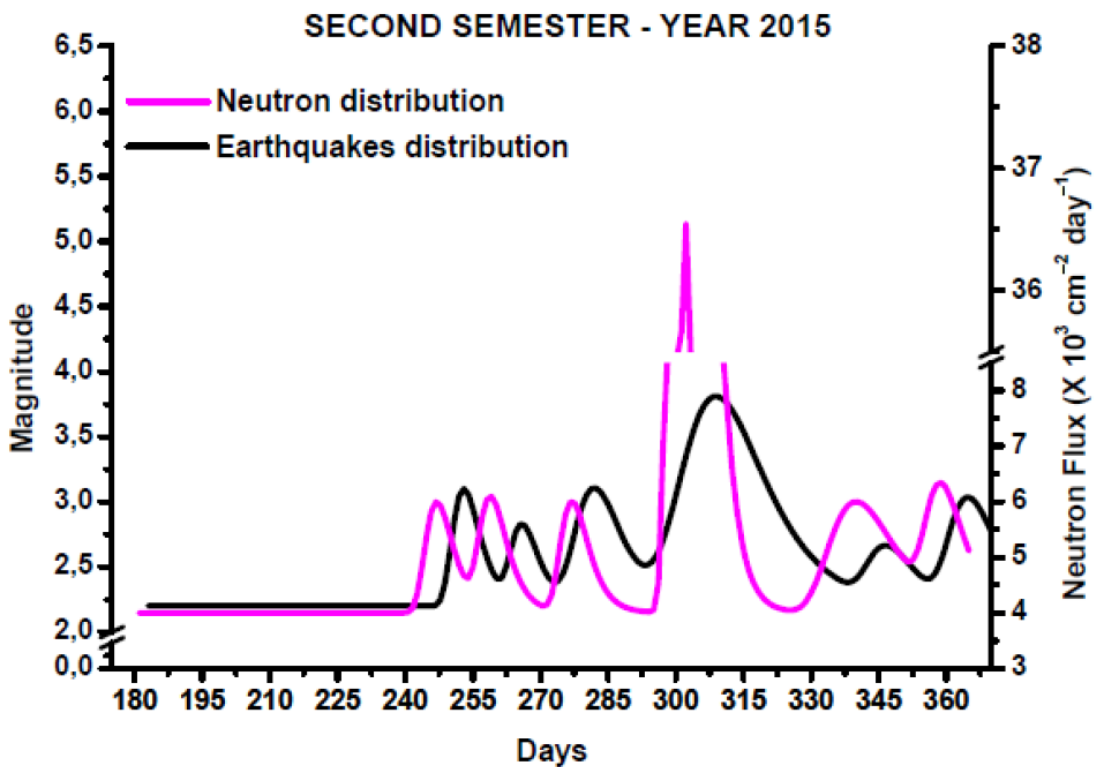


fig. 2.15: Multi-peak distribution of NE events and earthquakes for the second semester 2015

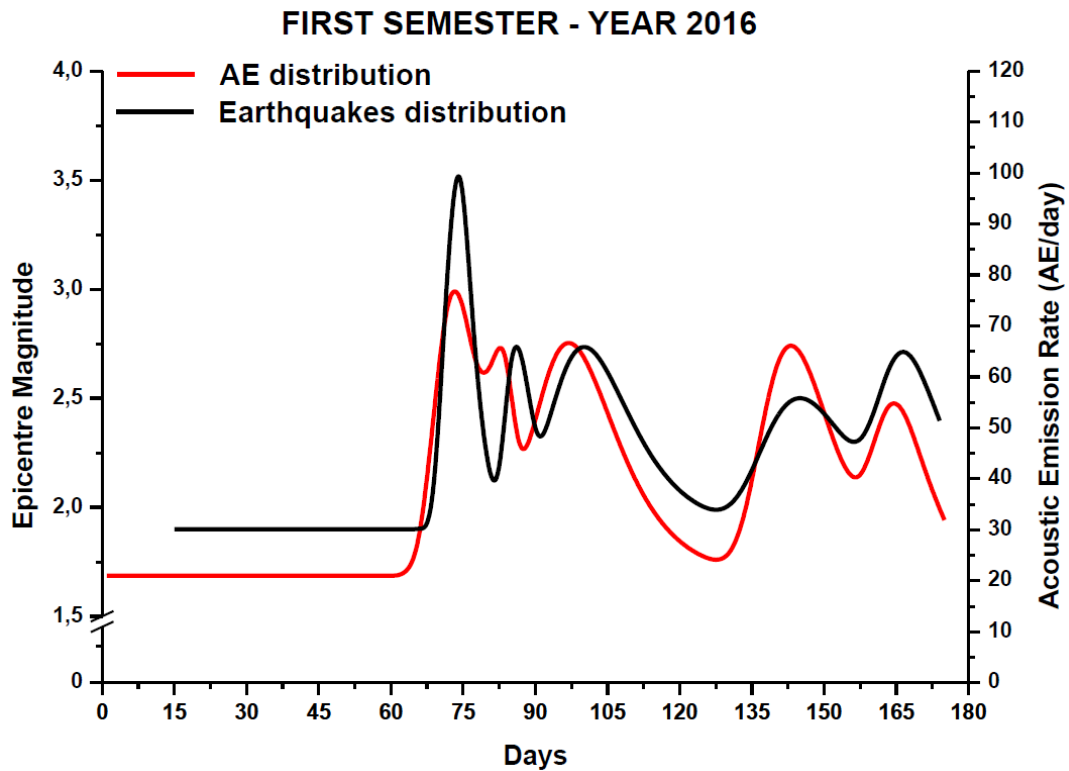


fig. 2.16: Multi-peak distribution of AE events and earthquakes for the first semester 2016

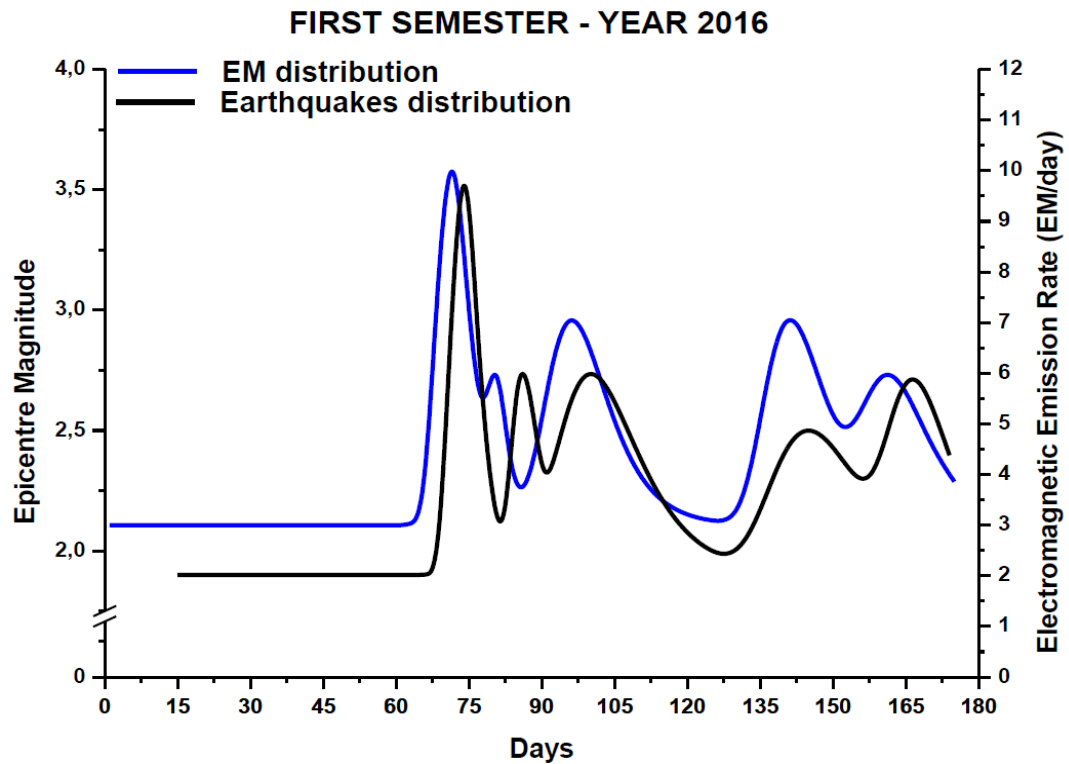


fig. 2.17: Multi-peak distribution of EME events and earthquakes for the first semester 2016

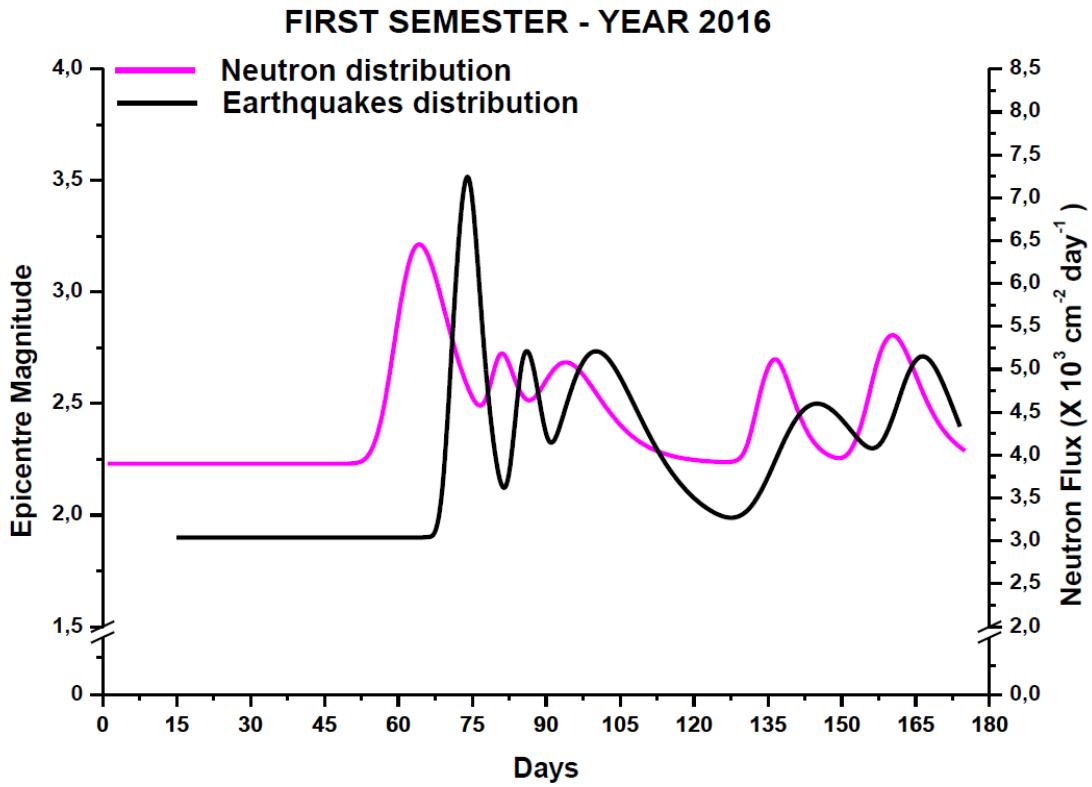


fig. 2.18: Multi-peak distribution of NE events and earthquakes for the first semester 2016

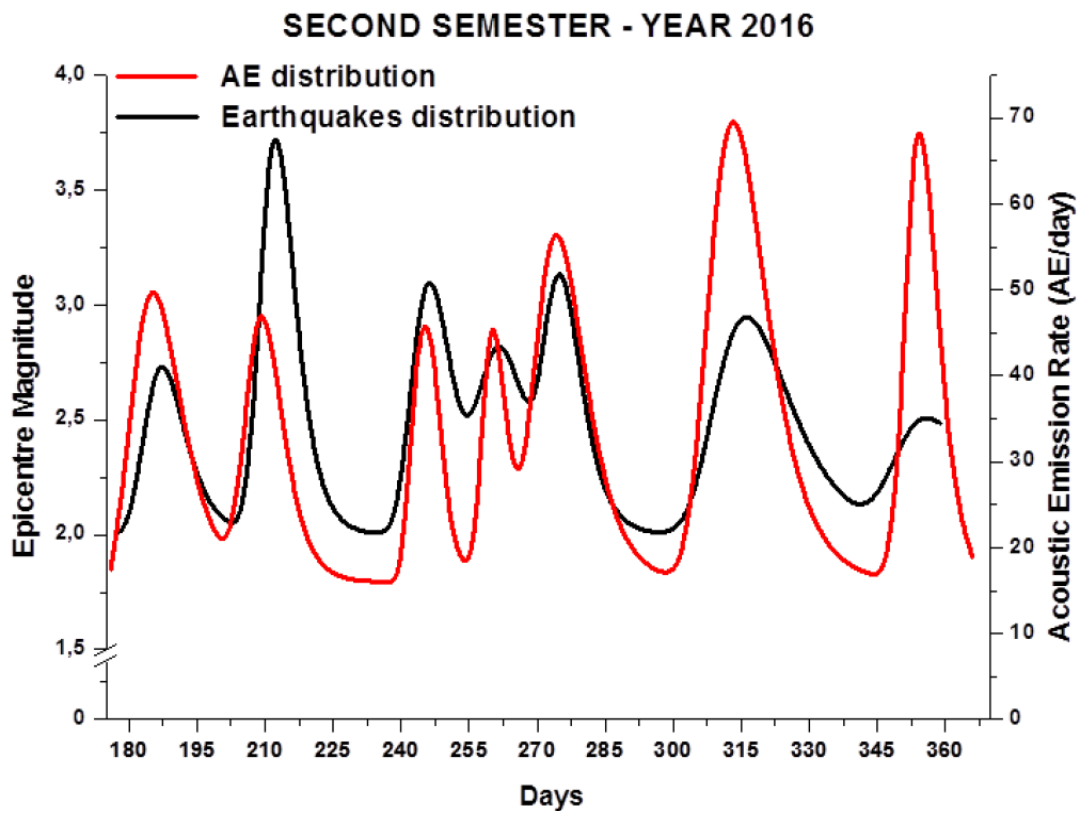


fig. 2.19: Multi-peak distribution of AE events and earthquakes for the second semester 2016

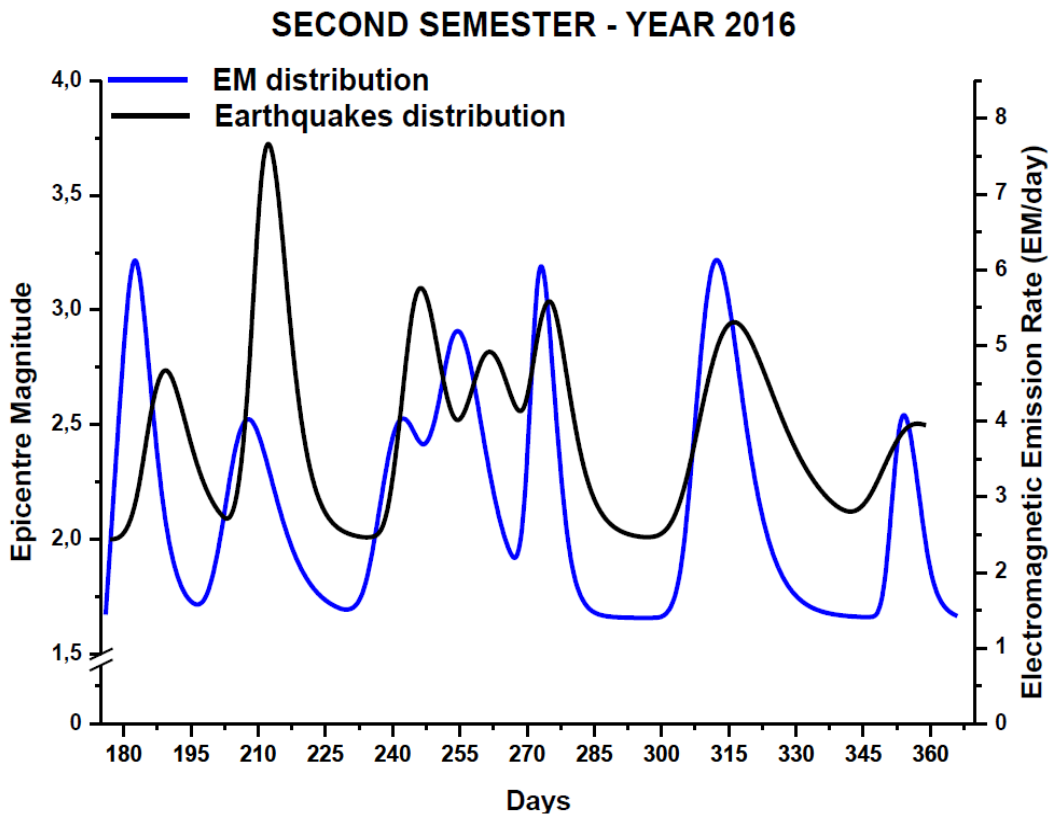


fig. 2.20: Multi-peak distribution of EME events and earthquakes for the second semester 2016

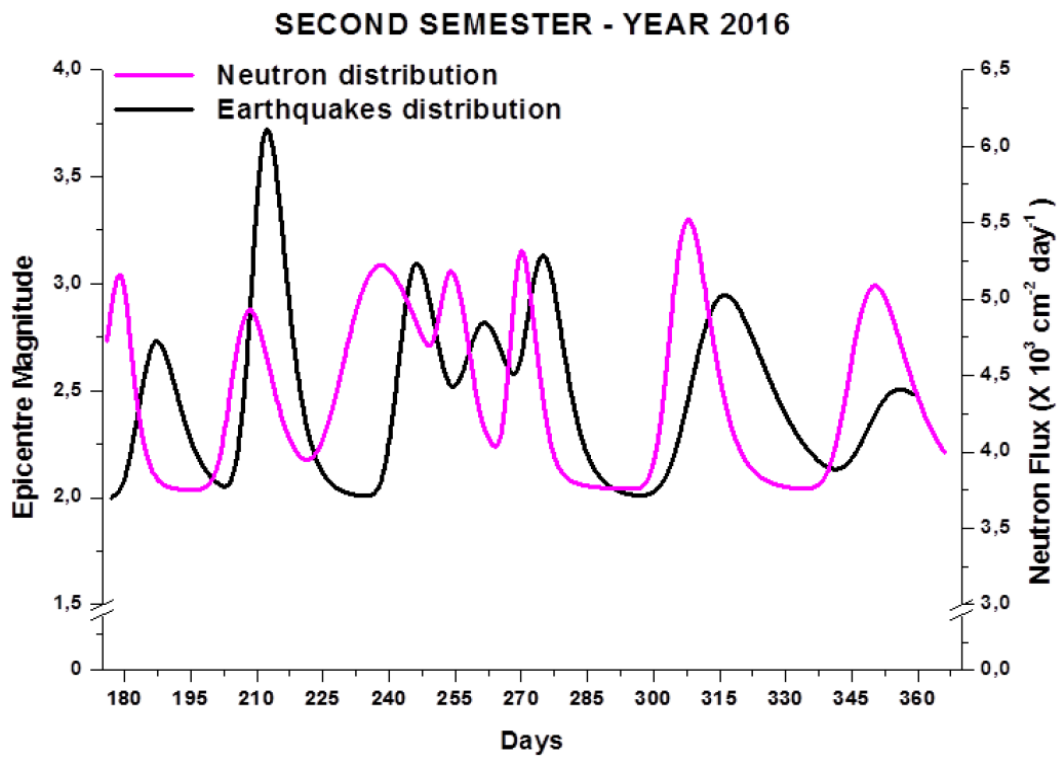


fig. 2.21: Multi-peak distribution of NE events and earthquakes for the second semester 2016

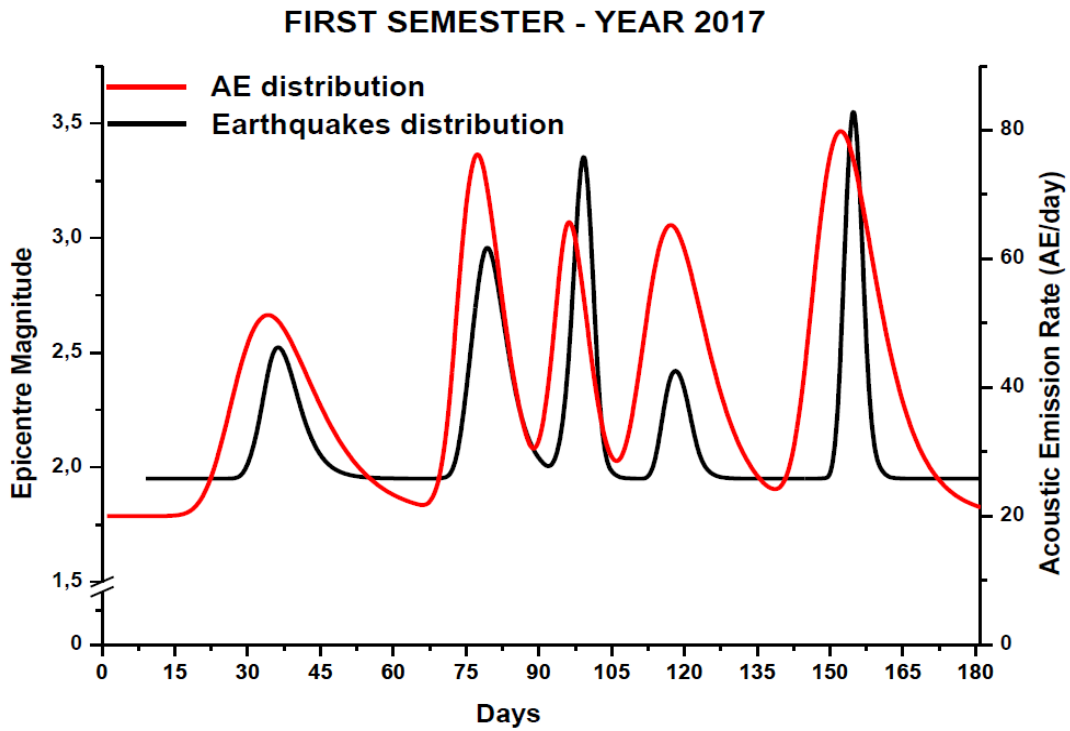


fig. 2.22: Multi-peak distribution of AE events and earthquakes for the first semester 2017

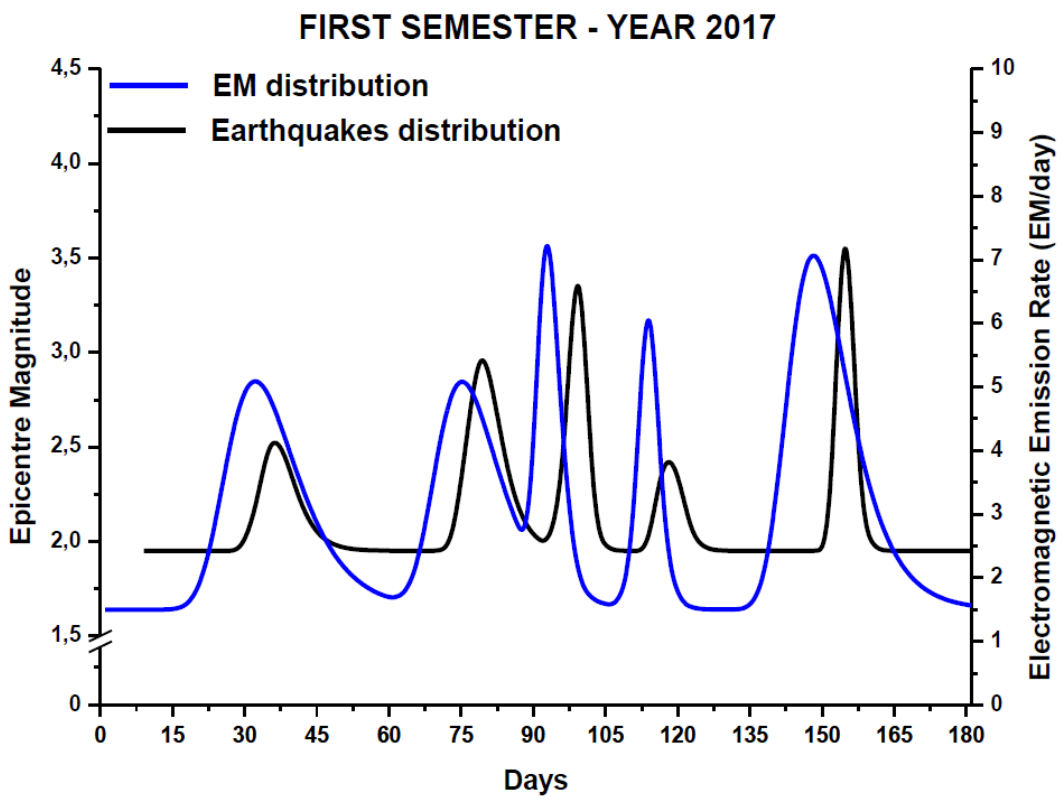


fig. 2.23: Multi-peak distribution of EME events and earthquakes for the first semester 2017

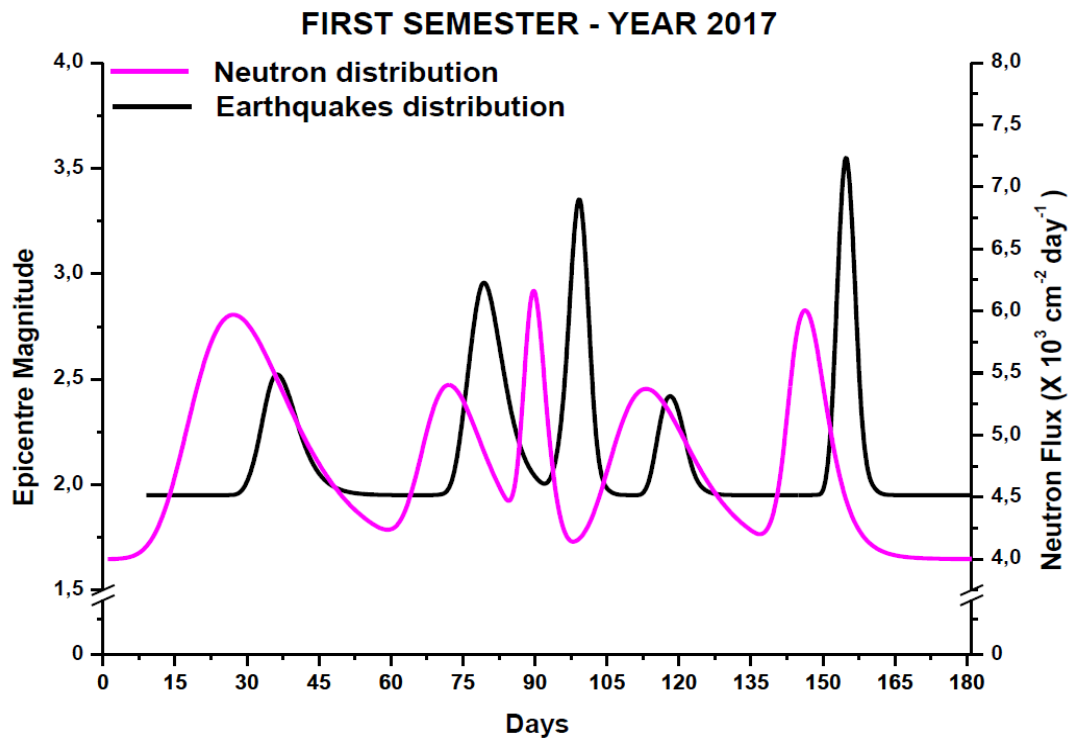


fig. 2.24: Multi-peak distribution of NE events and earthquakes for the first semester 2017

As we can see from the diagrams, and from the average time to the next earthquake (Table 2.1) fracto-emission's peaks anticipate main earthquakes from about one day for AE, 3 days for EME, and one week for NE. In the second column of the same table, we have the time after the previous earthquake. In chapter 4, also the temporal variation of *b*-value has been analyzed, in order to combine different methods but with the same scope to forecast earthquakes.

	Time to the next earthquake (days)	Time after the previous earthquake (days)	Standard deviation (days)
Acoustic Emissions	1,78	27,57	± 0,69
Electromagnetic Emissions	2,95	26,86	± 0,84
Neutron Emissions	7,05	22,76	± 2,08

Table 2.1: Average value of the time to the next earthquake, time after the previous earthquake and standard deviations for AE, EME and NE

2.3 Possible correlation between seismic activity and lunar phases

Studies demonstrate that the major earthquakes happened when Earth's crust was under the highest tidal stress. The moon is responsible for Earth's tides, and it involves modifications of the Earth's crust taking into account that everything depends on elasticity of Crust composition.

It is well accepted that earthquakes occur when the stress exceeds a particular critical value on a fault within the crust. As a matter of the fact, seismic risk is increased more during full and the new Moon respect to when Sun and Moon are aligned. The idea becomes from the fact that hydrostatic pressure exerted against rocks increases their state of stress until the point of fracturing, especially during full and new Moon. Recent studies have demonstrated that micro-earthquakes in volcanic and or hydrothermal areas have a strong correlation with tides (*Wilcock, 2001; Tolstoy et al., 2002; Stroup et al., 2007*). Regional and global tectonic events have also shown significant tidal influence (*Tanaka et al., 2002b, Cochran et al., 2004; Metivier et al., 2009; Wilcock, 2009*).

The hypothesis that tides may trigger seismic events is not new. Some scientists, in fact, found some correlation between magnitude and direction of tidal stress (Heaton 1975). Other scientists worked on this subject like M. Perrey (Klotz, O.,1914), in which he examined the influence of Moon on the production of earthquakes.

In his 7000 observations he noticed that:

- the frequency of earthquakes increases in syzygies (Period of Moon's revolution);
- that the frequency augments in the vicinity of the moon's perigee and diminishes towards the apogee.
- the shocks of earthquakes are more numerous when the moon is near the meridian.

He also gave a more scientific explanation: the interior of the earth that is in a liquid state tend to yield like the surface waters due to the attractive forces exerted by Moon and Sun, but these forces encounter the rigidity of the crust giving life to fractures and shocks.

According to Walsh Bryan J. in "Cycles of Enhanced Seismic Activity in California", large earthquakes are claimed to be three or more likely between new and full Moon than between full and new Moon (John T. Burns, 1997).

A test was performed by some scientists in the past (Heaton 1975,1982; Tsuruoka et al.,1995; Tanaka et al. 2002b, 2006) in order to find a correlation between the tidal components and the earthquakes occurrence using Schuster's test to examine the periodicity of seismicity. First of all, a tidal stress angle θ was assigned for the i earthquake, dividing linearly the time interval between them from 0° to 180° or from -180° to 0° where 0° and $\pm 180^\circ$ corresponding to the maximum or to the minimum of the tidal stress immediately before or after each earthquakes occurrence as we can see in fig. 2.25.

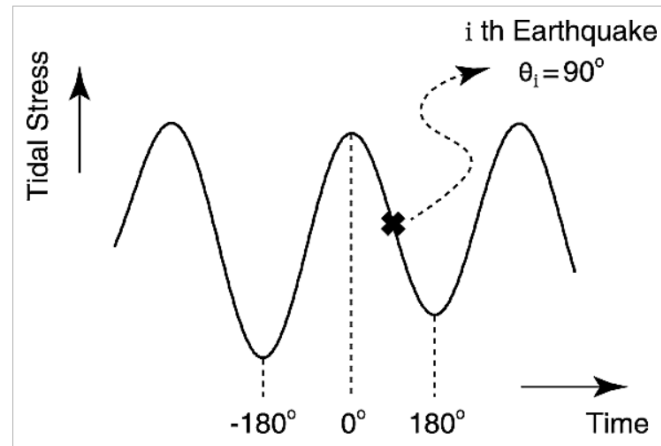


fig. 2.25: Linear time division from -180° to 180° , corresponding to the maximum or to the minimum of the tidal stress immediately before or after each earthquakes occurrence.

After having chosen a phase angle for each earthquake of a data set, the concentration around a particular phase angle was analyzed with the statistical method of Schuster. According to this method each earthquake is represented by a unit length vector in the direction of its tidal phase angle obtaining a vectorial sum D which is below defined as:

$$D^2 = (\sum_{i=1}^n \cos \theta_i)^2 + (\sum_{i=1}^n \sin \theta_i)^2 \quad (2.3)$$

where N is the number of earthquakes.

When θ_i are randomly distributed, the probability that the length of a vectorial sum is equal to or larger than D is given by:

$$\rho_s = e\left(\frac{-D^2}{N}\right) \quad (2.4)$$

$\rho_s < 5\%$ represents the null hypothesis that the earthquakes occurred randomly with respect to the tidal phase is rejected.

Significant tidal triggering evidence of intermediate earthquakes was obtained for the Vrancea region (Romania) by some researchers: N. Cadicheanu, M. van Ruymbeke, and P. Zhu, 2007. Vrancea seismic zone is located in the South-Eastern Carpathians (45° - 46° N, 25.5° - 27.5° E) and it is known for its seismicity in Europe.

To analyze the earthquakes the authors adopted a different statistical approach from Schuster's test even so this was a referring point for them to arrive to their conclusion. They choose the permutation test because it is always free to choose the statistic which best discriminates between hypothesis and the alternative as derive from biology and Genetic.

Permutation test is also used for calculating the significant level ρ_s explained before.

2.4 Relation between the phase of the moon and the micro-earthquakes

Some Japanese scientists investigated the correlation between Moon phase and the occurrence of micro-earthquakes in the Tamba region during the period from 31 January 1995 to 11 December 1996, close to the 1995 Kobe earthquakes (Iwata, Takaki & Katao, Hiroshi, 2006).

First of all they assigned a phase angle corresponding to the difference between the lunar and solar ecliptic longitude, attributing a value of 0° and 360° at a period of New Moon and 180° at a period of full Moon. They compared the situation of full/new Moon with the distribution of frequency of micro-earthquakes as shown in fig. 2.26

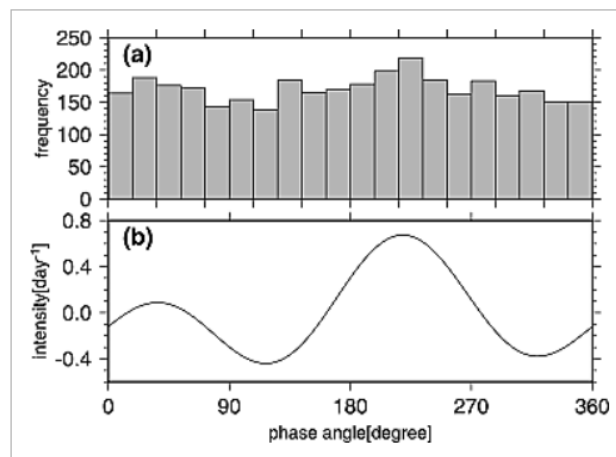


fig. 2.26: Comparison between the situation of full/new Moon with the distribution of frequency of micro-earthquakes

In order to find the statistical lunar correlation, the authors adopted the "point processing modelling" (Ogata 1983a) in which the periodicity is expressed as function of $\lambda(t)$:

$$\lambda(t) = \mu + (\text{trend}) + (\text{cluster}) + (\text{periodicity}) \quad (2.5)$$

where $\lambda(t)$ expresses the occurrence of micro-earthquakes in unit time.

To indicate the trend, the cluster and the periodicity they used respectively a polynomial function, the ETAS model (Ogata 1988), and a trigonometric function choosing the correct constraints (all equal to zero for some consideration).

$$\begin{aligned}
\lambda(t) = & \mu + \sum_{k=1}^N a_k t^k + \sum_{i:t_i < t} \frac{K \exp(\alpha (M_i - M_z))}{(t - t_i + c)^p} \\
& + A_1 \sin \theta(t) + B_1 \cos \theta(t) \\
& + A_2 \sin(2\theta(t)) + B_2 \cos(2\theta(t)), \\
& (a_k, K, c, p, \alpha, A_1, B_1, A_2, B_2 : \text{parameters}) \quad (2.6)
\end{aligned}$$

where t_i and M_i are the occurrence time and magnitudes of i -th micro-earthquake. M_z represents the lower threshold of the data set and $\theta(t)$ is a function that converts the actual time t in the phase angle.

2.5 Correlation between seismicity and lunar periodicity at the “San Pietro-Prato Nuovo” gypsum mine (July 2013 - June 2017)

A possible correlation between lunar phases and 48 seismic swarms was explored in the surrounding area of Murisengo in the period from July 1st, 2013 to December 31, 2017. Over a number of 396 earthquakes, 48 seismic swarms in the range of 1,8 to 4,7 magnitude can be identified, that is more or less an average of 6 seismic swarms per semester. For this reason, an hypothesis on the possible correlation between the two events emerged, also because the distance between two distinct seismic swarms was of about 30 days that is about the duration of the synodic month (which is the period of Moon's revolution). The assumption was later confirmed by the temporal correlation between lunar phases and seismic swarms. In the following diagrams (figs. 2.27-2.34), a sinusoidal curve is used to represent the lunar cycle with points of maximum and minimum coincident with the period of Full Moon and New Moon, respectively and black dots which represent the 48 seismic swarms. From the various diagrams a close correlation between lunar phases and seismic swarms emerged. Seismic swarms, in fact appear in correspondence or some days before or after (2-3 days) the occurrence of full and new Moon as the consequence of the attraction exerted by this natural satellite upon the Earth. From the experimental observation carried out at Murisengo, emerged that not only high magnitude earthquakes can be affected by the gravitational forces exerted by the Sun and the Moon, but also seismic swarms and low magnitude earthquakes tend to grow under the influence of our Star and our Satellite.

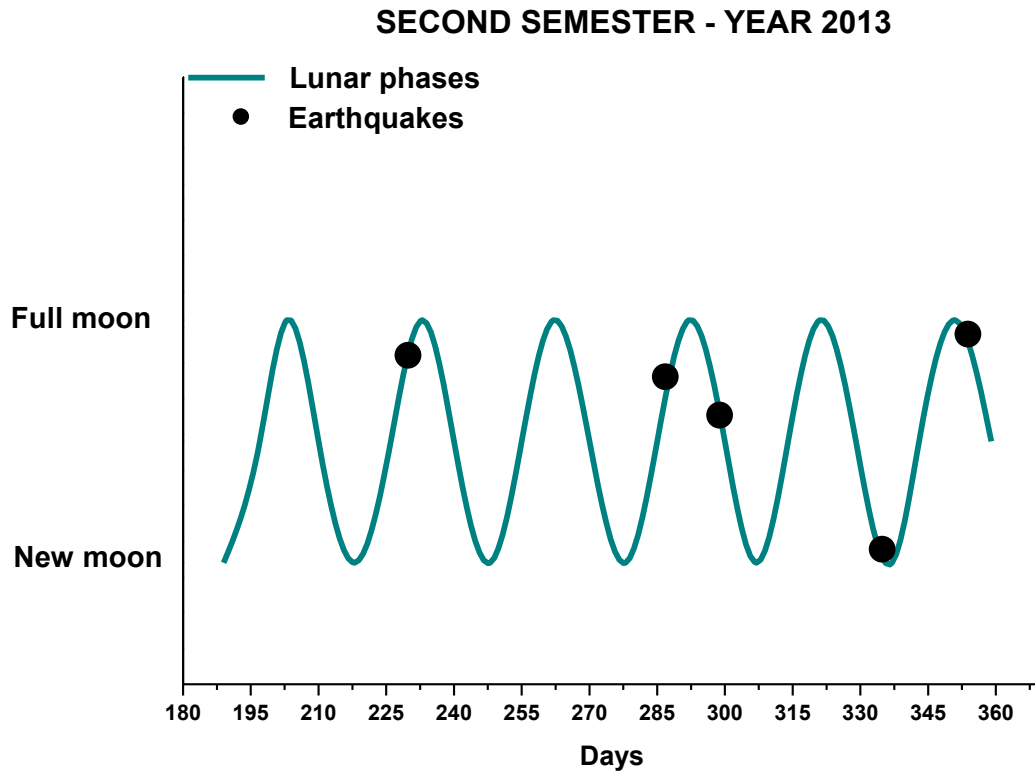


fig. 2.27: Correlation between lunar phases and seismic swarms for the second semester 2013

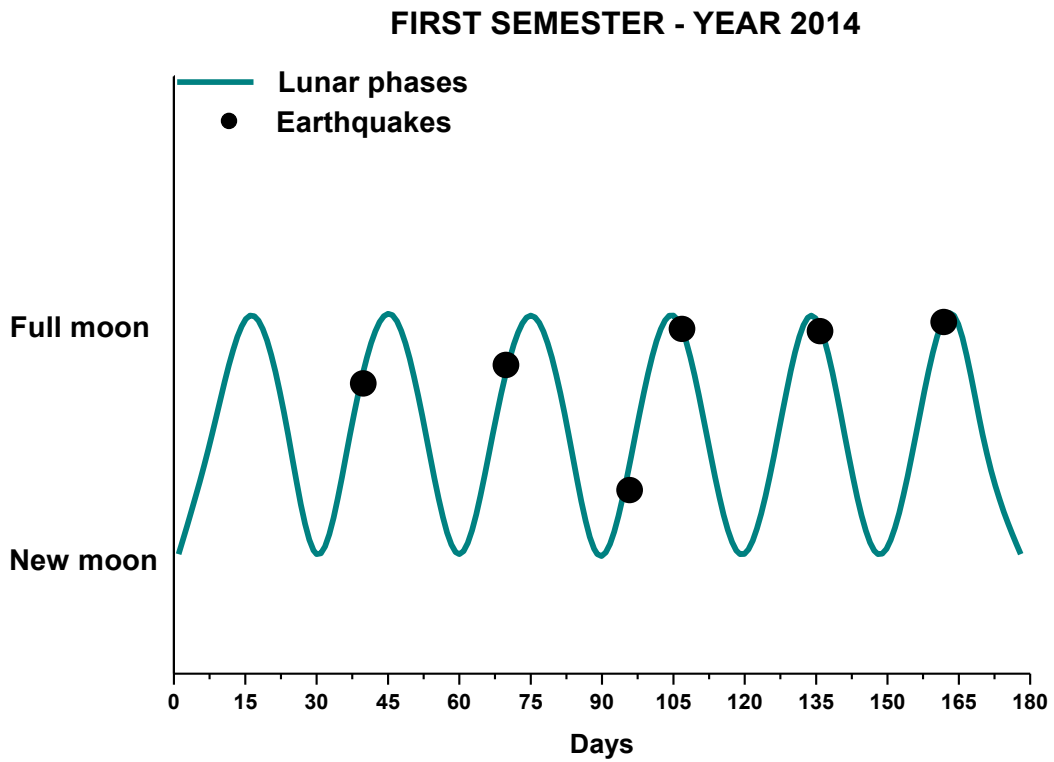


fig. 2.28: Correlation between lunar phases and seismic swarms for the first semester 2014

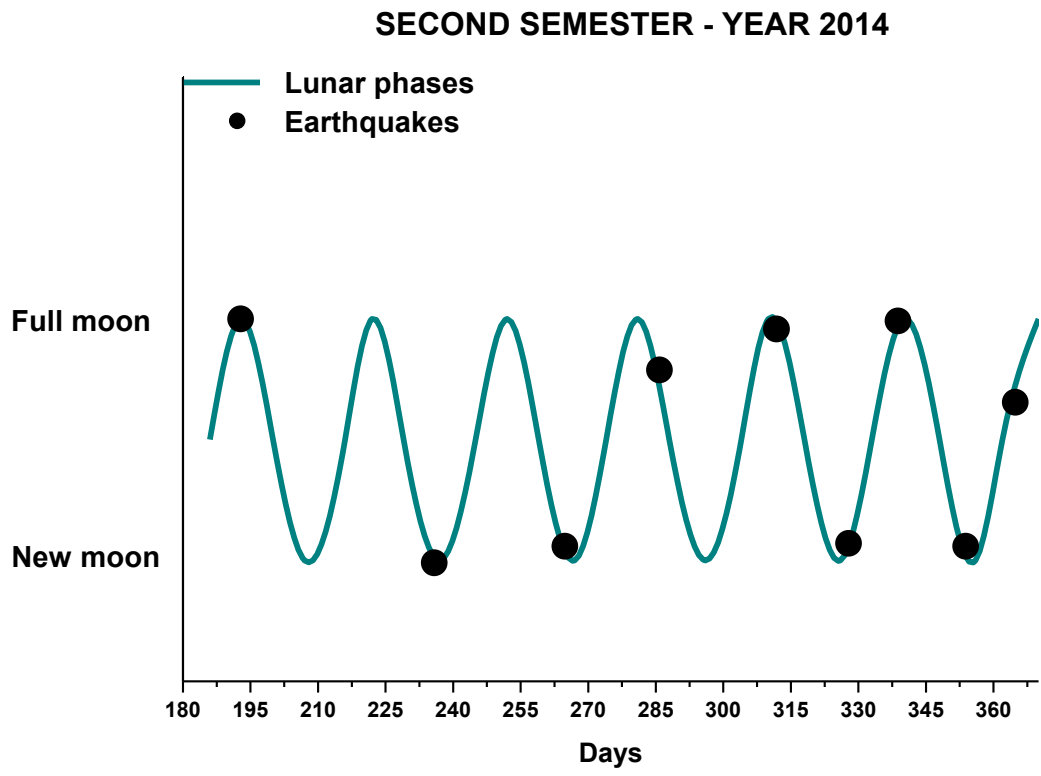


fig. 2.29: Correlation between lunar phases and seismic swarms for the second semester 2014

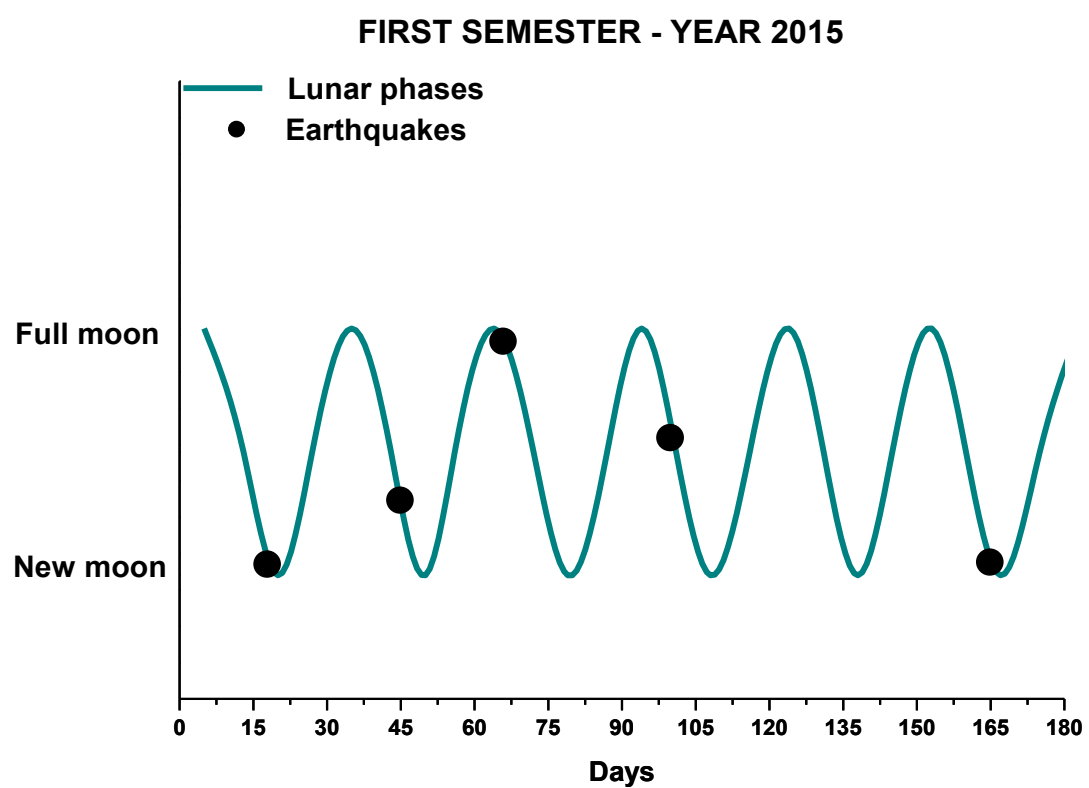


fig. 2.30: Correlation between lunar phases and seismic swarms for the first semester 2015

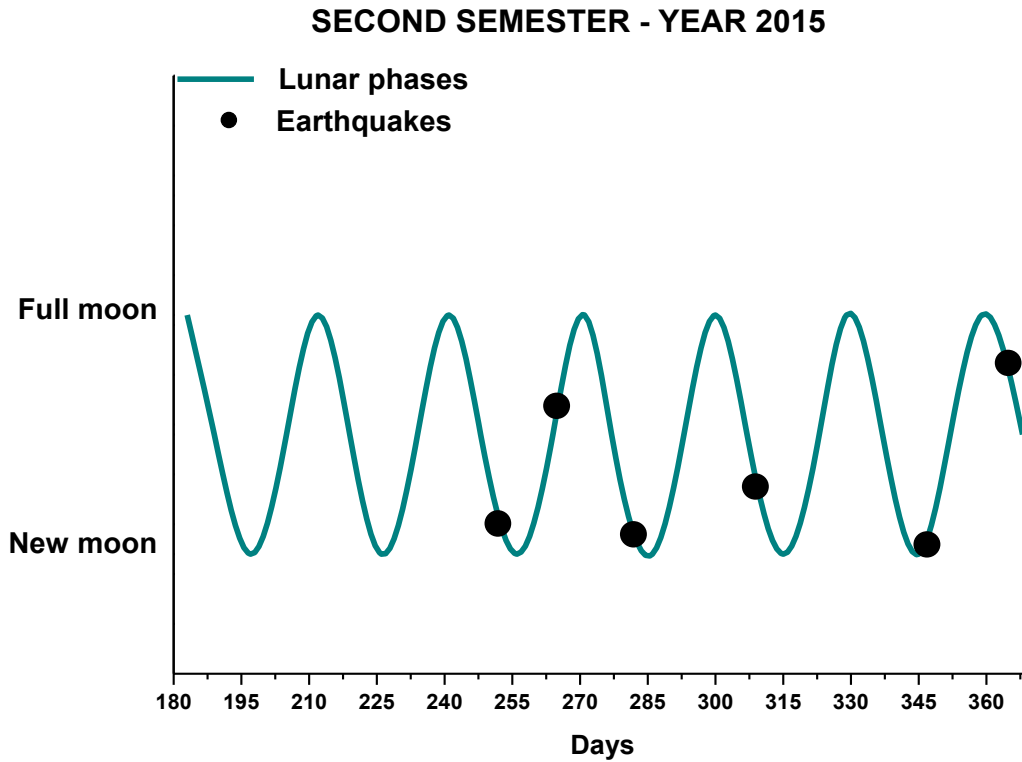


fig. 2.31: Correlation between lunar phases and seismic swarms for the second semester 2015

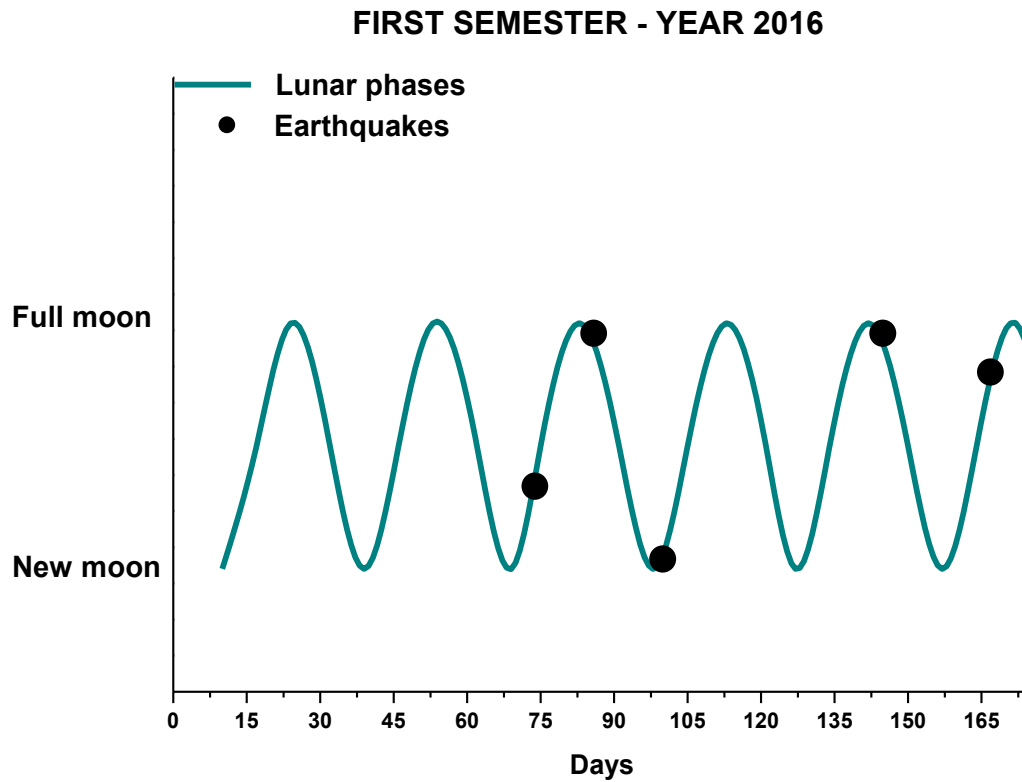


fig. 2.32: Correlation between lunar phases and seismic swarms for the first semester 2016

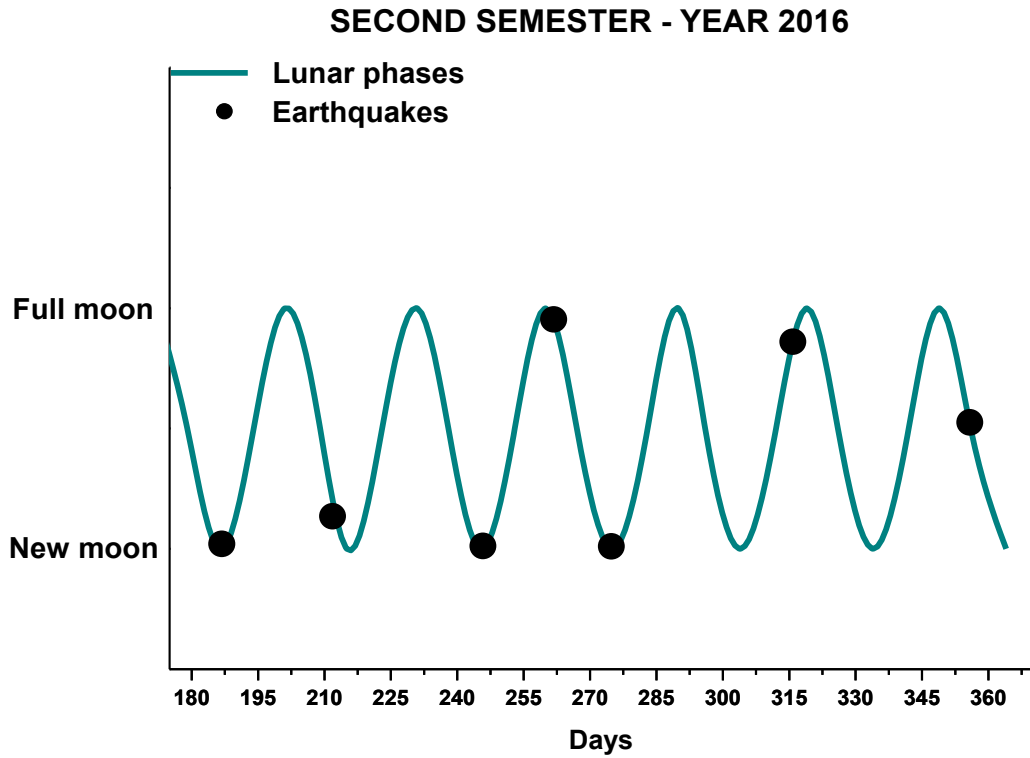


fig. 2.33: Correlation between lunar phases and seismic swarms for the second semester 2016

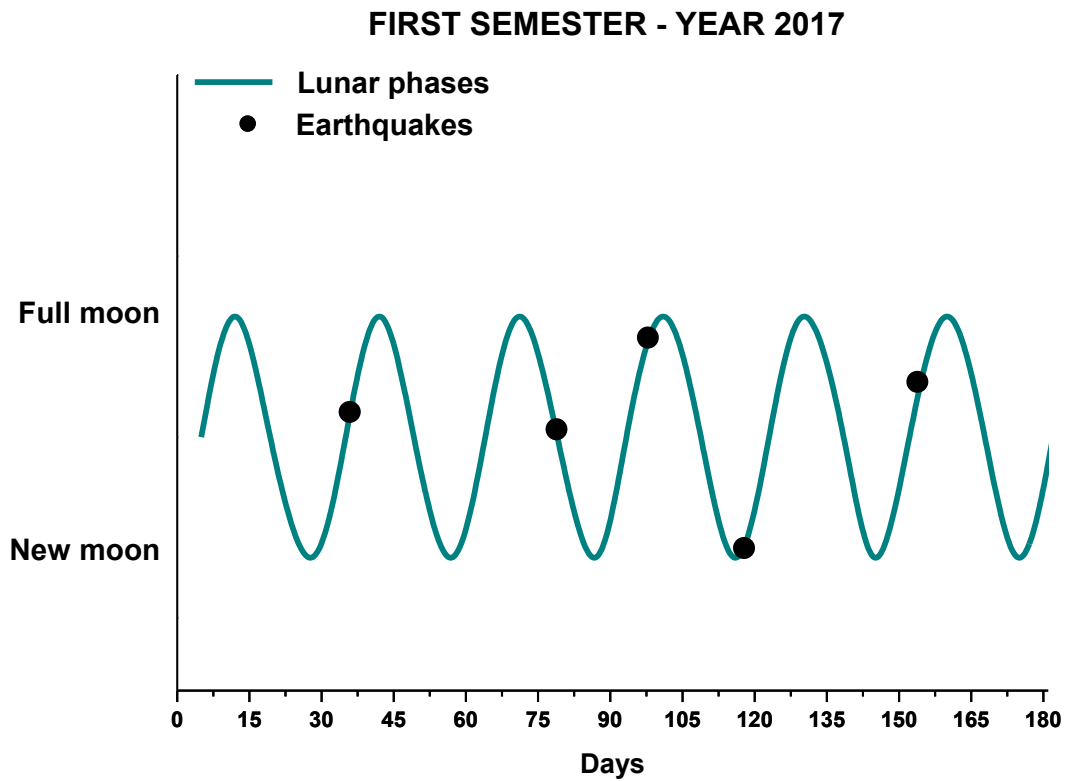


fig. 2.34: Correlation between lunar phases and seismic swarms for the first semester 2017

Chapter 3

NEW EXPERIMENTAL EVIDENCE FROM "SAN PIETRO-PRATO NUOVO" GYPSUM MINE

3.1 The recent experimental results of fracto-emissions (July 2017 - December 2017)

The following chapter exhibits the correlation between seismicity and the three fracto-emissions: Acoustic, Electromagnetic and Neutron emissions carried out by Polytechnic of Turin at San Pietro-Prato Nuovo gypsum mine on the period from July 1st, 2017 to December 31, 2017 (one semester) confirming the previous analysis and so reinforcing the idea of the great forecasting potentiality of fracto-emissions. The experimental results highlight how seismic events are anticipated by AE, EME and NE.

In this semester 48 earthquakes with a magnitude greater than 1,8 and comprised in the 1,8 to 3,7 magnitude range were detected and downloaded by INGV's site. By performing the multi-modal approach that is an iterative procedure that allows to obtain curves similar to Gaussians which best fit the discrete number of experimental data (just explained in Chapter 2), 4 seismic swarms emerged. As also for the previous analysis the threshold of 1,8 is chosen because no significant change in neutron flux was observed.

As regards fracto-emissions, the same multi-modal approach used for earthquakes has been performed. In the following diagrams the multi-modal analysis of earthquakes and fracto-emissions can be seen. In all cases, 4 peaks correspondent to the seismic swarms can be observed: two seismic swarms with a magnitude of 2,9; one with a magnitude of 3,3 and the last one with a magnitude of 3,7. On the x-axis we have the day of the year in which we can find each earthquake and precisely:

- September 10, 2017 for the first peak;
- October 27, 2017 for the second one;
- July 18, 2017 for the third one;
- December 19, 2017 for the last one.

The relative maximum of fracto-emissions peaks are in a range comprised from the background level to 4 times for AE and EME; from the background level to 2 times for NE, which are comparable with the order of magnitude of the previous analysis conducted over the 48 seismic swarms.

In the order we have:

1. the graph relative to the multi-modal analysis of seismic swarms and shown by a black line (fig. 3.1);
2. the graph relative to the multi-modal analysis of Acoustic emissions (AE) and shown by a red line (fig. 3.2);
3. the graph relative to the multi-modal analysis of Electromagnetic emissions (EME) and shown by a blue line (fig. 3.3);
4. the graph relative to the multi-modal analysis of Neutron emissions (NE) and shown by a violet line (fig. 3.4);

By superimposing the singular multi-peaks analysis of the three fracto-emissions with the one relative to the earthquake swarms (figs. 3.5-3.7), we can clearly see their precursory nature. As a matter of the fact, fracto-emissions peaks anticipate major earthquakes from few days (for the AE and EME) until several days (NE) as a confirmation of the potentiality of this methods as a forecasting tool for earthquakes.

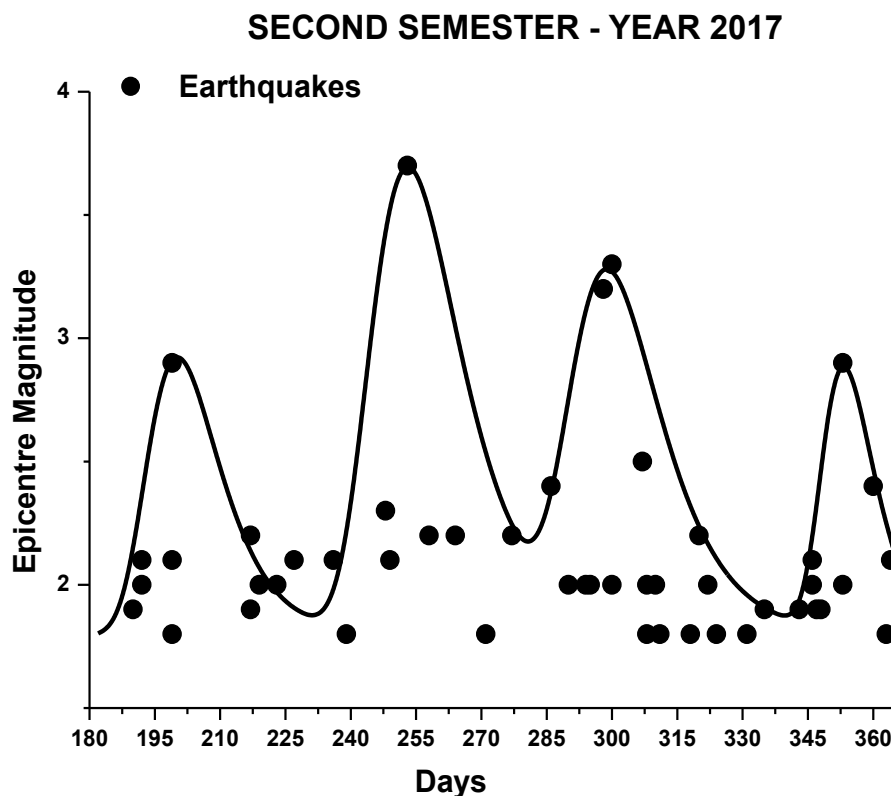


fig. 3.1: Multi-peak distribution of earthquakes for the second semester 2017.

SECOND SEMESTER - YEAR 2017

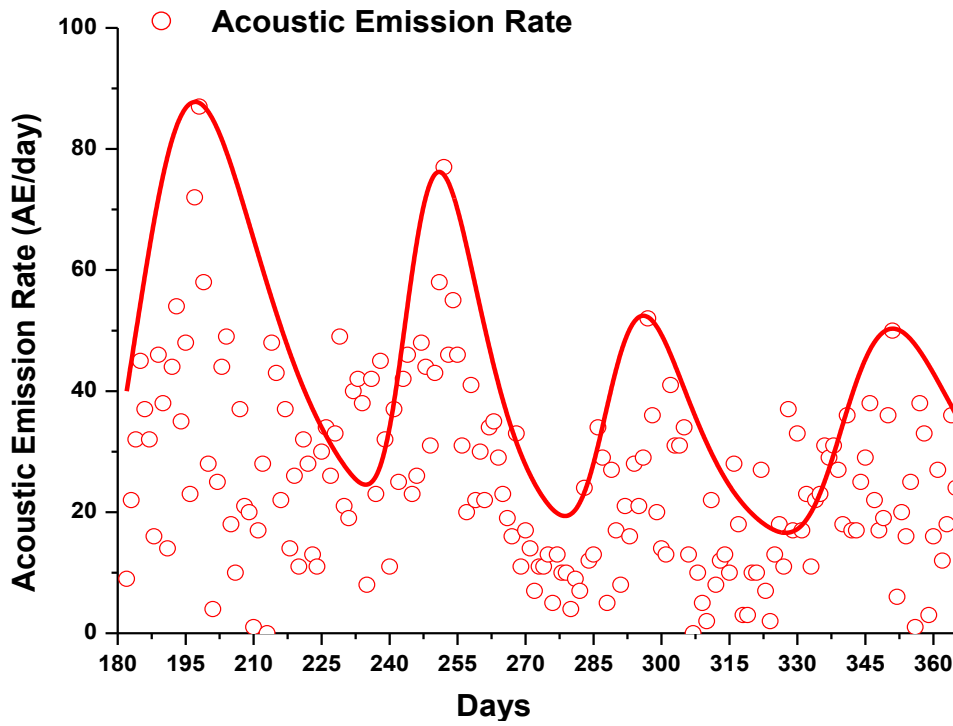


fig. 3.2: Multi-peak distribution of AE events for the second semester 2017.

SECOND SEMESTER - YEAR 2017

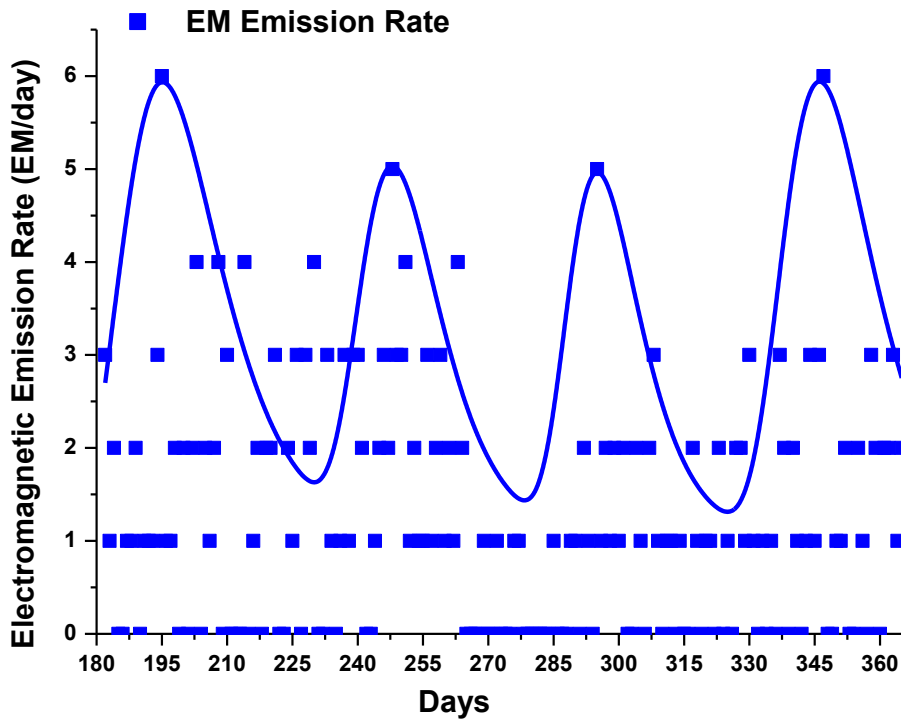


fig. 3.3: Multi-peak distribution of EME events for the second semester 2017.

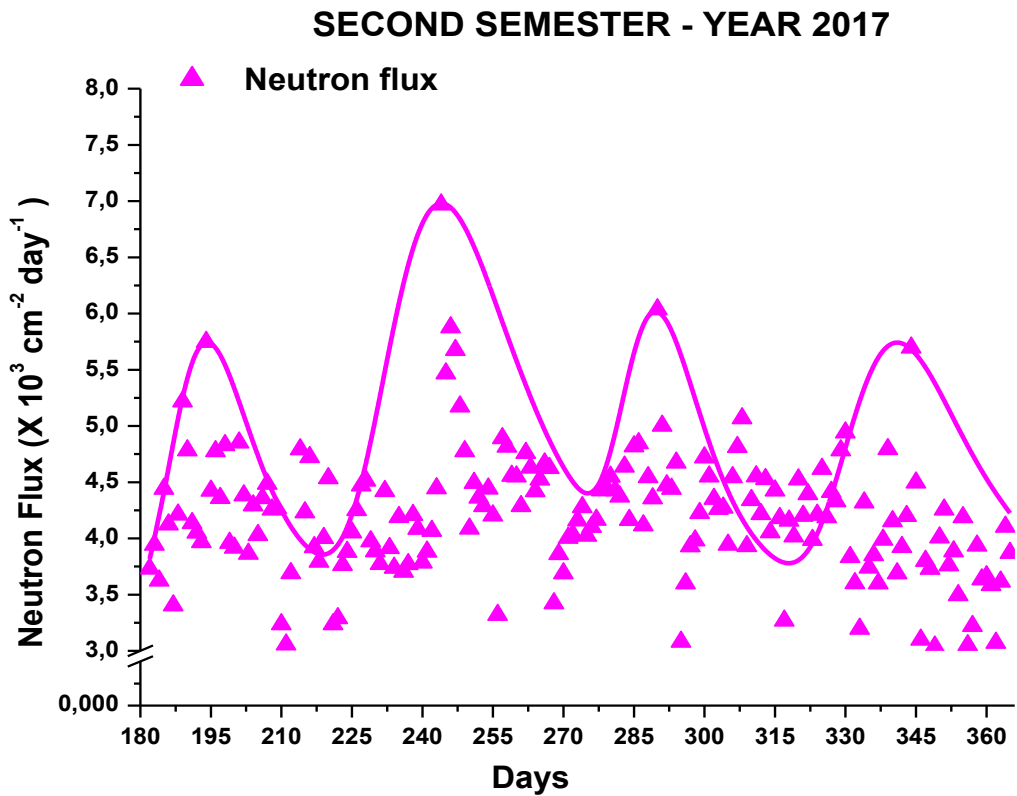


fig. 3.4: Multi-peak distribution of NE events for the second semester 2017.

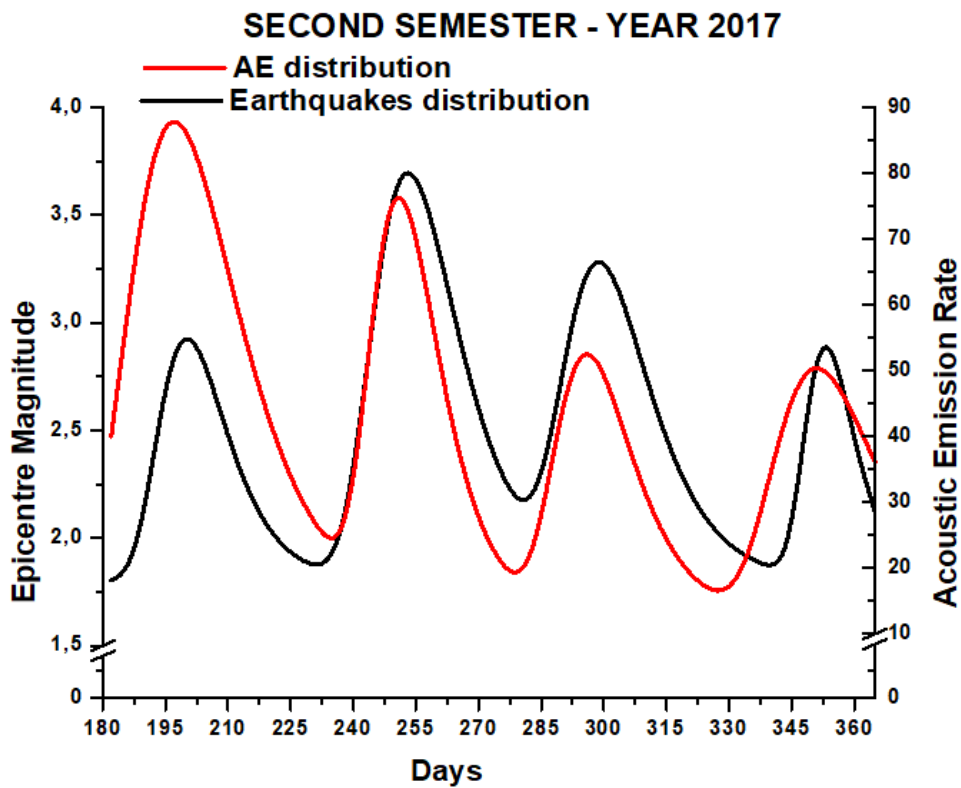


fig. 3.5: Multi-peak distribution of AE events and earthquakes for the second semester 2017

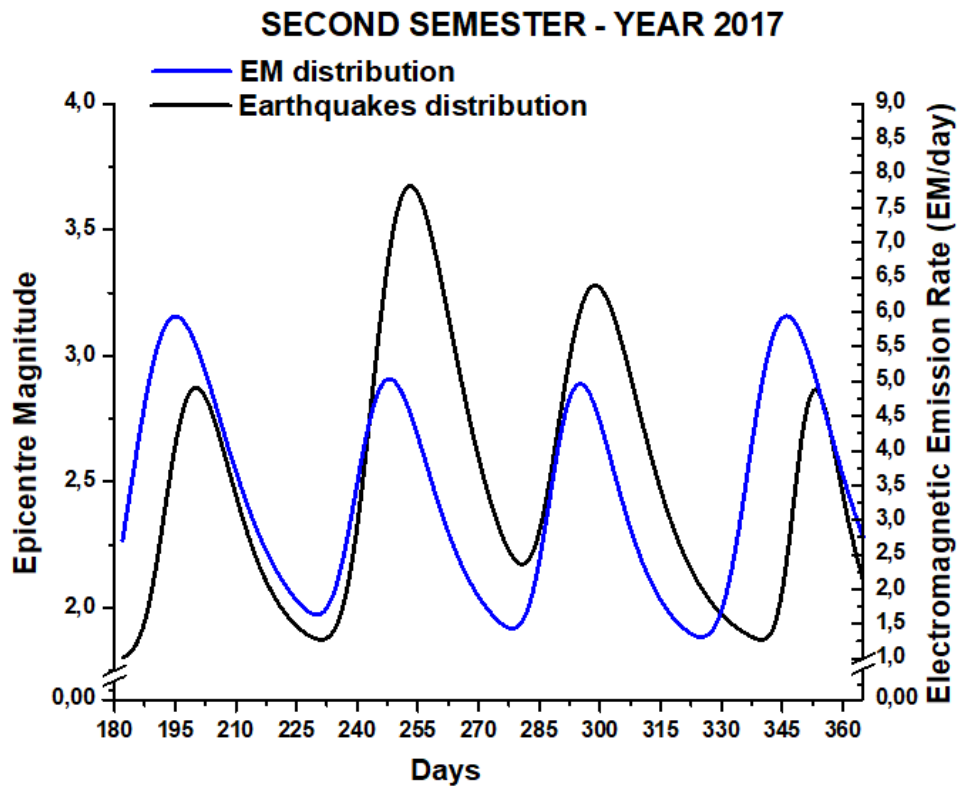


fig. 3.6: Multi-peak distribution of EME events and earthquakes for the second semester 2017

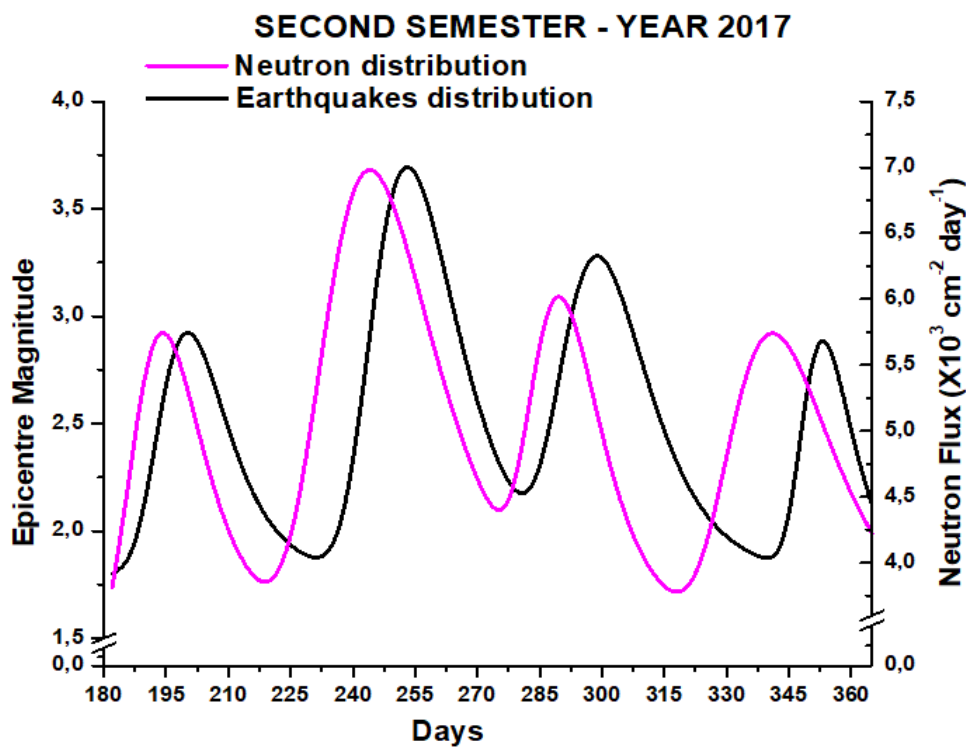


fig. 3.7: Multi-peak distribution of NE events and earthquakes for the second semester 2017

Comparing the peaks of the curves regarding the earthquakes distribution with those concerning the three kind of fracto-emissions, it can be deduced that the results obtained during the last semester of monitoring, and discussed in this thesis, confirm the results related to the period from July: the AE, EME, and NE anticipate the seismic event.

As it was deduced by the previous studies, the acoustic emissions happen about two-three days before the earthquake, the electromagnetic emissions anticipate the event of about five days while the neutron ones of about nine days. If we compare these values with those coming from table 2.1 referred to the previous 48 seismic swarms, we can notice a little difference but anyway it seems to be comprised in the confidence intervals, as can be deduced from the standard deviation values. After having analyzed the previous semesters and the new one it can be confirmed the strong potentiality of fracto-emissions as a seismic tool to forecast earthquakes.

The Table 3.1 reports the occurrence of the fracto-emissions with respect to that of the corresponding seismic swarm, instead the Table 3.2 reports the average values of the occurrence times of the AE, EME and NE that precede the seismic swarm and their standard deviations.

SECOND SEMESTER - YEAR 2017				
		Time to the next earthquake (days)		
Date of seismic swarm	magnitude	AE	EME	NE
18/07/2017	2,9	3	5	6
10/09/2017	3,7	2	5	9
27/10/2017	3,3	3	4	9
19/12/2017	2,9	2	7	12

Table 3.1: Occurrence of AE, EME and NE with respect to the corresponding seismic swarm

PRECURSORS	Time to the next earthquake (days)	Standard Dev.
Acoustic Emissions	2,5	±0,58
Electromagnetic Emissions	5,25	±1,26
Neutron Emissions	9	±2,45

Table 3.2: Average value of the time to the next earthquake for AE, EME and NE and standard deviations

In the next diagrams (figs. 3.8-3.10), it is possible to observe the comparison between the seismic swarm of December 19, 2017, whose main event was of 2,9 degree in the Richter

scale, and the correlated energy distribution. From the correlation the temporal shift of fracto-emissions from the incoming earthquake can be clearly seen.

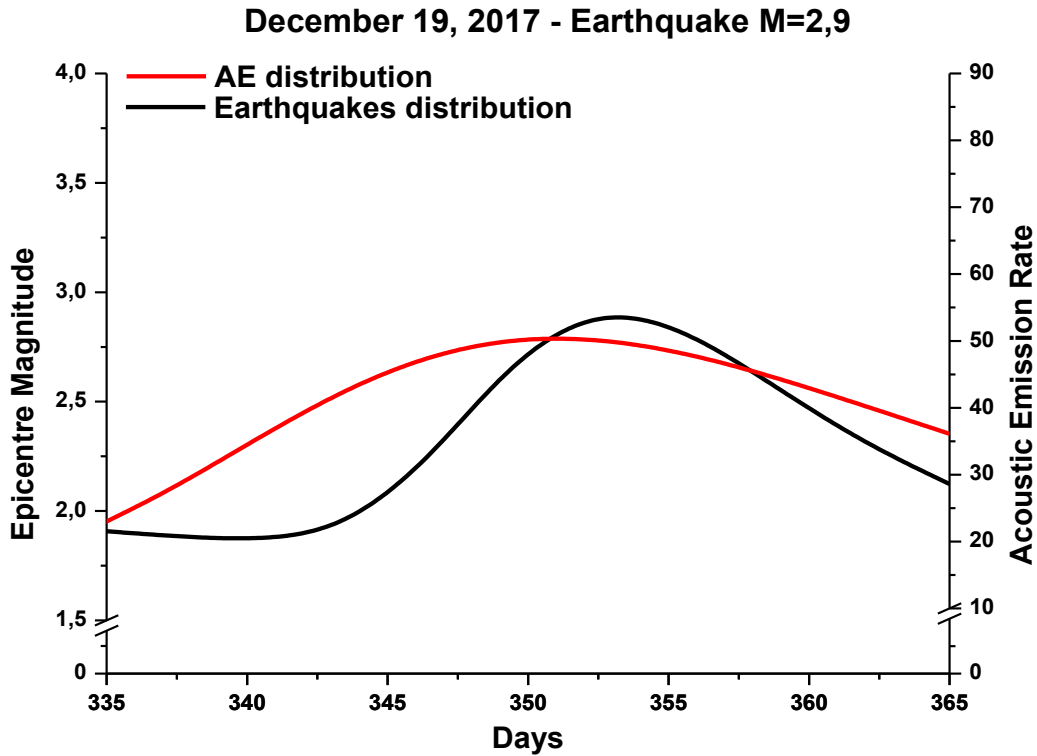


fig. 3.8: Statistical distribution of AE events related to December 19, 2017 earthquake

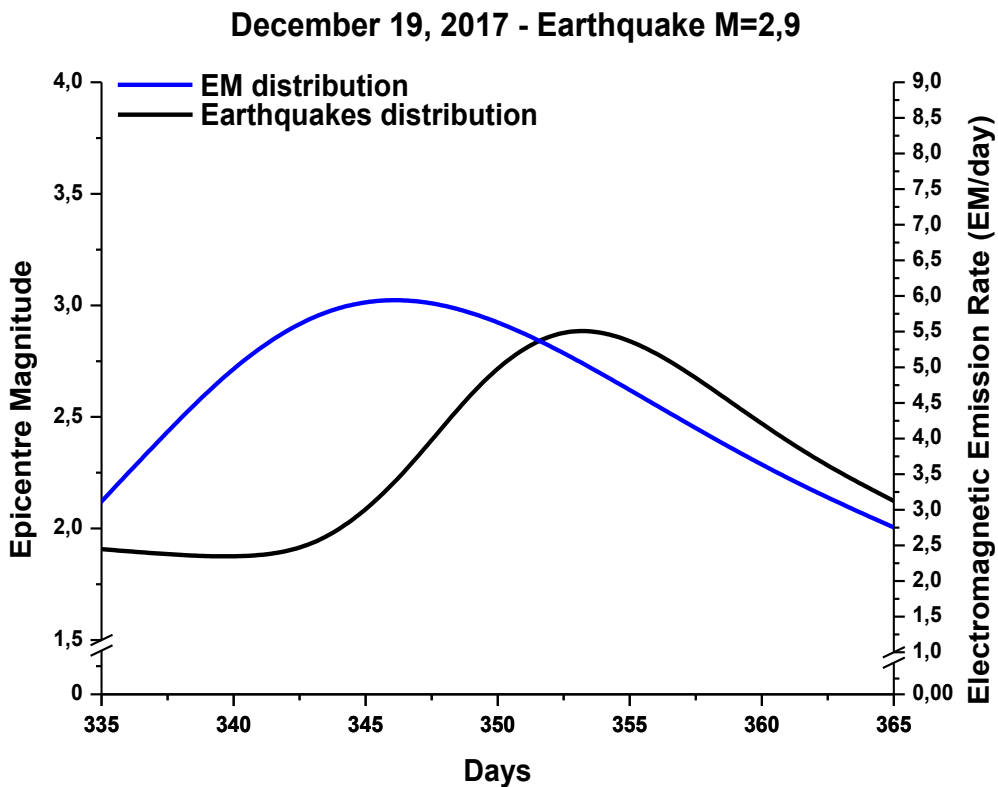


fig. 3.9: Statistical distribution of EME events related to December 19, 2017 earthquake

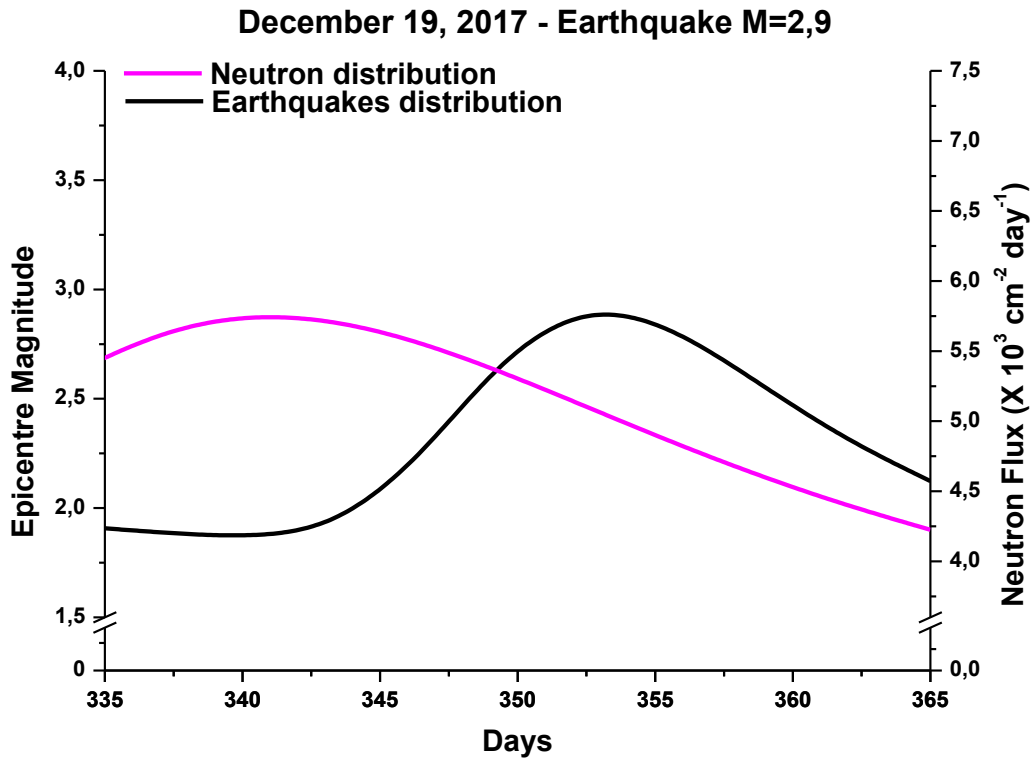


fig. 3.10: Statistical distribution of NE events related to December 19, 2017 earthquake

3.2 The recent analysis of lunar phases (July 2017 - December 2017)

In this paragraph, the possible correlation between seismicity and lunar phases is addressed for the period from July, 1st 2017 to December, 31 2017 regarding the surrounding area of "San Pietro-Prato Nuovo". By comparing the temporal distribution of the same seismic swarms coming from the multi-modal approach of the previous paragraph with the cycle of the Moon, a possible connection seems to exist. As a matter of fact, the first two events happen after 4 days the period of new and full Moon, respectively, the third seismic swarm happens about 8 days before the Full Moon, the last one happens just day before the New Moon. For all events the range of variation is of about 4 ± 2 days as a confirmation of the previous results. Even in this case, the same conventions are adopted: a green line is used to represent the cycle of the Moon, the black dots that lie on the same track of the Moon are the seismic swarms. On x-axis are represented the days of the second semester of the year 2017.

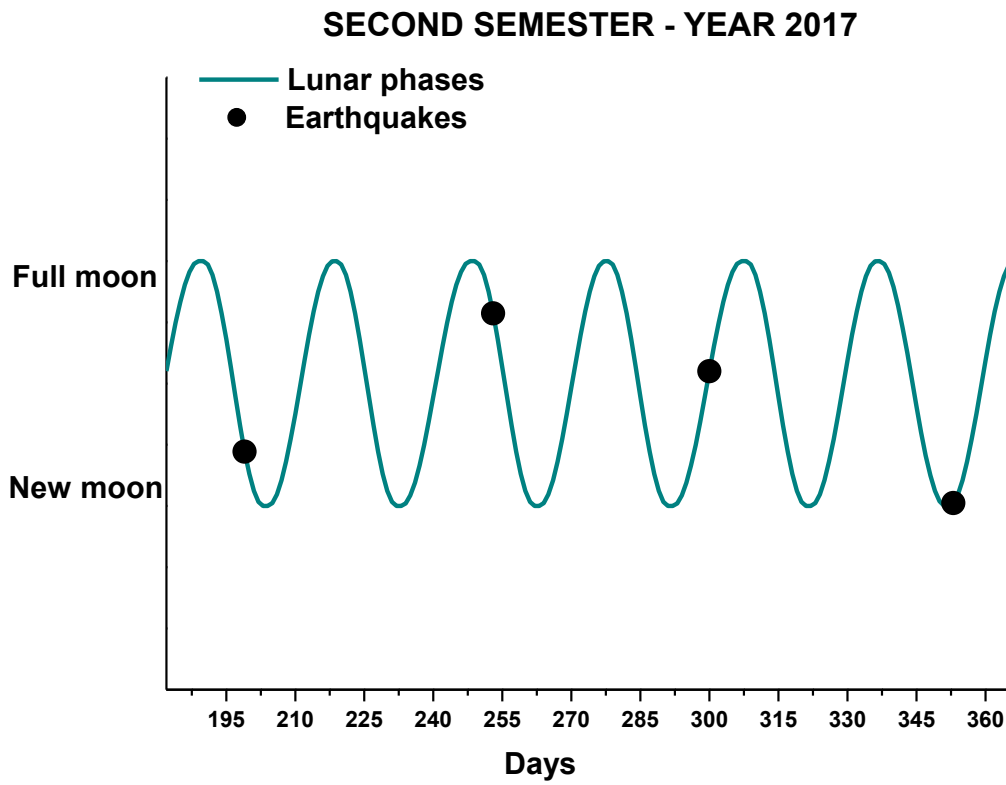


fig. 3.11: Correlation between lunar phases and seismic swarms for the second semester 2017

Chapter 4

***b*-VALUE STATISTICAL SEISMIC PRECURSOR OF LOW-MAGNITUDE EARTHQUAKES**

4.1 *b*-value as statistical seismic precursor

Complex phenomena often exhibit power law (fractal) scaling (Mandelbrot, 1967, 1992; Turcotte, 1997). It has been seen that earthquakes seem to comply some fractal criteria, such as some other natural phenomena (De Rubeis et al., 1993; 1997; Smalley et al., 1987; Turcotte, 1989; Kagan and Jackson, 1991). A non linear behaviour of earthquakes can be represented by a multifractal phenomenon (Enescu et al., 2005; Geilikman et al., 1990; Goltz, 1998; Godano et al., 1997; Hirabayashi et al., 1992; Peitgen et al., 1992; Wang and Lee, 1996). Aki showed that Gutenberg-Richter law and the formula $N = CA^{-y}$ are equivalent; where N represents the number of earthquakes per unit time with area greater than A in a specified are, C and y are two constants, instead the fractal dimension is $D = 2y$ (Turcotte et al., 2000). Gutenberg-Richter relation means that there is no characteristic fracture size and that size distribution has a self-similar property. Aki also presented another relation:

$$D = \frac{3b}{c} \quad (4.1)$$

between b -value and the fractal dimension D .

C is a constant of the log (moment) versus magnitude relation and equal to 1.5 (Kanamori and Anderson 1975). According to him earthquake moment is proportional to fault length and smaller earthquakes are generated by the segmentation of large earthquakes. The two limit cases of the equation (4.1) are:

1. for $b = \frac{3}{2}$ $D = 3$ that is small defects are uniformly distributed through a volume (critical condition);
2. for $b = 1$ $D = 2$ when energy release takes place on a surface (imminent collapse).

Other studies focus on the relation between b -value and the fractal dimension D_c (Wyss et al. 2004) to understand the seismotectonic activities. According to Scholz 1968 D_c is related to the seismicity and the stress condition of a region. D_c was evaluated with the integral technique (Grassberger and Procaccia 1983):

$$C(r) = \frac{2}{N(N-1)} N(R < r) \quad (4.2)$$

where N is the number of the earthquakes analyzed and $N(R < r)$ is the number of events pairs separated by a distance $R < r$. If the distribution is fractal the same relation can be expressed as:

$$C(r) \sim r^{D_c} \quad (4.3)$$

In this current work the seismicity of "San Pietro-Prato Nuovo" gypsum mine has been analyzed. For this scope, Gutenberg-Richter's law expressed in the previous chapter was used. The FMD (frequency-magnitude distribution) describes the number of earthquakes occurring in a given region as a function of their magnitude M as:

$$\log(N \geq m) = a - bM \quad (4.4)$$

where a and b are two constants and b is the so-called " b -value". The parameter a characterizes the general level of seismicity in a given area during the study period; i.e. if higher is the a value, higher is the seismicity. The parameter b is believed to depend on the stress regime and tectonic character of the region (Allen et al., 1965; Mogi, 1967; Scholz, 1968; Hatzidimitriou et al., 1985; Tsapanos, 1990). Many studies have been suggested to measure b and its confidence limits (Aki, 1965; Utsu, 1965; Bender, 1983; Shi and Bolt, 1982). High and low b -value probably means low and high stressed zone respectively and decreasing of b -value has been found before major earthquakes (Kanamori, 1981). This variation of b -value as a stress indicator has also demonstrated to hold for small magnitudes and microfractures (Mogi 1962).

Some scientists adopted variations of b -value as a seismic precursor for small events (rock bursts) in Zinkgruvan mine (Sweden) and for tectonic (large) earthquakes (Nuannin Paiboon, 2006). They analyzed the frequency variations of earthquakes with a magnitude in the range of 2,4 - 2,6 for a period from 1996 to April 2004. Moreover to compute b -value they adopted sliding time windows which contained 50 events shifted with steps of 5 events. The result was a decreasing of b -value preceding rock bursts of magnitude equal to 1,6. The same approach was used for tectonic earthquakes in Sumatra with a magnitude of about 4,1. Also in this cases, b -values presented a drop preceding earthquakes. They supported the hypothesis that the observed variations in time and space of b -value have a precursory potential which can be applied from micro-earthquakes ($M < 3$) to giant tectonic shocks ($M \cong 9$) and for both independents shocks and aftershocks.

We have different methods to evaluate b -value:

- through the Maximum Likelihood technique;
- as the slope of the linear regression line calculated to starts from such a number of events considered (this method will be used in the next paragraph because it's more stable and less sensitive to M_c variations (Han et al. 2015)).

This law was found for the Californian earthquakes and so with high magnitudes, however our scope is to demonstrate its validity also for low seismic zone such as San Pietro-Nuovo gypsum mine.

4.2 Maximux Likelihood technique (MLE)

This method was proposed for the first time by Aki and Utsu in 1965. The magnitude M was considered a continuous Random Variable (RV) and the probability density function of M is:

$$f(M) = b \ln(10) \frac{10^{-bM}}{10^{-bM_{\min}} - 10^{-bM_{\max}}} \quad (4.5)$$

where M_{\min} and M_{\max} are the minimum and the maximum magnitude allowed, respectively.

If $M_{\max} \gg M_{\min}$ the equation results to be:

$$f(M) = b \ln(10) 10^{-b(M-M_{\min})} \quad (4.6)$$

The Maximum Likelihood technique consists of choosing the b -value which maximises the likelihood function (Fisher, 1950) that is:

$$\hat{b} = \frac{1}{\ln(10)(\hat{\mu} - M_{\text{thresh}})} \quad (4.7)$$

where $\hat{\mu}$ is the sampling average of magnitudes; M_{thresh} is the magnitude of completeness. the symbol '^' distinguishes the estimate value from the true value. The uncertainty of \hat{b}^* was estimated for the first time by (Aki, 1965)

$$\hat{\sigma}_b = \frac{\hat{b}}{\sqrt{N}} \quad (4.8)$$

where N is the number of earthquakes.

Shi and Bolt (1982) provided a new formula to estimate the error of b -value:

$$\hat{\sigma}_b = 2.30 \hat{b}^2 \sqrt{\frac{\sum_{i=1}^n (M_i - \mu)^2}{N(N-1)}} \quad (4.9)$$

4.3 Ordinary Least Squares

In statistic, Ordinary Least Squares is a statistical method which minimizes the sum of the squares of the residual of the differences between the observed and the predicted values in a dataset. This technique is used to evaluate the parameters a and b of the frequency-magnitude distribution. The sum of the residual as like as the medium is equal to zero as it's expressed in the following relation as:

$$S = \sum_{i=1}^n r_i^2 = \sum_{i=1}^n (y_i - \hat{y}_i)^2 \quad (4.10)$$

where n is the number of events, y_i is the actual value and \hat{y}_i is the expected value.

The aim is to minimize the sum of the areas of the squares created by the coordinates of the actual and the expected value. From the Ordinary Least Squares we can derive the regression line optimizing the linear intercept and the slope which is the b -value.

The regression line has this equation:

$$\hat{y} = bx + a \quad (4.11)$$

$$\text{where the slope } b = \frac{\sum_{i=1}^n (x_i - \bar{x})(y_i - \bar{y})}{\sum_{i=1}^n (x_i - \bar{x})^2} \quad (4.12)$$

$$\text{and the intercept } a = \hat{y} - bx \quad (4.13)$$

4.4 Magnitude of completeness (M_c)

For a lot of Italian earthquakes, ISide reports the local magnitude (ML), that should be corrected when the instrument is less or bigger 100 km far from the hypocenter. Seismologists don't have a correction for Italian territory and so they use the American correction developed by Hutton and Boore (1987). This formula is reliable when instruments are bigger 100 km far from the hypocenter, instead it tends to overestimate in the opposite case.

According to the studies of Schorlemmer et al. 2010 M_c in Italy is 2,4 until the '90, 2,2/2,3 until the 2005 and equal to 1,6 after the 16th of April 2008. Spatial variability of M_c presents a value of 1,5 for the central-south Appennino and a value of about 1,9 for Sicily. The magnitude of completeness is an important parameter for many studies related to seismicity: it is defined as the lowest magnitude of the catalogue at which all the events are reliably detected (Rydelek and Sacks, 1989). We can derive M_c from parametric or non-parametric techniques. Parametric techniques consists on fitting FMD, instead the non-parametric ones are based on the evaluation of changes of FMD. Below are presented some of these methods:

1. the maximum curvature (MAXC) method (Wiemer and Wyss, 2000) in which the completeness magnitude is defined as the point where the first derivative of the frequency magnitude curve assumes its maximum of the non-cumulative frequency-magnitude distribution;
2. the goodness of fit (GFT) method (Wiemer and Wyss, 2000) consists in evaluating M_c by comparing the observed FMD with synthetic ones. The goodness of fit is evaluated by the parameter R, which is the absolute difference between the observed and synthetic G-R distribution. Synthetic distributions are calculated using the same a and b and M_i previously evaluated in G-R as a function of the minimum magnitude $M \geq M_i$, which represents a perfect fit to a power law. M_c is evaluated as the cut-off line at which the 90% of the observed data is modelled by a straight line;

3. the entire magnitude (EMR) firstly developed by Ogata and Katsura (1995) and then modified by Woessner and Wiemer (2005). This method includes the complete and the incomplete part of FMD. The first is represented by a power law distribution which adopts a and b parameters and the second one by a normal distribution with μ and σ which are respectively the average and the standard deviation of the normal distribution.

A small error on this parameter could lead to highly significant errors on b -value. Therefore, four periods have been considered in order to evaluate the most accurate value for this parameter. The magnitudes of the earthquakes of the surrounding area of Murisengo were necessary in this regard. They were downloaded by the Italian site of seismology called "ISIde" choosing a radius of about 100 km from Murisengo. The four periods considered for the analysis are:

1. From 1985 to 31th December of 2017 (fig. 4.1)
2. From 2000 to 31th December of 2017 (fig. 4.2)
3. From 2007 to 31th December of 2017 (fig. 4.3)
4. From 2013 to 31th December of 2017 (fig. 4.4)

If we try to search the oldest event that took place in the considered area we find that the first earthquakes date back to the 1985. In fact, when M_c was calculated, it was found a similar value for the last three periods and equal to $1.3 \pm 0,1$ and a different value for the first period and equal to $1.6 \pm 0,1$. A different value (increased) was found probably due to the fact that from that date only considerable earthquakes were registered or because seismologists adopted little sensible instrument for their records in the first periods.

M_c changes, as can be seen, in time but also in space. Space variations are due to the obvious fact that some seismic stations are excluded from the calculus since the moment that a radius of inspection of about 100 km was chosen for the examination. M_c values were calculated from the non cumulative frequency-magnitude distribution, dividing the scale of magnitudes in classes with step of 0,1 until the maximum magnitude ever recorded in the area (4,8). Then by putting each earthquake in the correspondent class, summing the number of events with the same magnitude of each class and transforming them in base-10 logarithm, M_c was obtained. We could achieve the same result by using the software ZMAP of Wymer 2001. This means that the values with a magnitude lesser than M_c , will be neglected for the next calculation of b -values. By plotting b -value for the region, the same value of M_c for each period has been found as a confirmation of the previous calculation. Starting now from the cumulative FMD, b -value was derived as the slope of the regression line made on a number of events with a magnitude bigger or equal to a fixed magnitude M (even in this case, the same vector uniformly spaced for the calculation of M_c was considered) (fig. 4.5). M_c can be find, also in this case to the intersection between the constant line of the cumulative FMD (transformed in the logarithm to the base of 10) and the regression line; in other words M_c corresponds to the curve's knee of the diagram (fig. 4.5). Also in these cases the reliability of M_c is confirmed by

obtaining more or less the same values for the three previous considered periods (2000-2014; 2007-2014; 2013-2014). Therefore for the next calculation of b -value as a statistical seismic precursor the threshold of magnitude of M_c between 1.3 and 1.4 will be adopted.

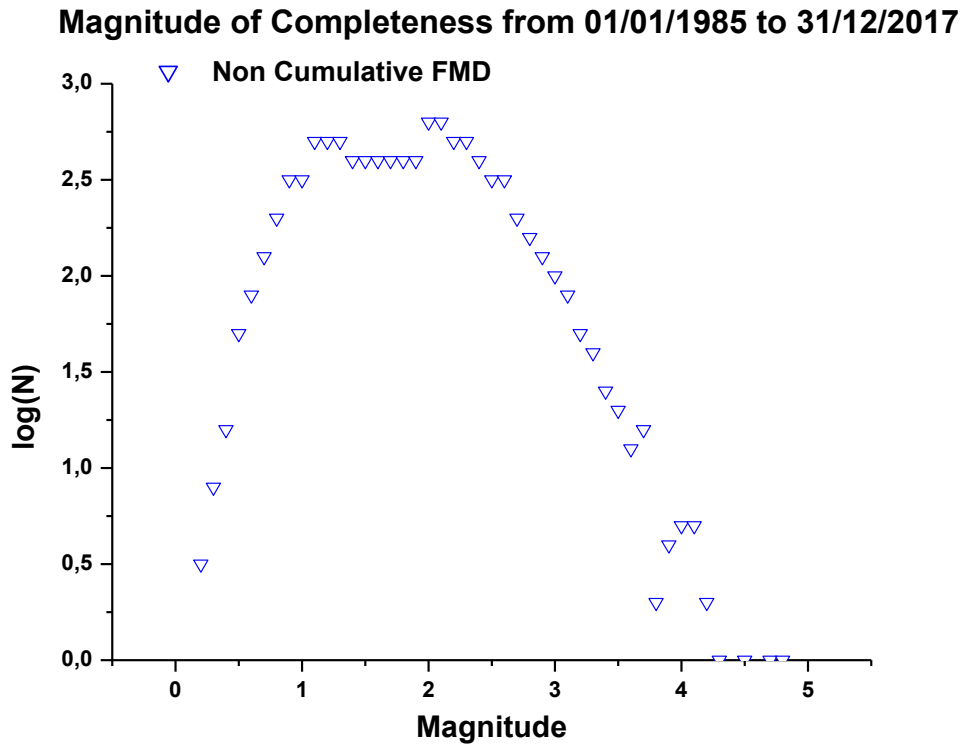


fig. 4.1: M_c for the period from January 1, 1985 to December 31, 2017

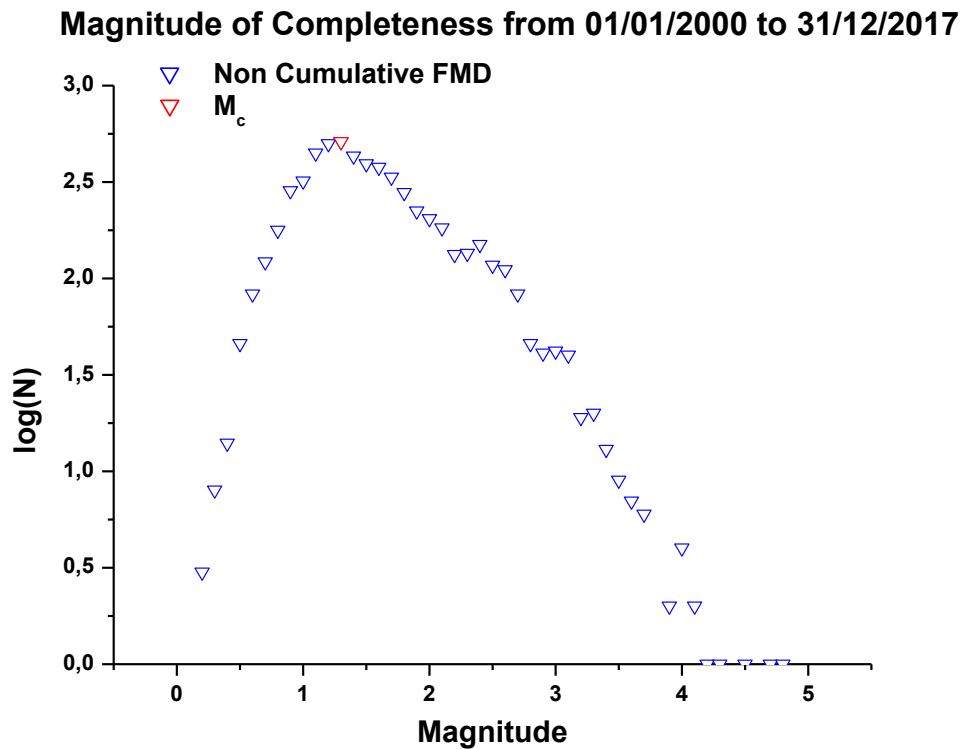


fig. 4.2: M_c for the period from January 1, 2000 to December 31, 2017

Magnitude of Completeness from 01/01/2007 to 31/12/2017

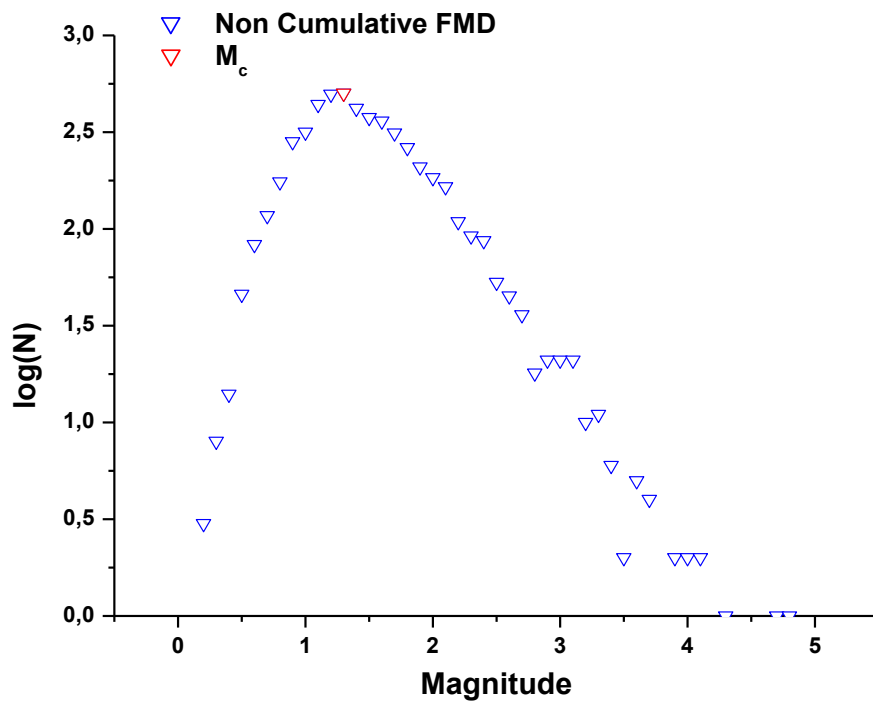


fig. 4.3: M_c for the period from January 1, 2007 to December 31, 2017

Magnitude of Completeness from 01/01/2013 to 31/12/2017

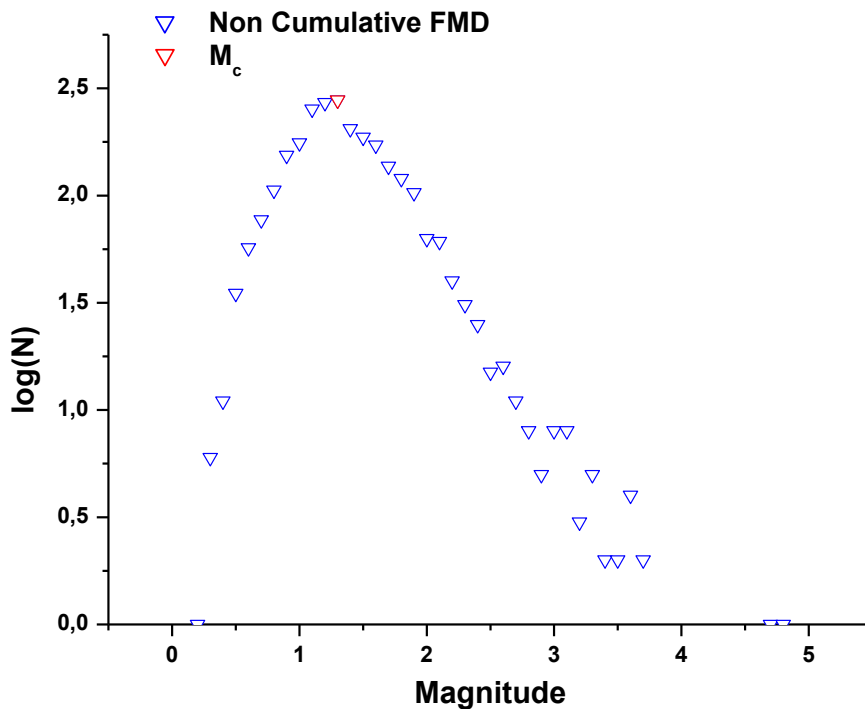


fig. 4.4: M_c for the period from January 1, 2013 to December 31, 2017

Least square regression: 2007-2017

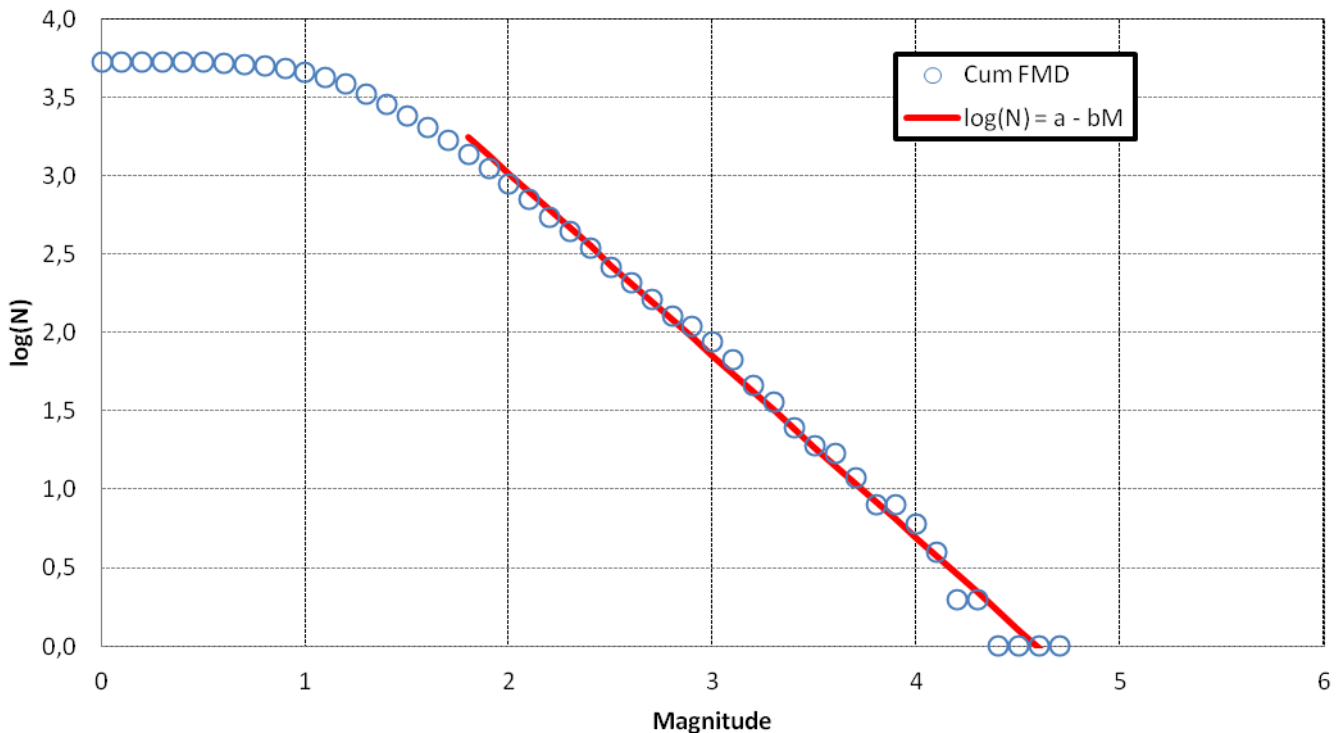


fig. 4.5: Cumulative FMD and Least square regression for the period from 2007-2017. The equation of the regression line is $\log(N) = a - bM$ where $a = 5,34$ and $b = 1,16$. The intersection between the horizontal line $\log(N) = 3,7$ and the regression line is equal more or less to 1,3 that is the Magnitude of Completeness.

4.5 *b*-value analysis for the seismic swarms at the "San Pietro-Prato Nuovo" gypsum mine (July 2013 - December 2017)

52 seismic swarms with a magnitude greater than 1,8 were analyzed in the period from July 1st, 2013 to December 31, 2017 for the surrounding area of Murisengo in order to calculate the changing in time of *b*-value, which is a statistical seismic precursor coming from frequency-magnitude Richter law (§ 4.2). After fixing the Magnitude of Completeness (with the methods described in § 4.4 and equal to $1,3 \pm 0,1$ as we can see from figs. 4.2-4.4), only earthquakes with a magnitude greater than M_c were considered. Previous analysis demonstrated the validity of the statistical precursor for earthquakes of high magnitude in high-seismicity regions; in this chapter we are going to check its precursory function also for low-magnitude earthquakes. To deal with a new unknown problem, first of all, it was tried to adapt Richter's law to the more significant seismic swarm that took place in the area. After having overlooked earthquakes with magnitudes lesser than M_c , different temporal windows were tested and among these the best window was chosen whose temporal variation of *b*-value better follows the trend of earthquakes. At the end, a temporal window of about 15 days was selected, defined considering the seismicity of the

monitored area. b -value is calculated as the slope of the regression line made on the temporal window of the cumulative-frequency distribution using the Least Square Method. A different method was used too at the same scope, using floating windows on a number of about 15 events (rather than having number of days) to make stronger the seismic tool used for the changing in time of b -value. As it turns out, the different methods led to the same results. In the next pages, only the first method has been taken into account since it makes a better idea about the definition of b -value as a statistical seismic precursor. Curves were also tested for different values of M_c (which is the beginner value from which we started the calculation) and can be observed that they are shifted upwards. According to this fact, when M_c increases are more numerous the events with an higher magnitude and so also b -value increases too and vice versa. Since some values of the cumulative frequency distribution were the same around the 2,3-2,4 magnitude giving a not exact interpolation of them and so a non reliable value of the statistical precursor, it was tried to reduce the number of points to the minimum (imposed equal to 4) changing the scale of magnitude.

As we can see in the following diagrams, there are some curves which perfectly fit the trend of seismic swarms: b -value which is in general comprised in the range 1,5 to 1, decreases in correspondence of the main seismic events or some days before reaching the value of 0,5, on the contrary, it increases reaching the value of 1,5 in correspondence of earthquakes of very small magnitude. Higher values for this parameter have been correlated with the occurrence of earthquakes with small magnitude spread over a wide geographical area, lower values are related to a concentration of major earthquakes localized along a fault (Carpinteri et al. 2009a).

As concerns for the period from July 2013 to December 2017 (nine semesters), over a number of 52 seismic swarms 36 verify the correct trend of b -value (about 69% of the cases), in the other 16 cases its precursory function turns lesser than 1 and maintains the same values in the preparation time, for two main reasons:

1. we have a poor statistic, that is a small data of events in the considered period;
2. the seismic ratio (equal to the number of seismic events over the number of days in which they take place) is too high, that is when a big number of events in few days occurs, and so the geographical area is in a sort of permanent critical state.

In the following diagrams the changing in time of b -value is plotted considering a referring time of about one week before the main seismic event. The blue line used to connect the different points corresponds to the changing in time of b -value, an horizontal red line is used to indicate the transition of the statistical precursor from a "stable" to a "critical" state assumed equal to 1, a vertical black line is used to represent the local magnitude of the seismic swarm. Each point represents the slope of the FMD regression line calculated by means temporal windows of 15 days containing seismic events with a magnitude higher or equal to the M_c defined considering the seismicity of the monitored area (figs. 4.6-4.38 and figs. 4.40-4.42).

This means that the incoming earthquake depends on the foreshocks which anticipate it in the preparation time.

A strict correlation between the seismic swarms and the statistical seismic precursor emerged from this analysis. b -value (in the accepted cases) behaves like the acoustic emissions: it can anticipate earthquakes from 1 to about 2 days. Anyway, fracto-emissions are more reliable than the statistical seismic precursor, as they seem to strongly anticipate the incoming earthquakes.

In the last figure, 3 of the 15 cases in which the b -value shows a less evident behavior in terms of statistical seismic precursor (as its value remains constantly around 1) are shown (fig. 4.39).

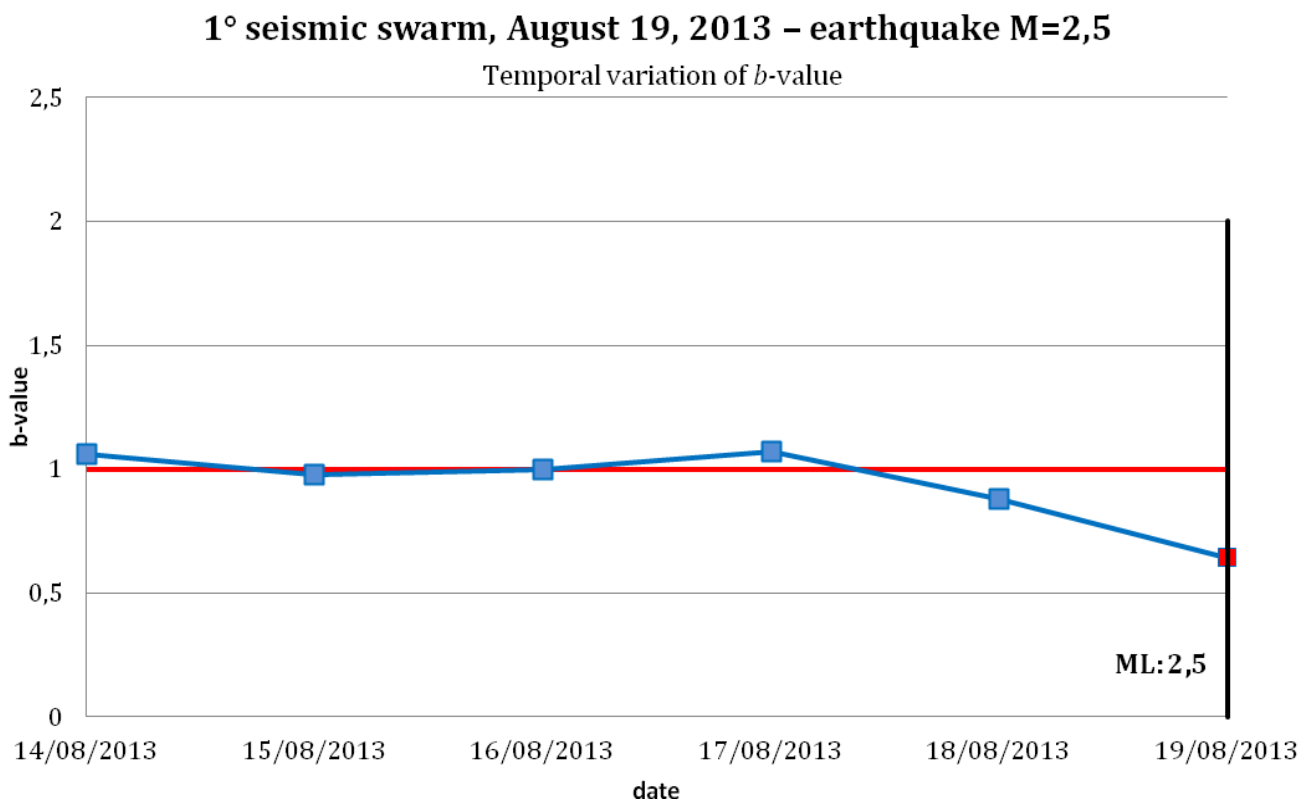


fig. 4.6: Temporal variation of b -value from August 14, 2013 to August 19,2013.

2° seismic swarm, October 15, 2013 – earthquake M=3,4

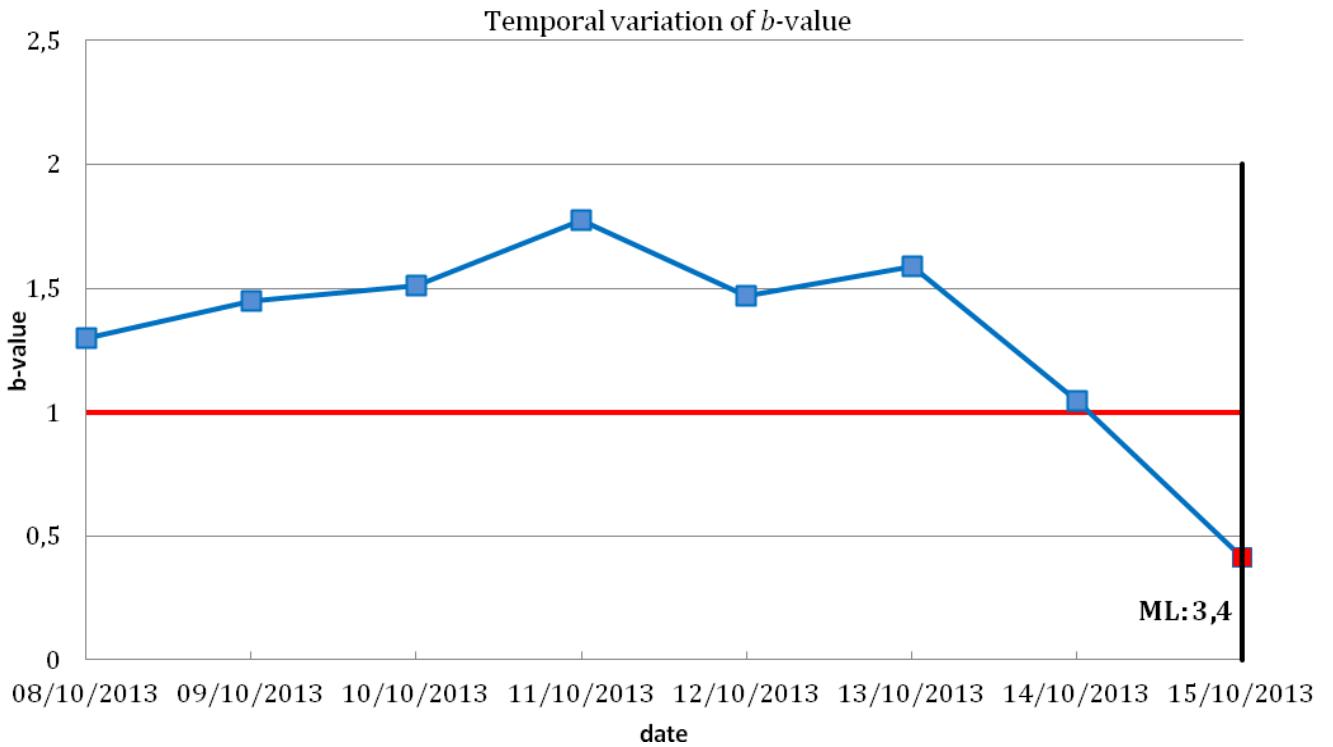


fig. 4.7: Temporal variation of b -value from October 8, 2013 to October 15, 2013.

5° seismic swarm, December 21, 2013 – earthquake M=3

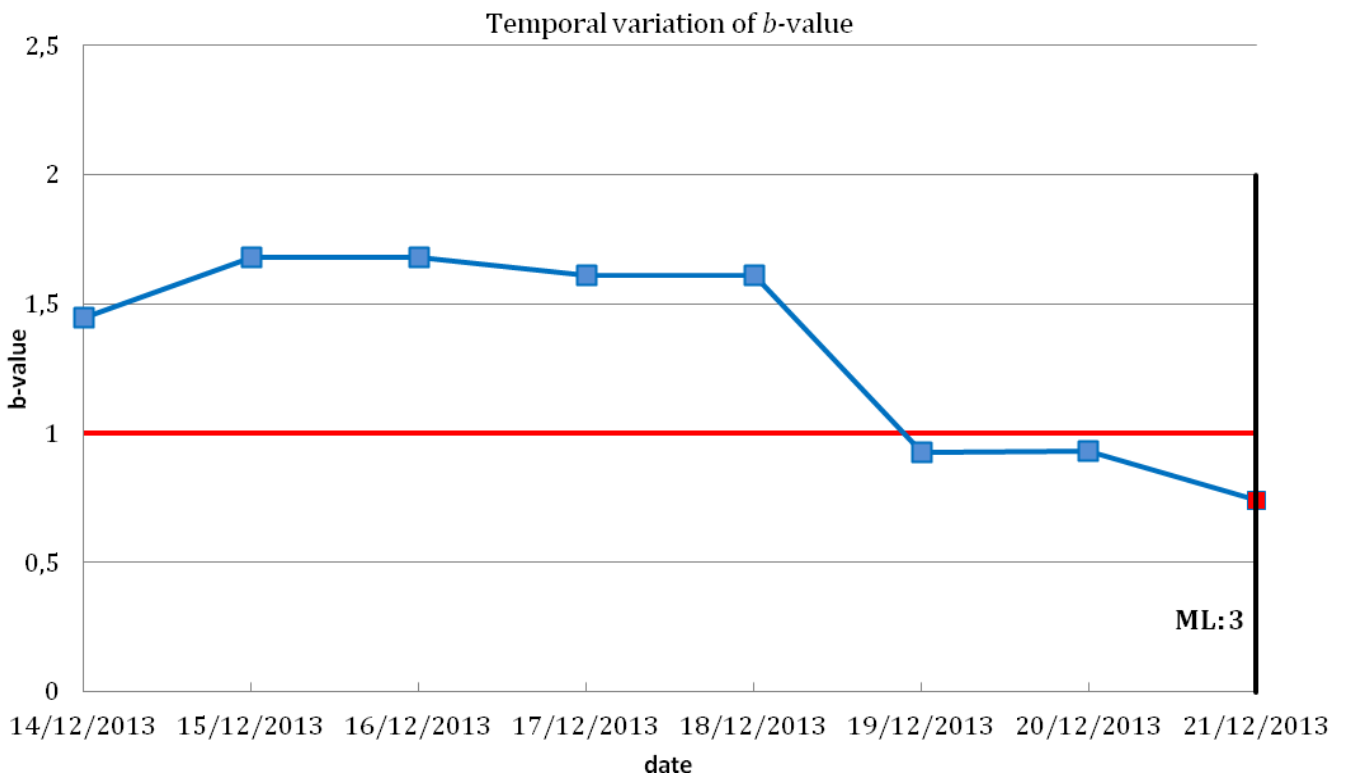


fig. 4.8: Temporal variation of b -value from December 14, 2013 to December 21, 2013.

6° seismic swarm, February 10, 2014 – earthquake M=2,6

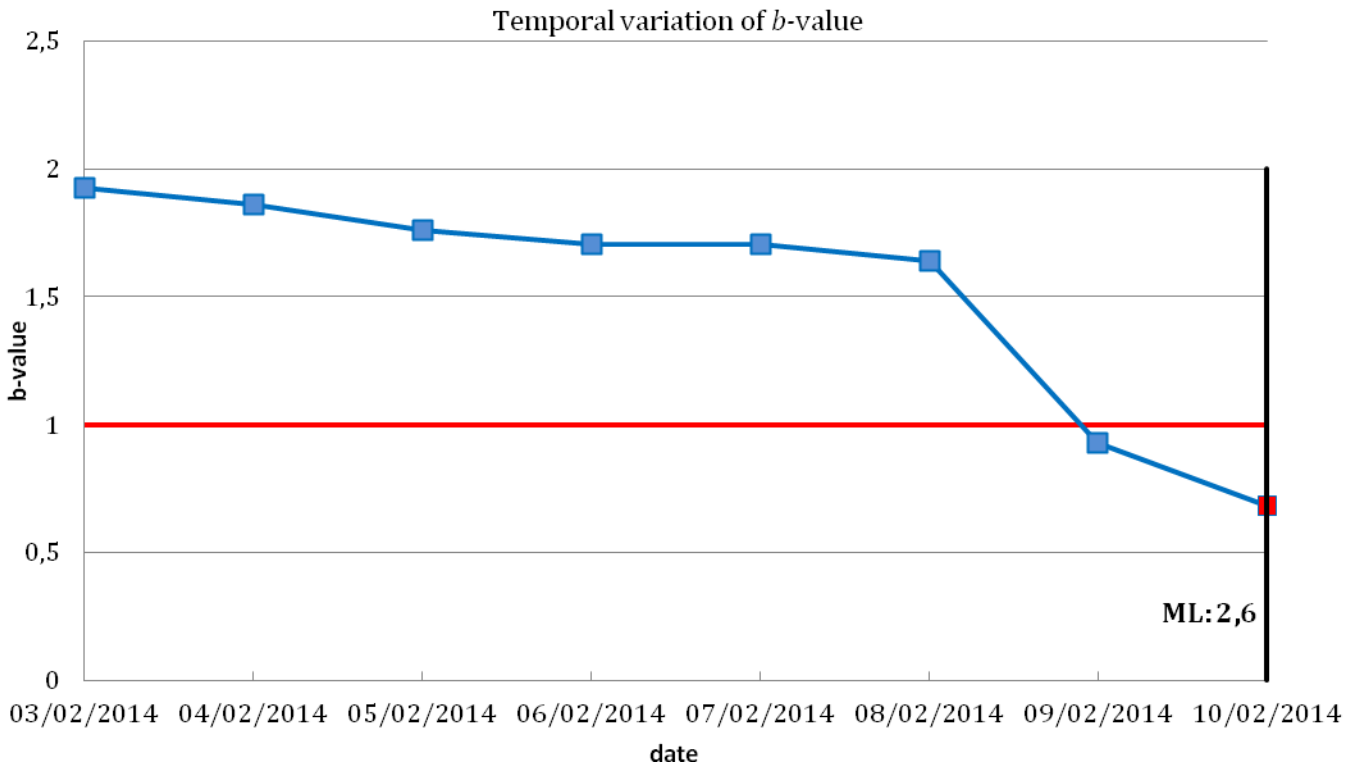


fig. 4.9: Temporal variation of b -value from February 3, 2014 to February 10, 2014.

7° seismic swarm, March 12, 2014 – earthquake M=2,6

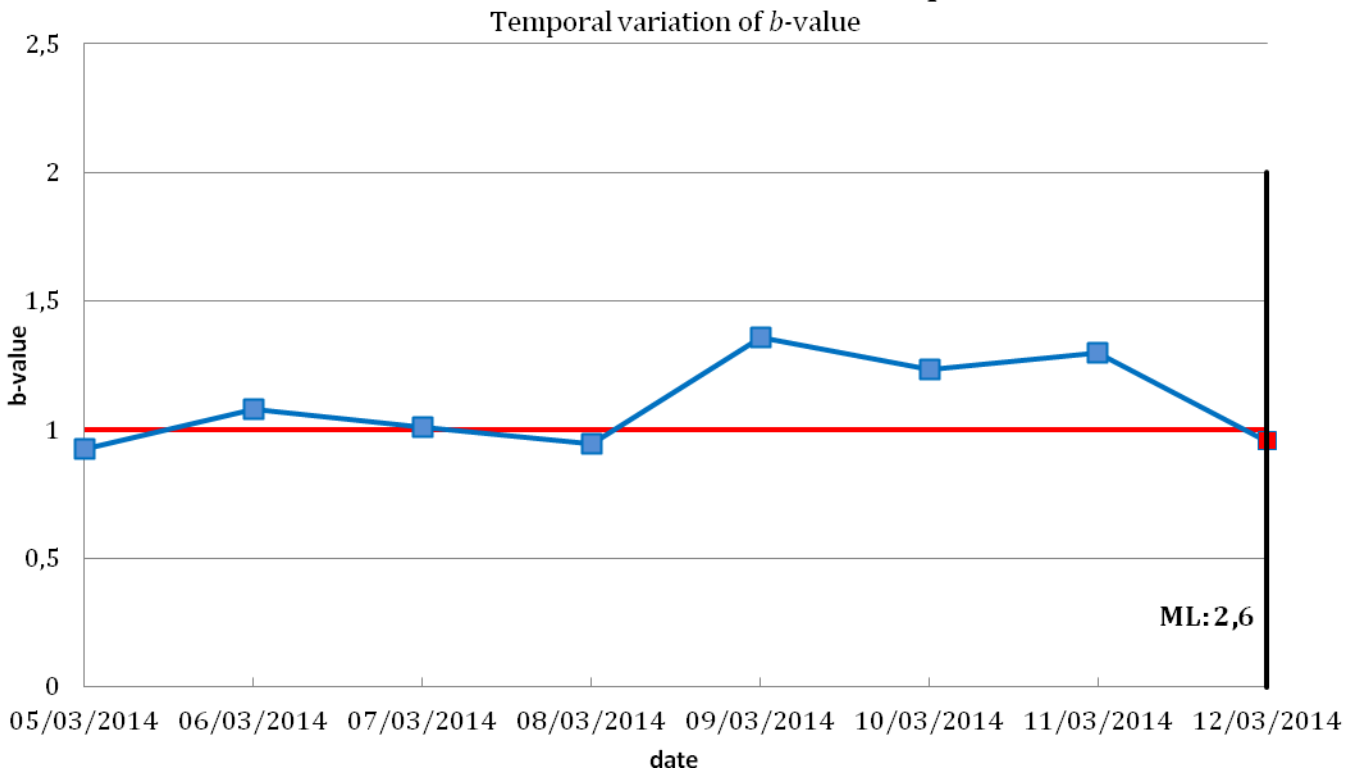


fig. 4.10: Temporal variation of b -value from March 5, 2014 to March 12, 2014.

8° seismic swarm, April 7, 2014 – earthquake M=4,7

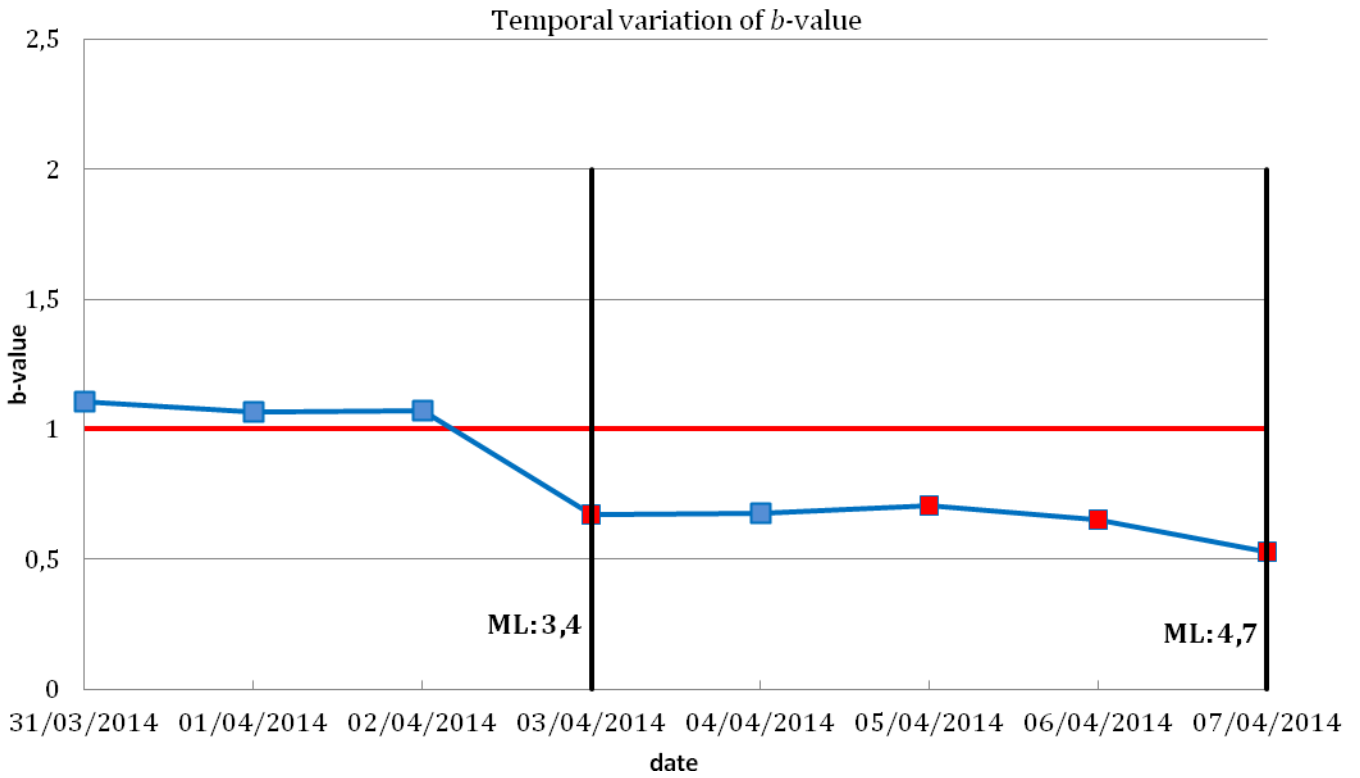


fig. 4.11: Temporal variation of b -value from March 31, 2014 to April 7, 2014.

9° seismic swarm, April 18, 2014 – earthquake M=2,6

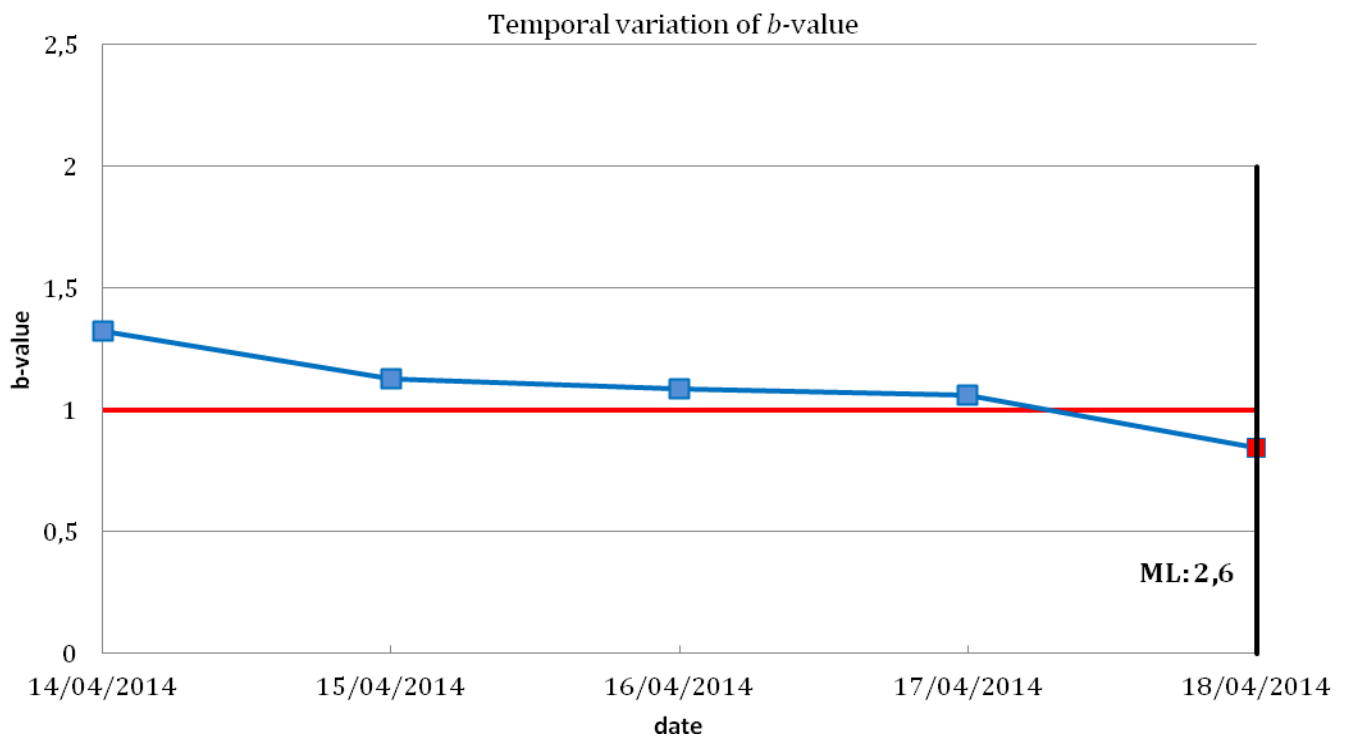


fig. 4.12: Temporal variation of b -value from April 14, 2014 to April 18, 2014.

10° seismic swarm, May 17, 2014 – earthquake M=2,8

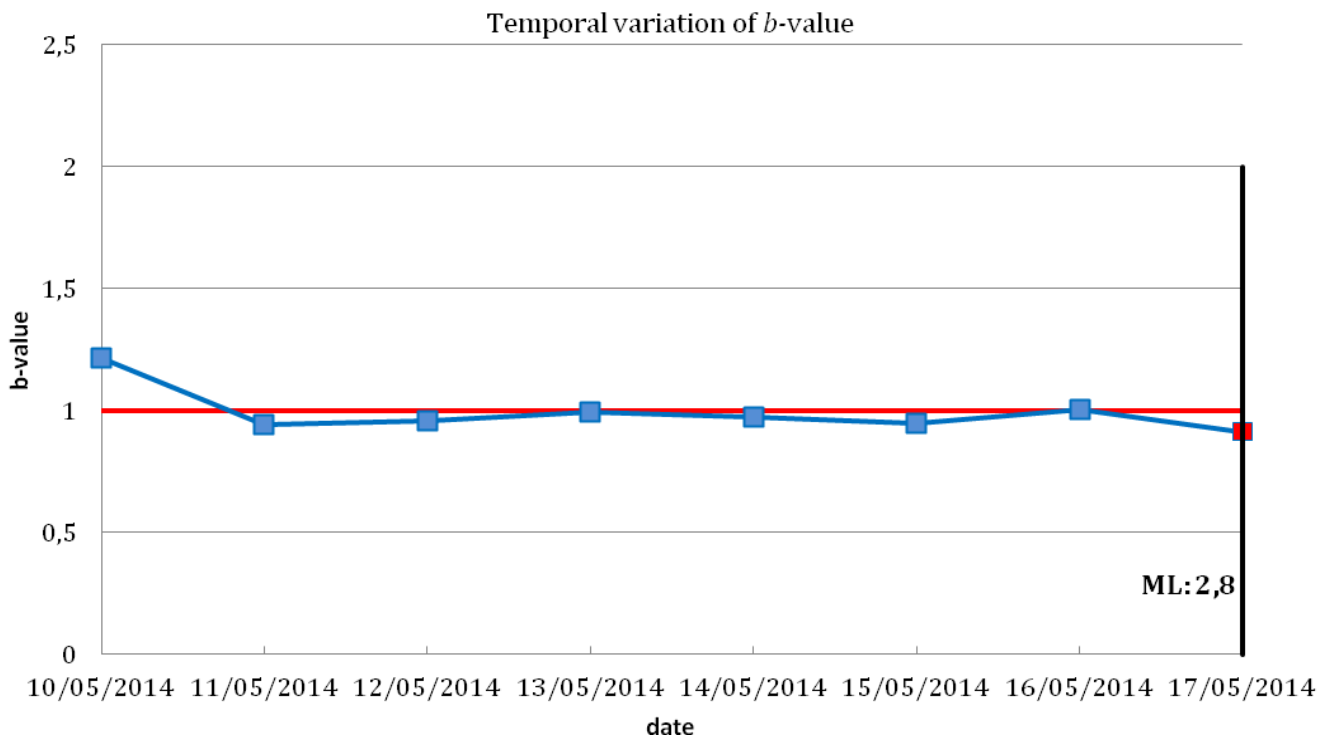


fig. 4.13: Temporal variation of b -value from May 10, 2014 to May 17, 2014.

11° seismic swarm, June 12, 2014 – earthquake M=3,3

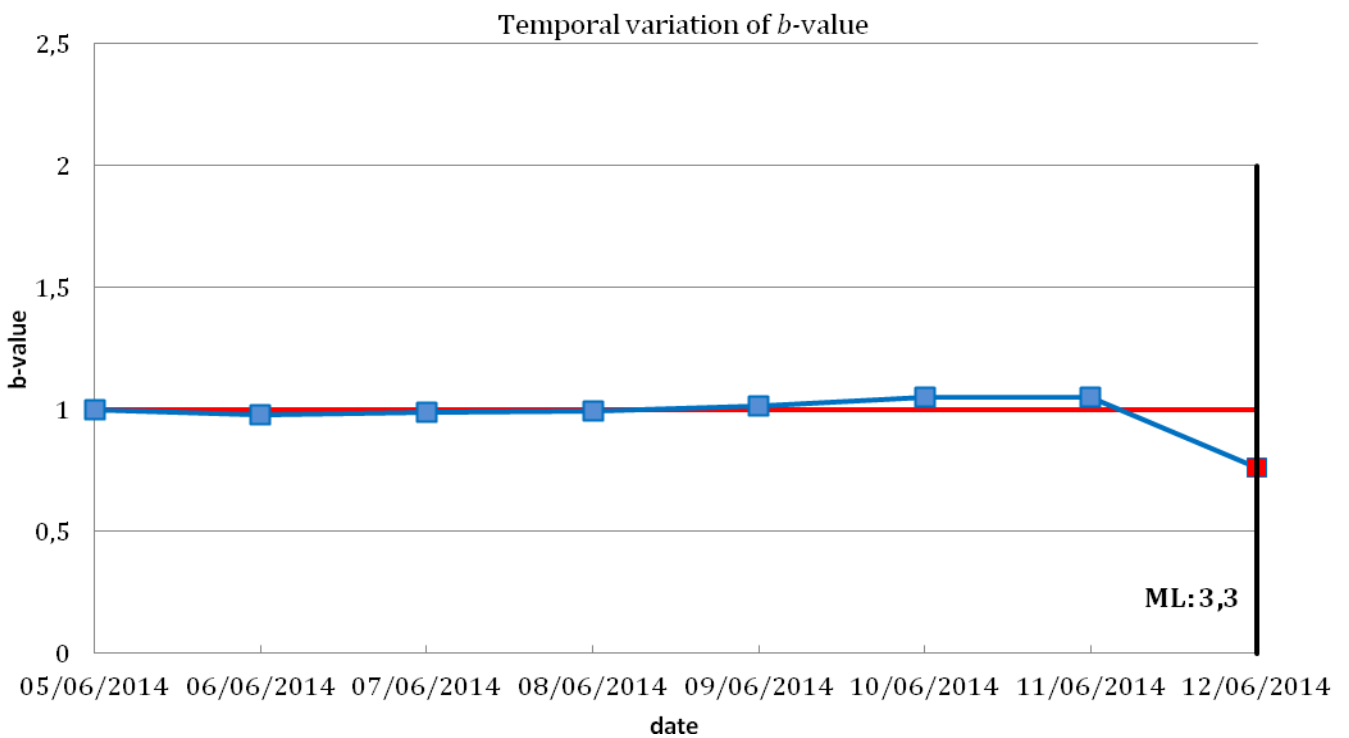


fig. 4.14: Temporal variation of b -value from June 5, 2014 to June 12, 2014.

12° seismic swarm, July 14, 2014 – earthquake M=3,3

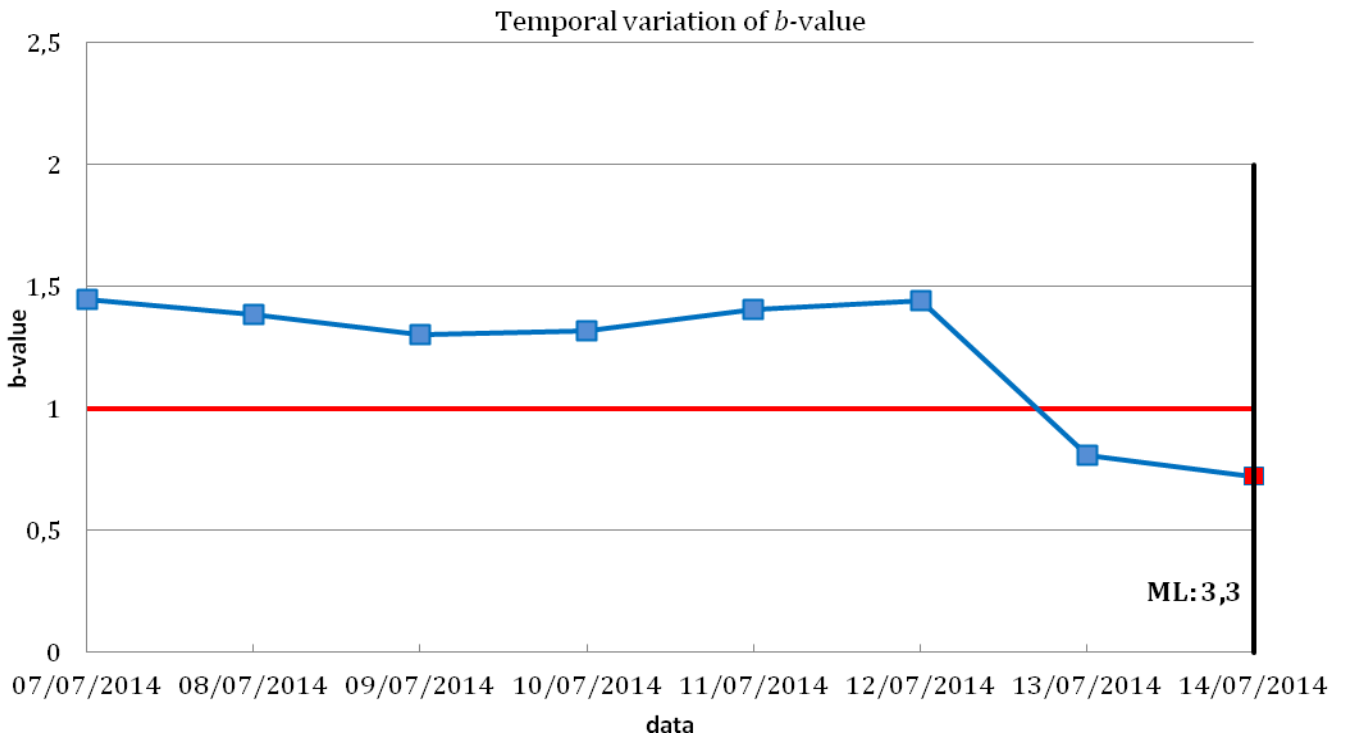


fig. 4.15 : Temporal variation of b -value from July 7, 2014 to July 14, 2014.

13° seismic swarm, August 19, 2014 – earthquake M=2,5

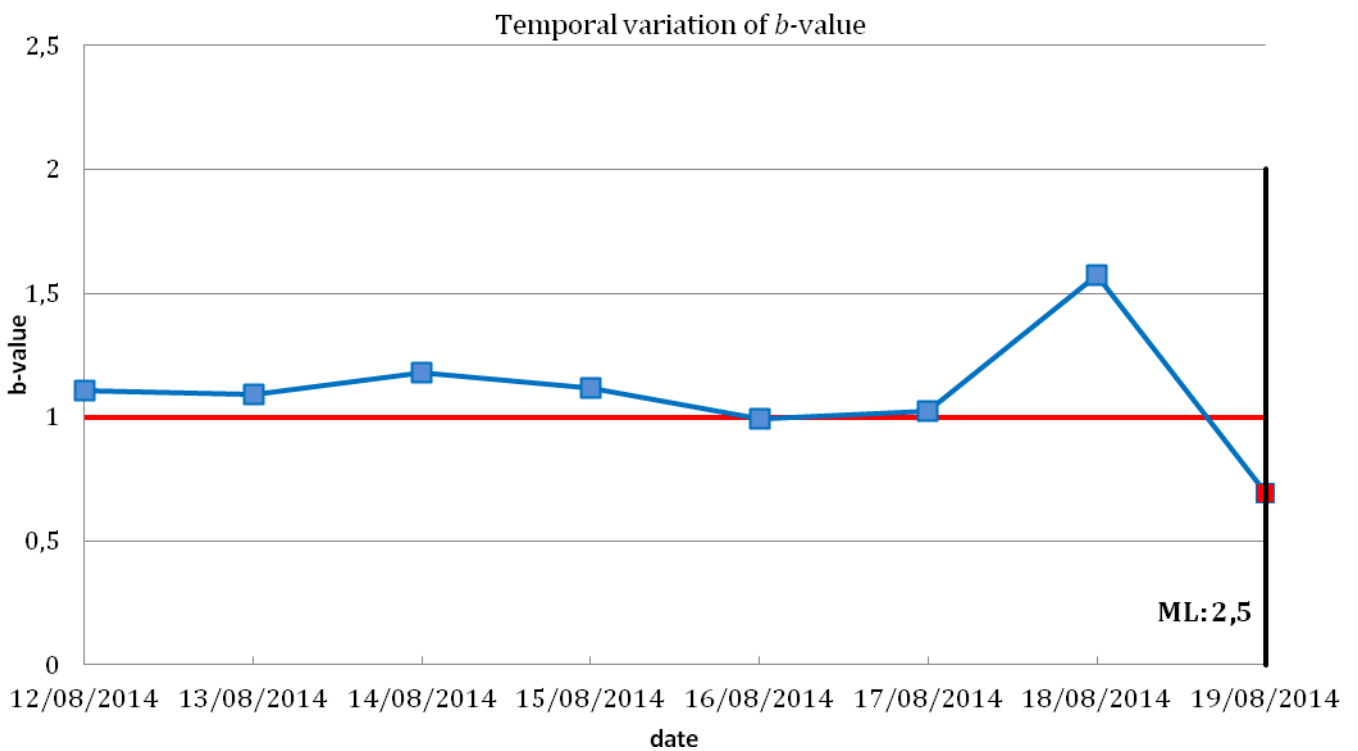


fig. 4.16: Temporal variation of b -value from August 12, 2014 to August 19, 2014.

15° seismic swarm, October 14, 2014 – earthquake M=2,7

Temporal variation of b -value

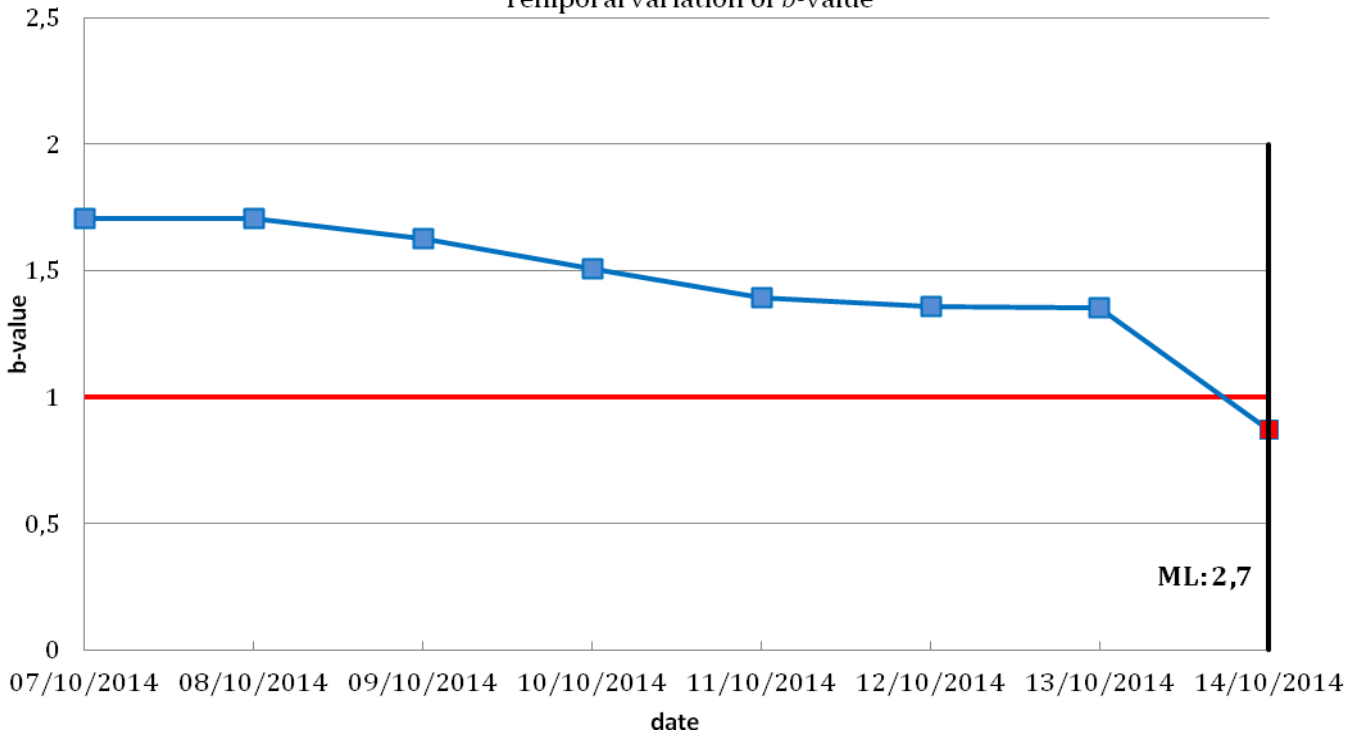


fig. 4.17: Temporal variation of b -value from October 7, 2014 to October 14, 2014.

16° seismic swarm, November 6, 2014 – earthquake M=3

Temporal variation of b -value

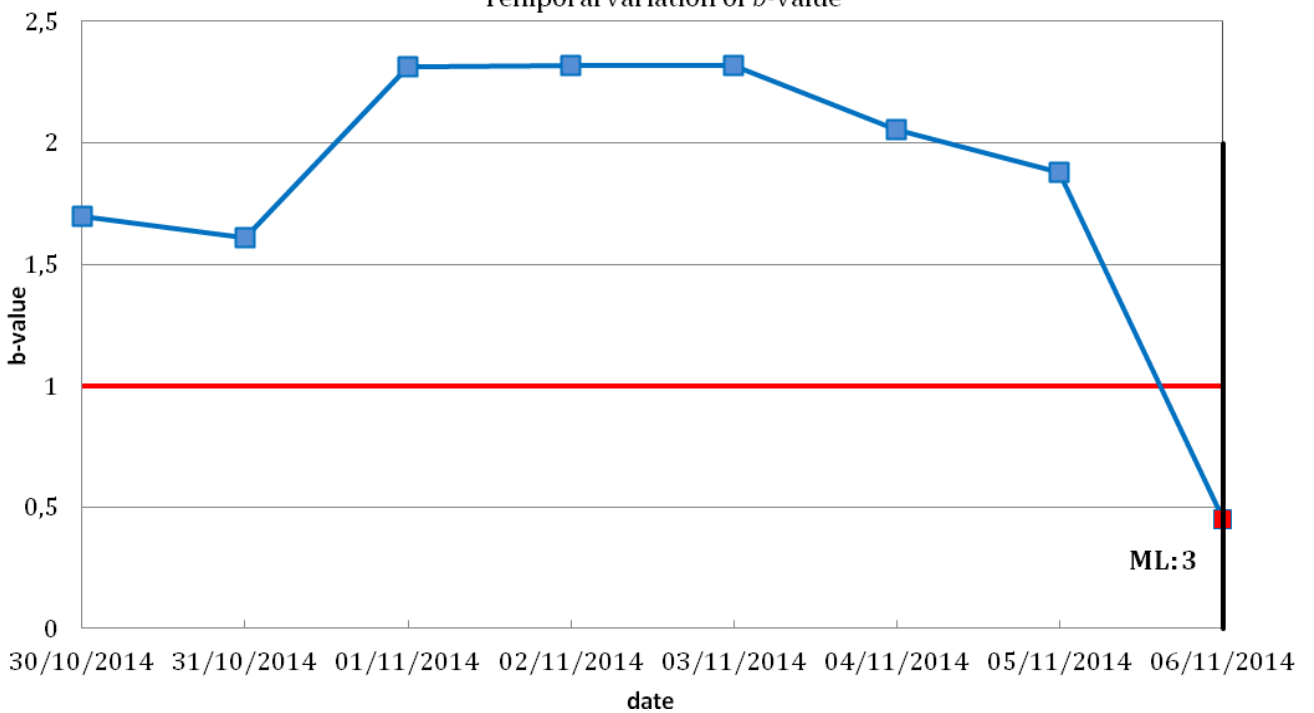


fig. 4.18: Temporal variation of b -value from October 30, 2014 to November 6, 2014.

20° seismic swarm, December 31, 2014 – earthquake M=2,7

Temporal variation of b -value

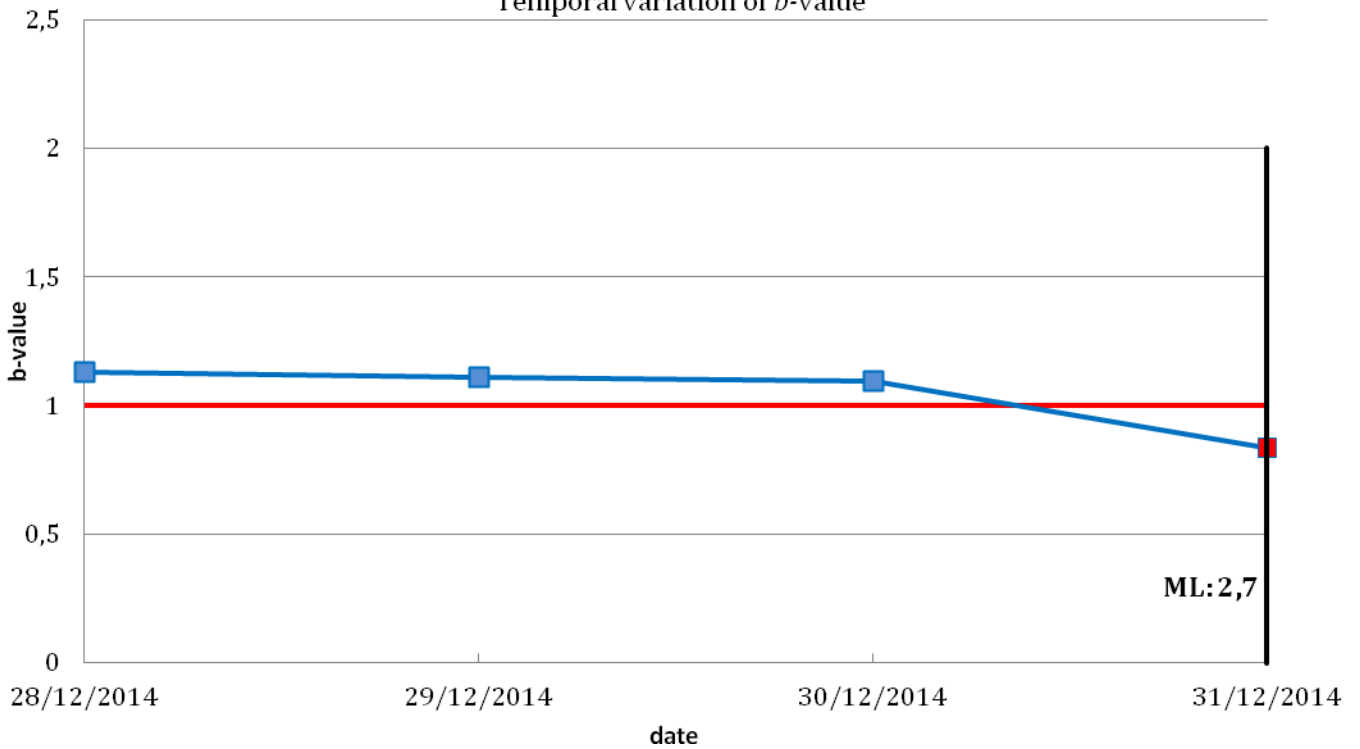


fig. 4.19: Temporal variation of b -value from December 28, 2014 to December 31, 2014.

21° seismic swarm, January 18, 2015 – earthquake M=3,1

Temporal variation of b -value

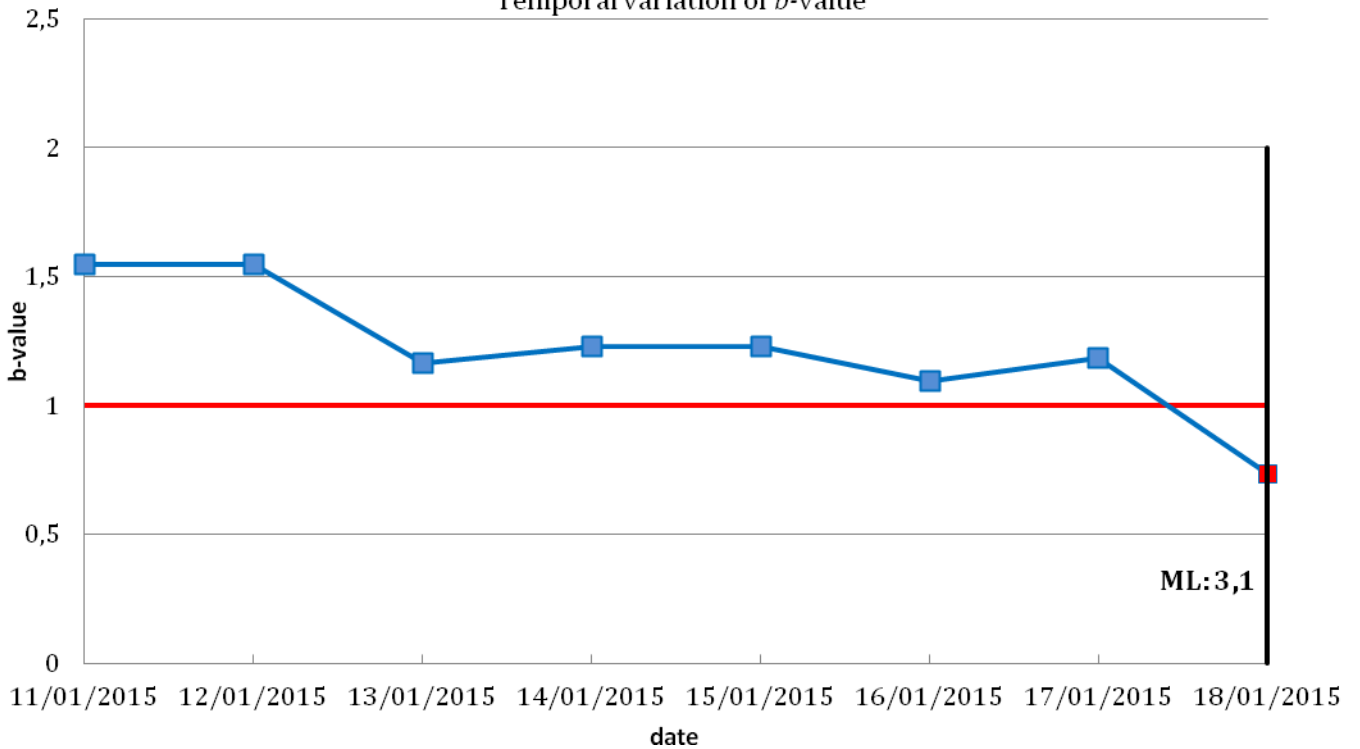


fig. 4.20: Temporal variation of b -value from January 11, 2015 to January 18, 2015.

22° seismic swarm, February 14, 2015 – earthquake M=2,9

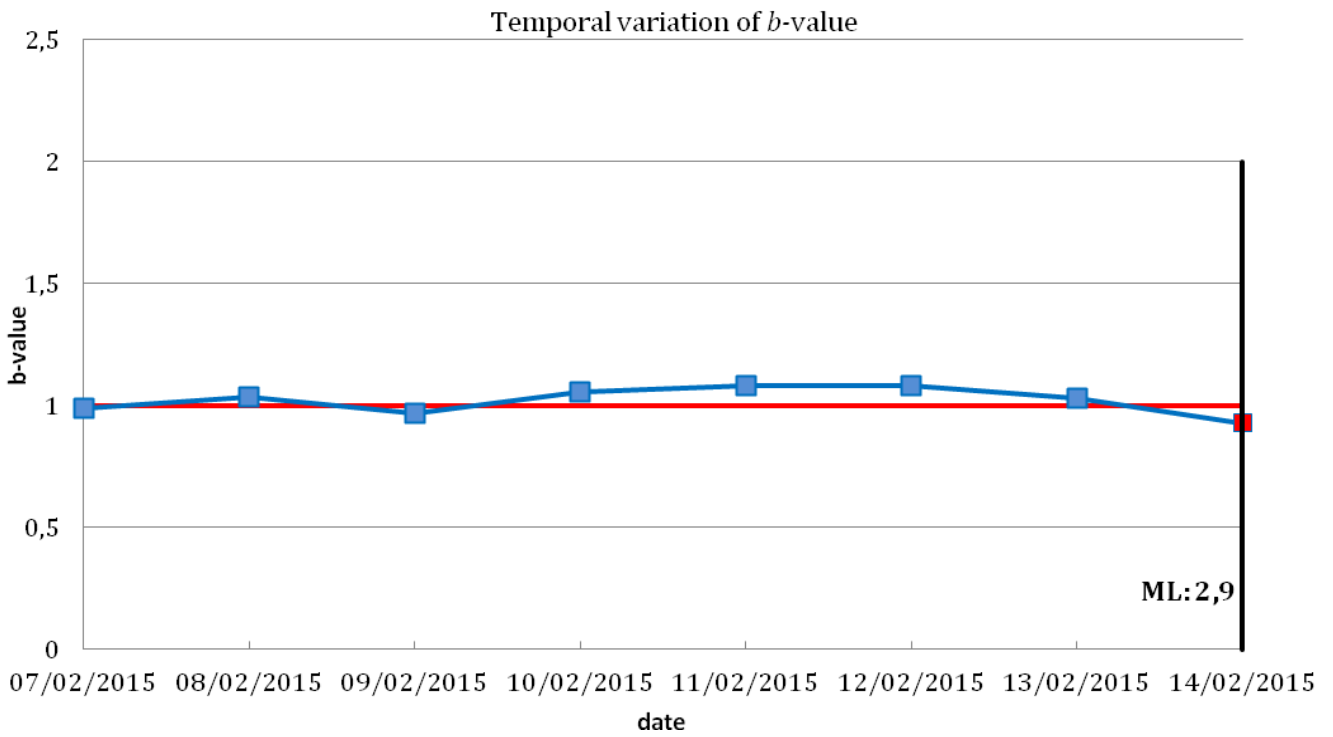


fig. 4.21: Temporal variation of b -value from February 7, 2015 to February 14, 2015.

24° seismic swarm, April 11, 2015 – earthquake M=3,2

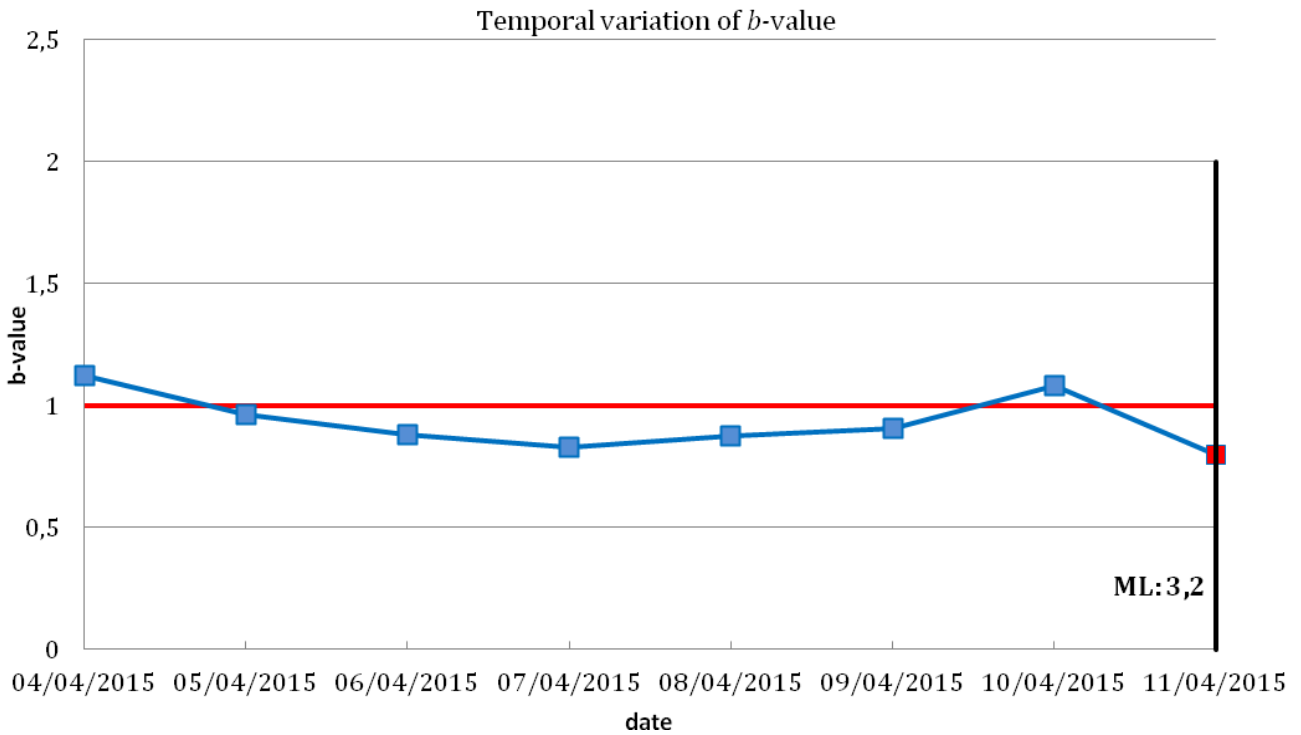


fig. 4.22: Temporal variation of b -value from April 4, 2015 to April 11, 2015.

25° seismic swarm, June 15, 2015 – earthquake M=2,9

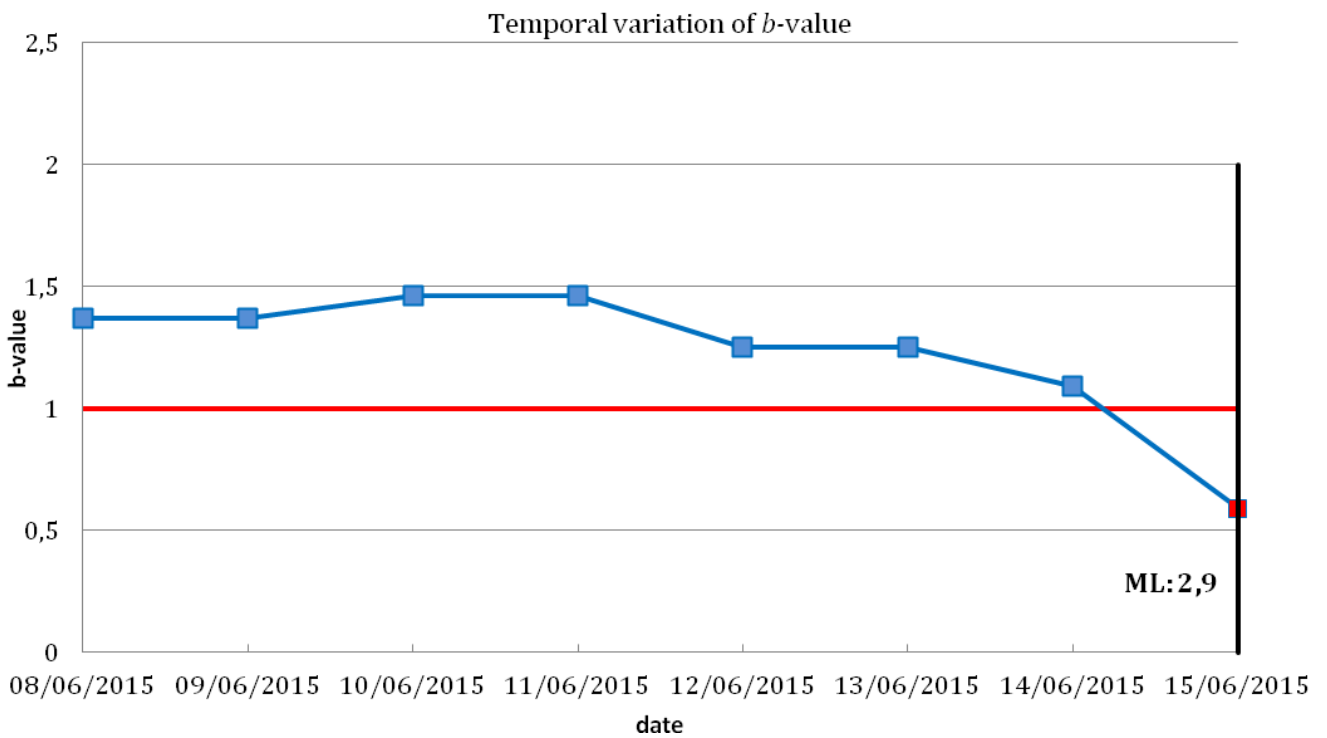


fig. 4.23: Temporal variation of b -value from June 8, 2015 to June 15, 2015.

26° seismic swarm, September 10, 2015 – earthquake M=3,1

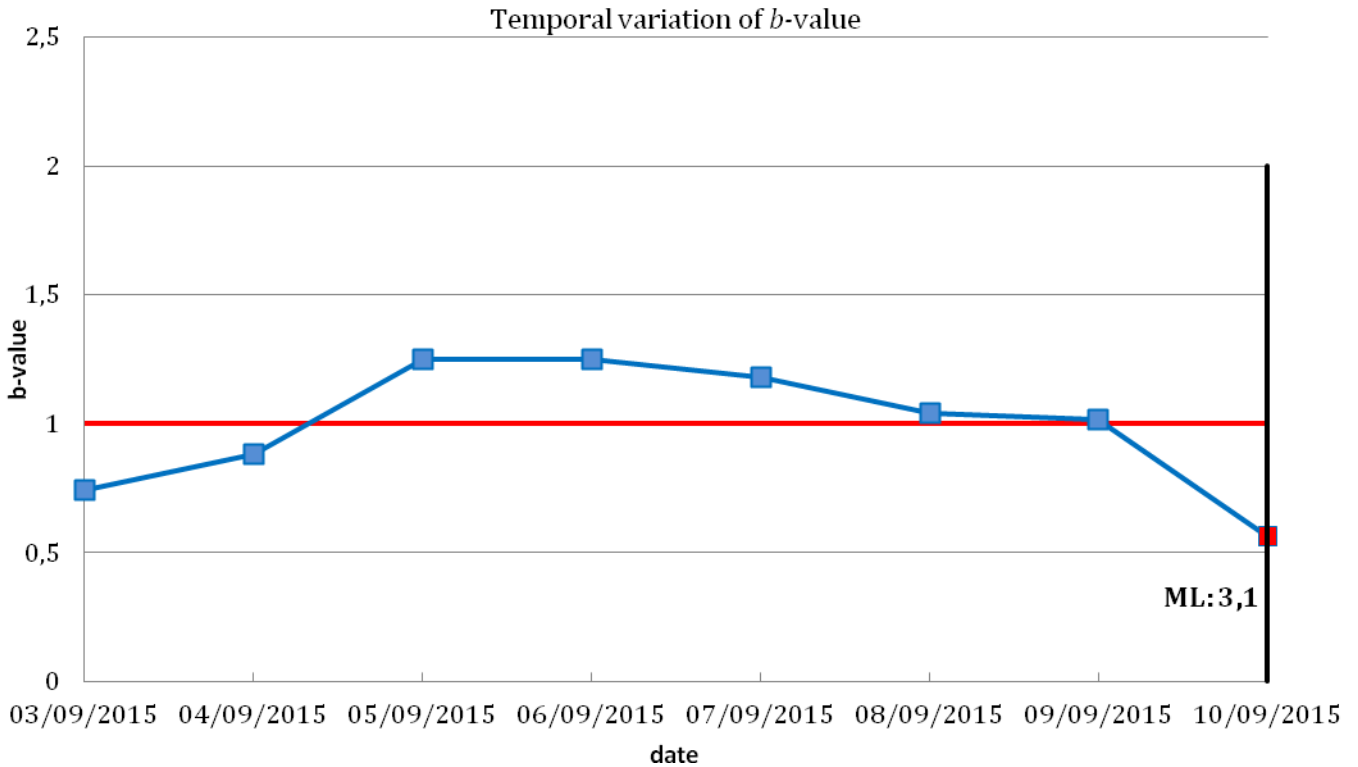


fig. 4.24: Temporal variation of b -value from September 3, 2015 to September 10, 2015.

28° seismic swarm, October 10, 2015 – earthquake M=3,1

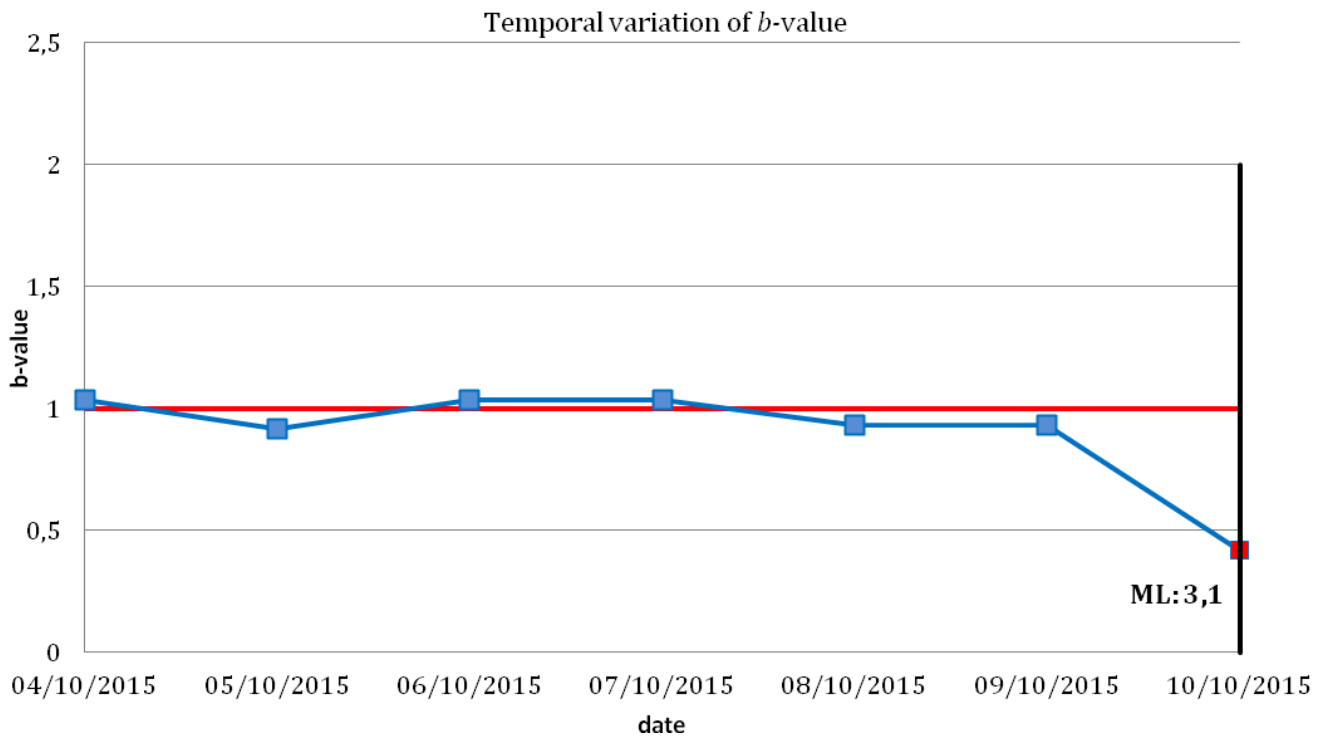


fig. 4.25: Temporal variation of b -value from October 4, 2015 to October 10, 2015.

32° seismic swarm, March 14, 2016 – earthquake M=2,7

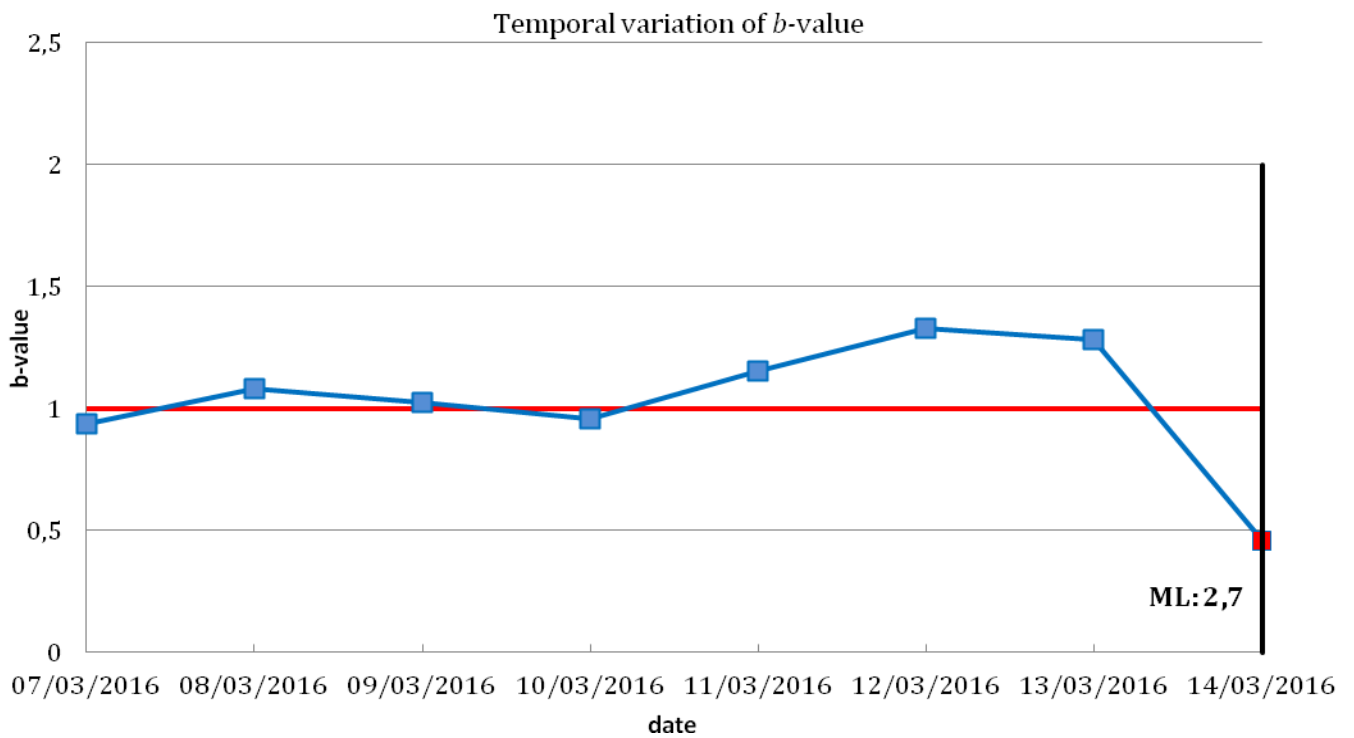


fig. 4.26: Temporal variation of b -value from March 7, 2016 to March 14, 2016.

34° seismic swarm, April 9, 2016 – earthquake M=2,7

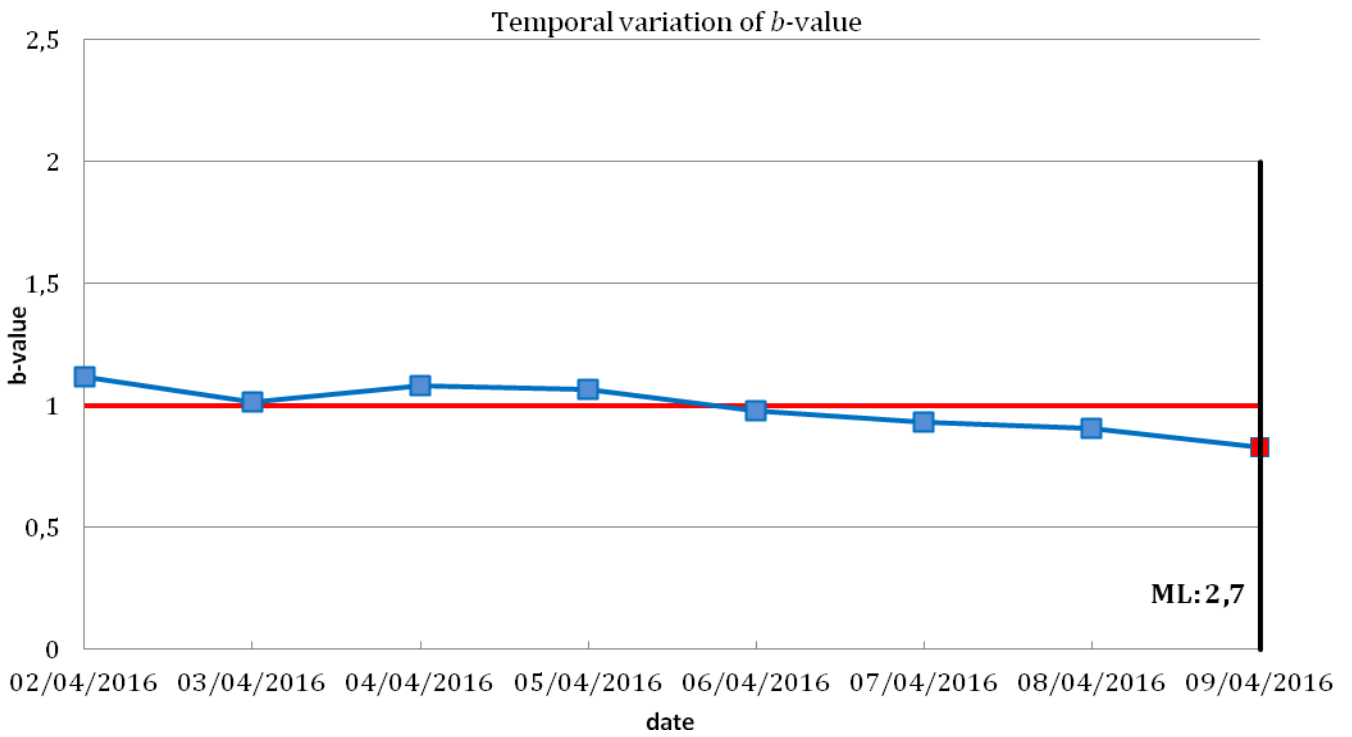


fig. 4.27: Temporal variation of b -value from April 2, 2016 to April 9, 2016

35° seismic swarm, May 24, 2016 – earthquake M=2,5

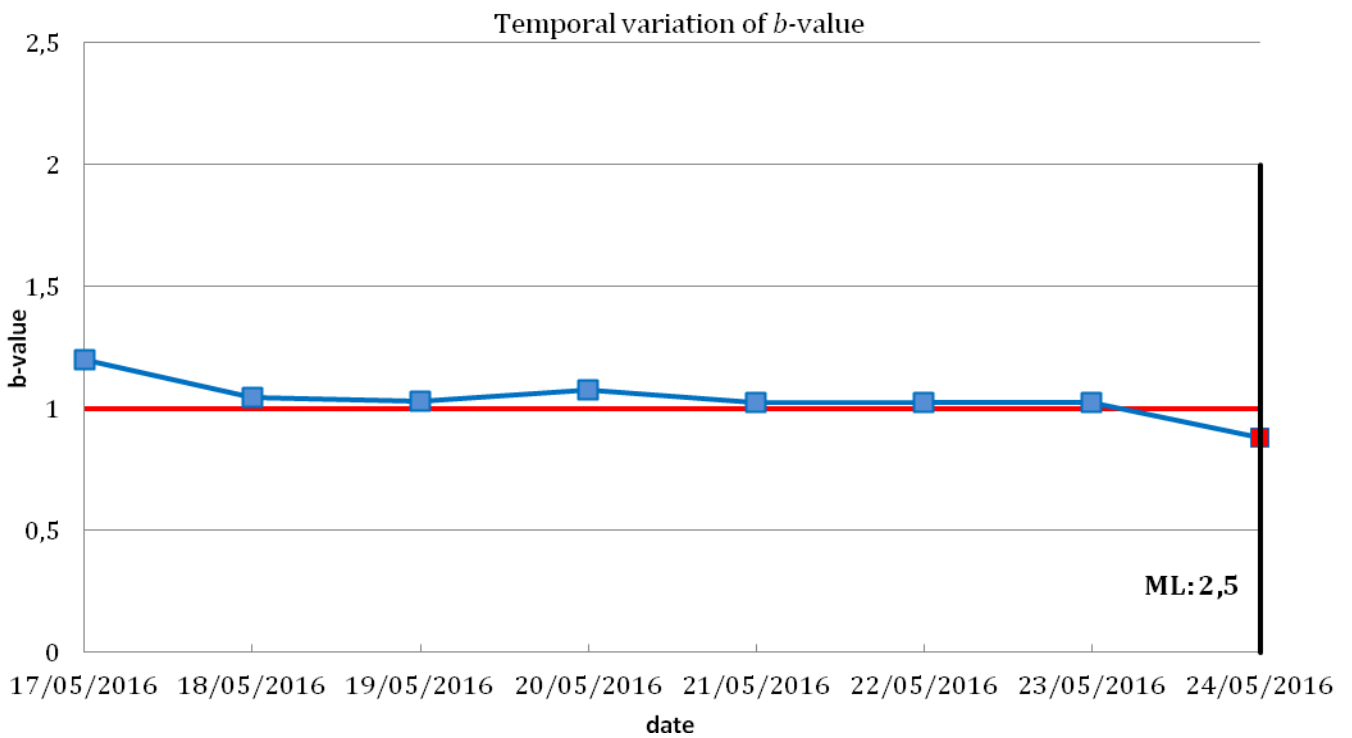


fig. 4.28: Temporal variation of b -value from May 17, 2016 to May 24, 2016.

36° seismic swarm, June 15, 2016 – earthquake M=2,7

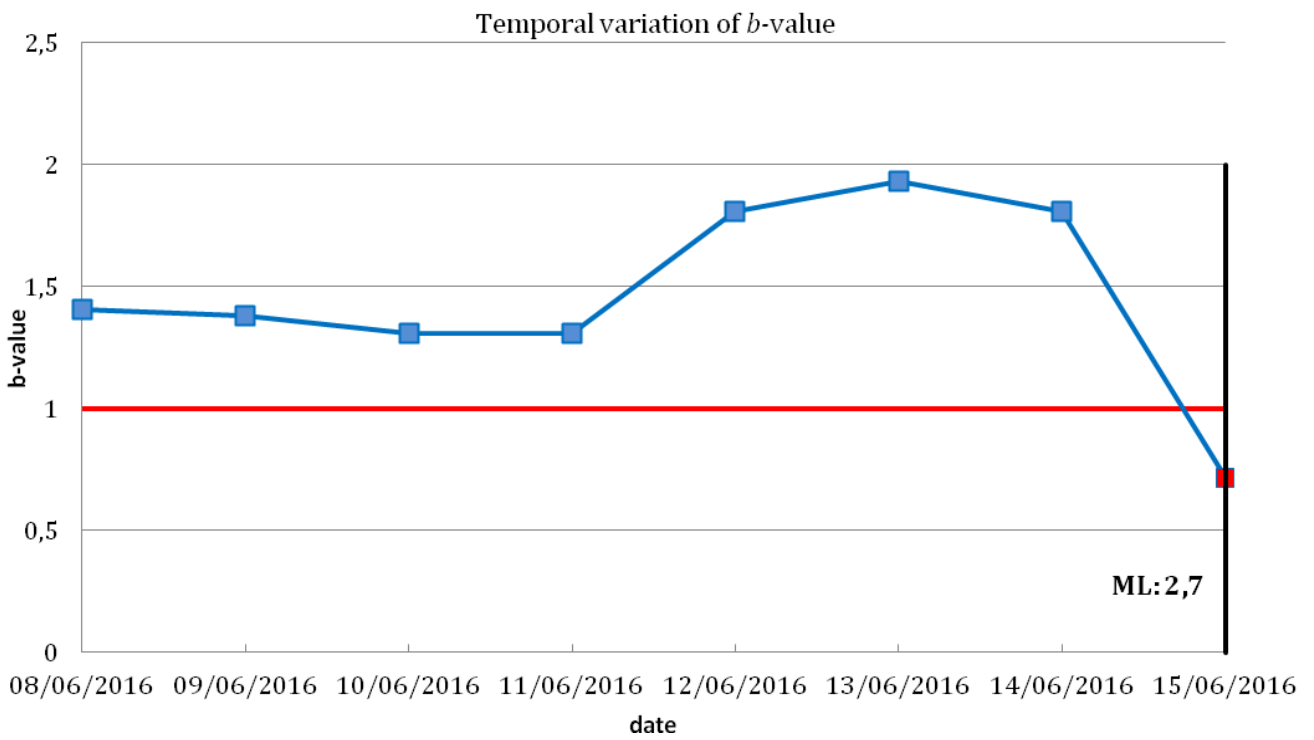


fig. 4.29 : Temporal variation of b -value from June 8, 2016 to June 15, 2016.

37° seismic swarm, July 5, 2016 – earthquake M=2,7

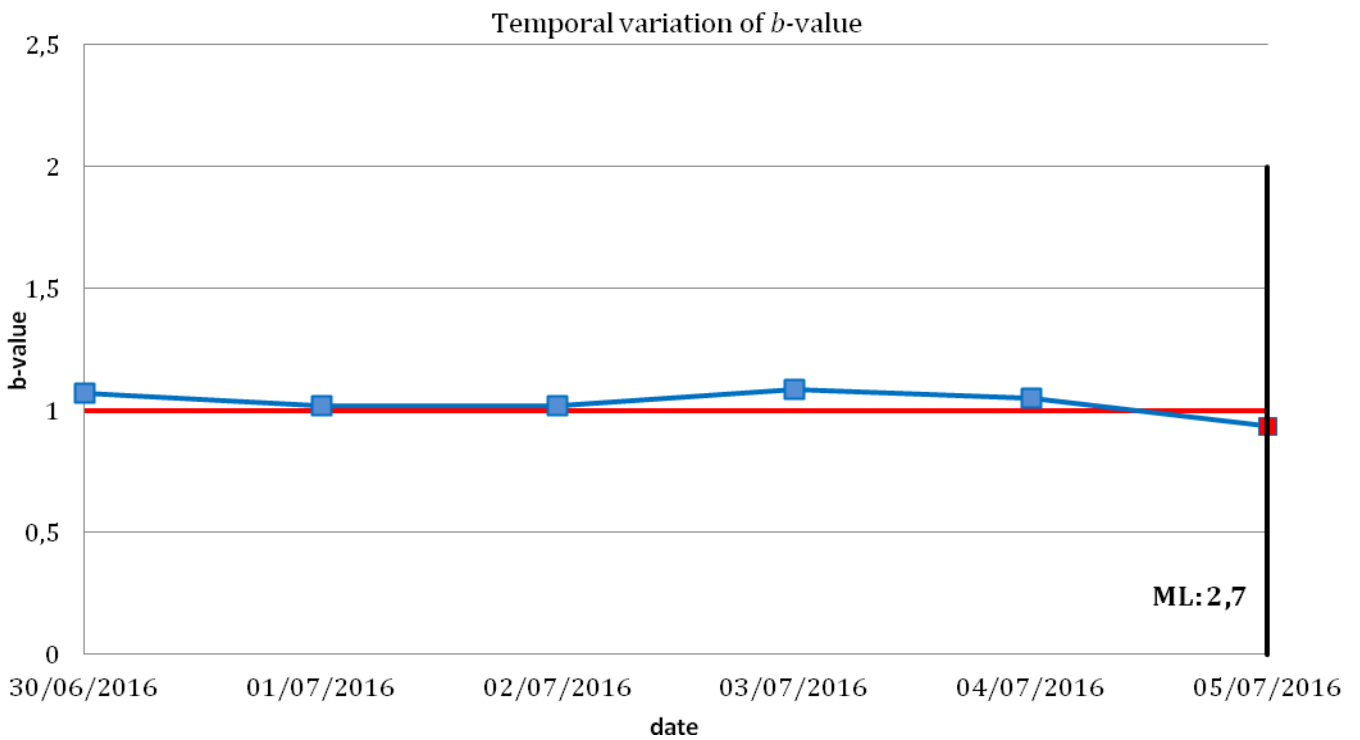


fig. 4.30: Temporal variation of b -value from June 30, 2016 to July 5, 2016.

38° seismic swarm, July 30, 2016 – earthquake M=3,7

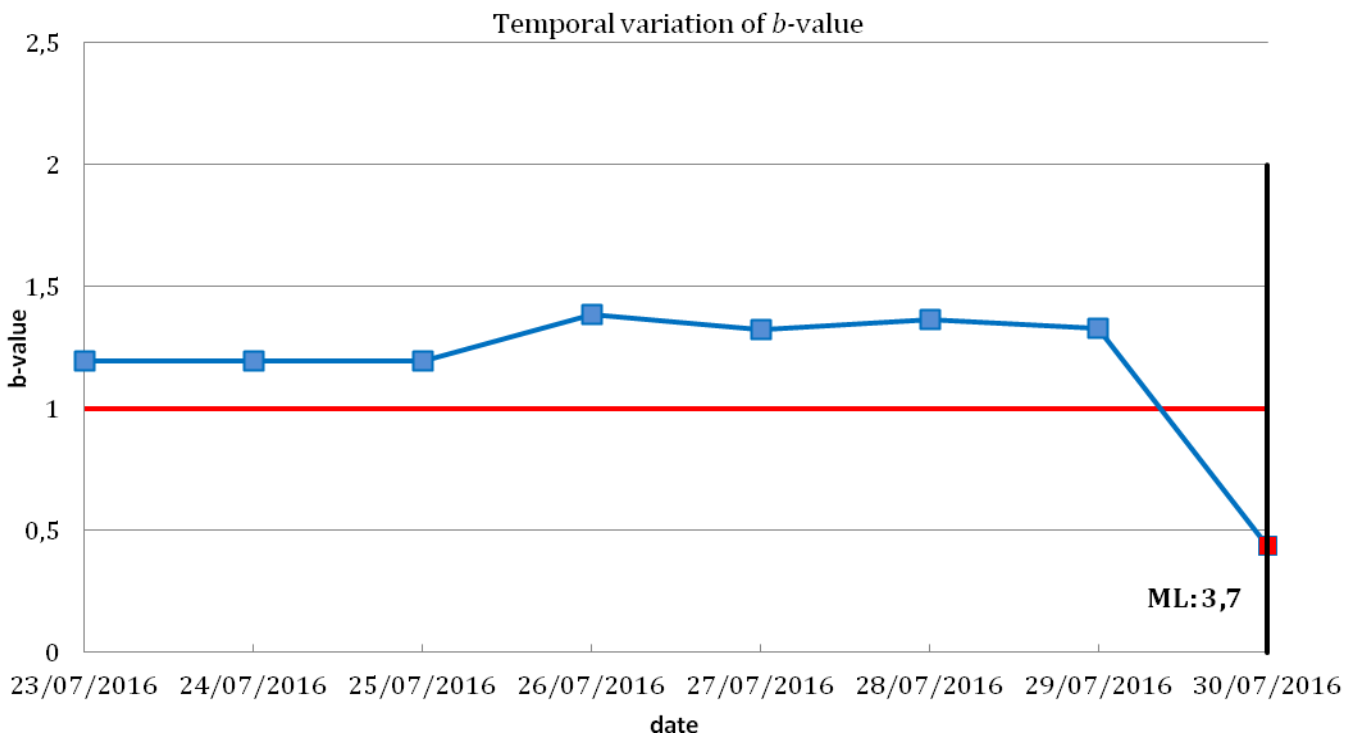


fig. 4.31: Temporal variation of b -value from July 23, 2016 to July 30, 2016.

39° seismic swarm, Semptember 2, 2016 – earthquake M=3,1

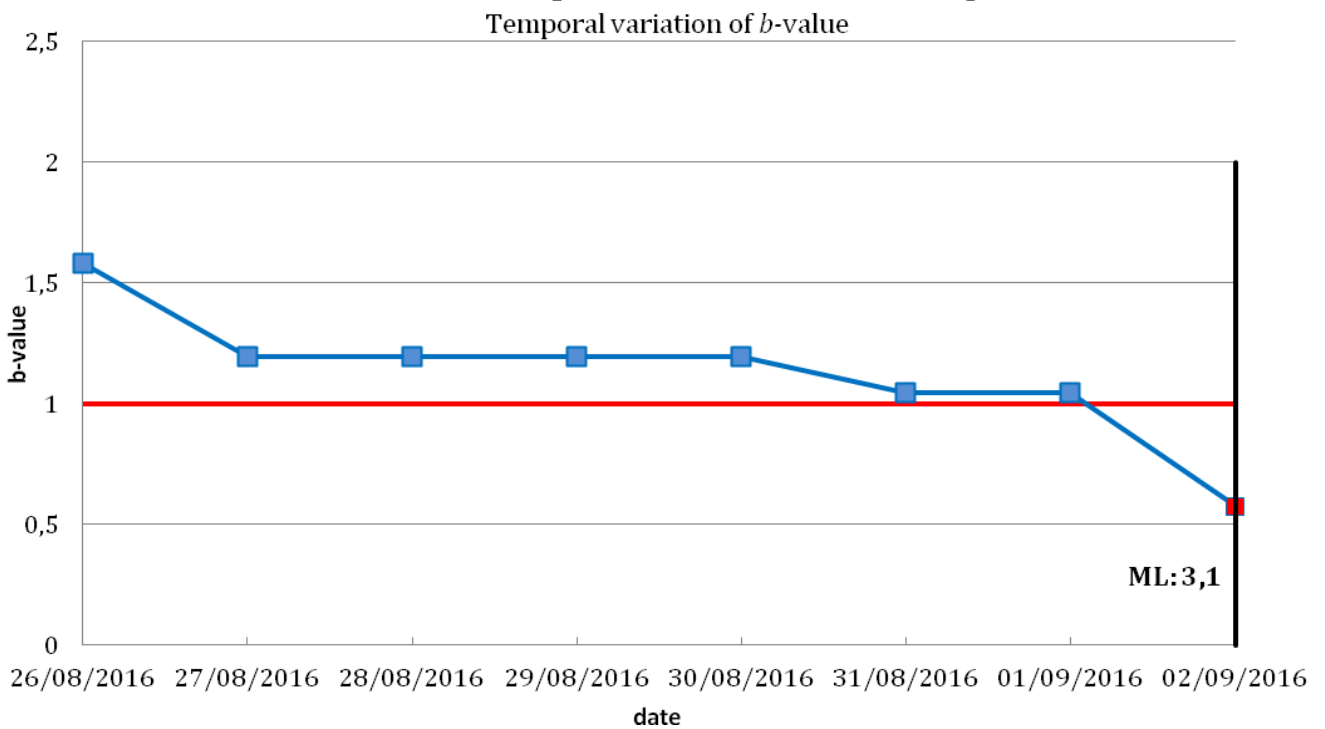


fig. 4.32: Temporal variation of b -value from August 26, 2016 to September 2, 2016.

41° seismic swarm, October 1, 2016 – earthquake M=3

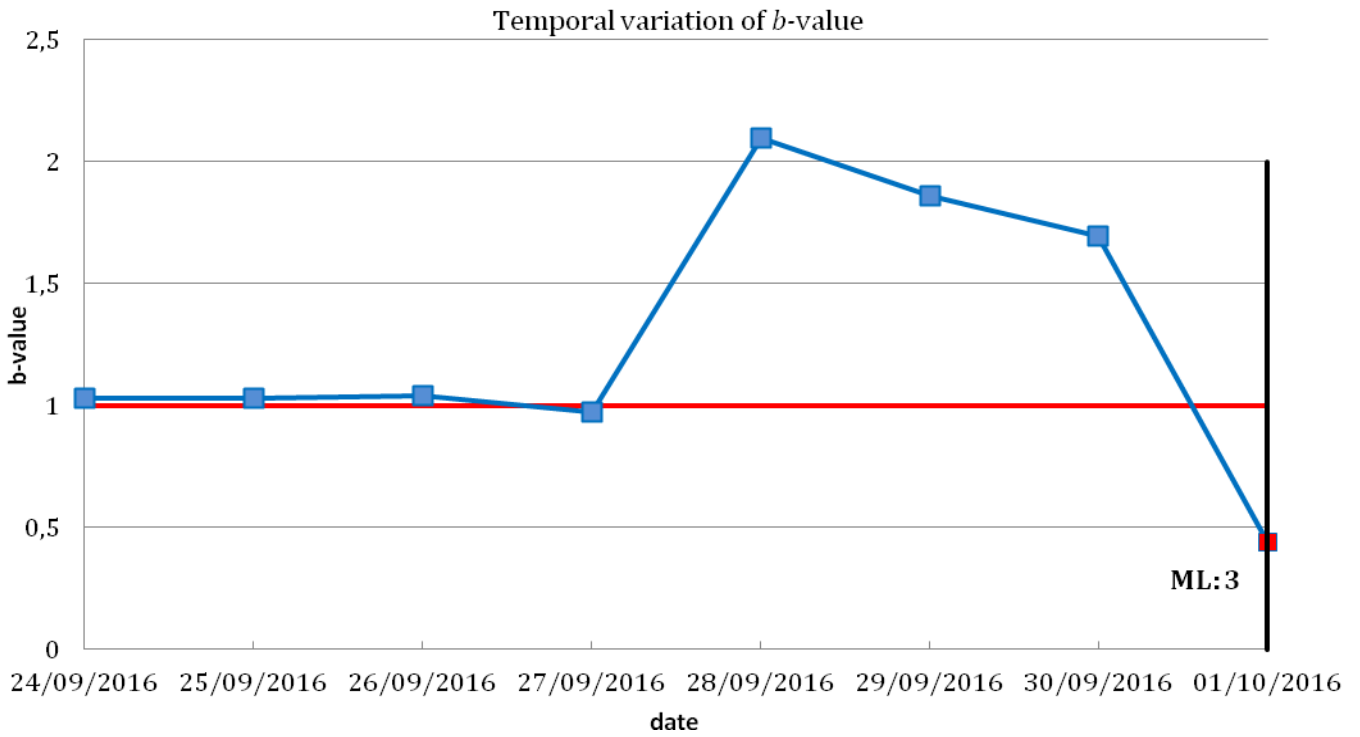


fig. 4.33: Temporal variation of b -value from September 24, 2016 to October 1, 2016.

42° seismic swarm, November 11, 2016 – earthquake M=3

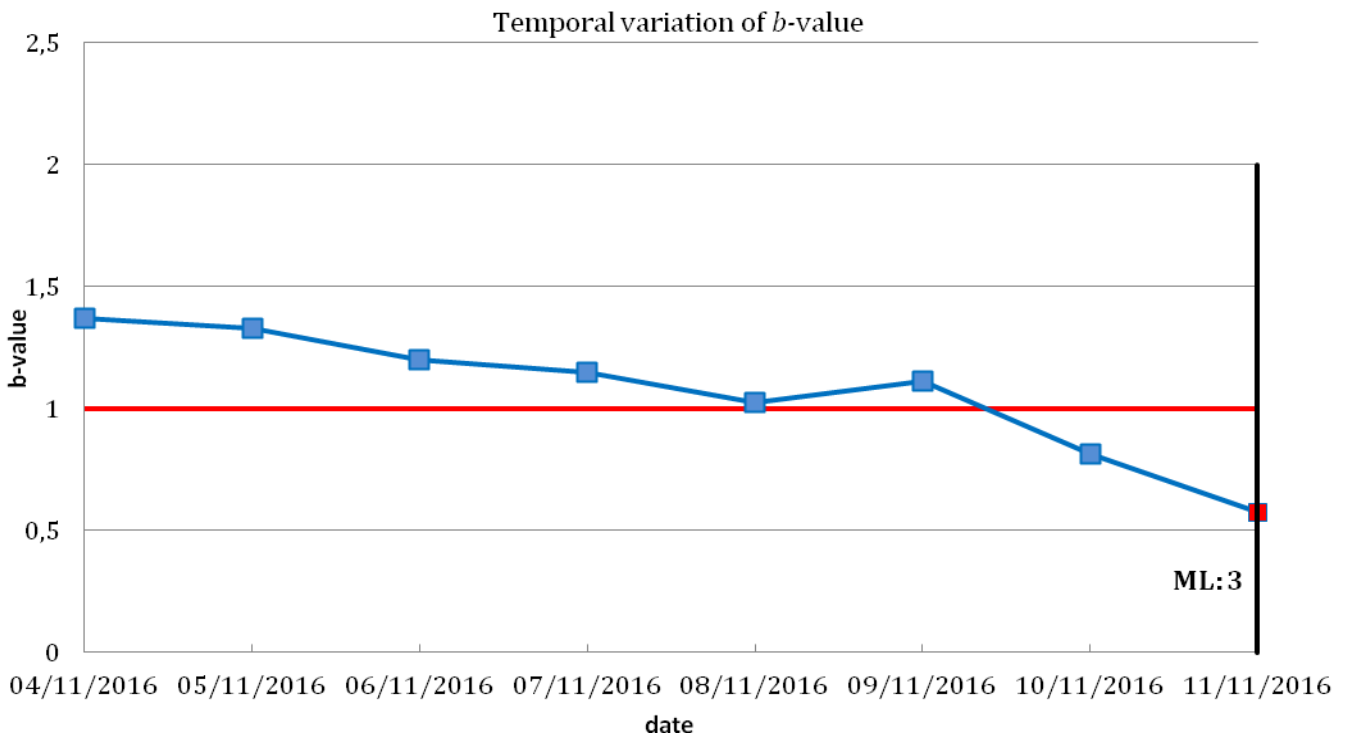


fig. 4.34: Temporal variation of b -value from November 4, 2016 to November 11, 2016.

43° seismic swarm, December 21, 2016 – earthquake M=2,4

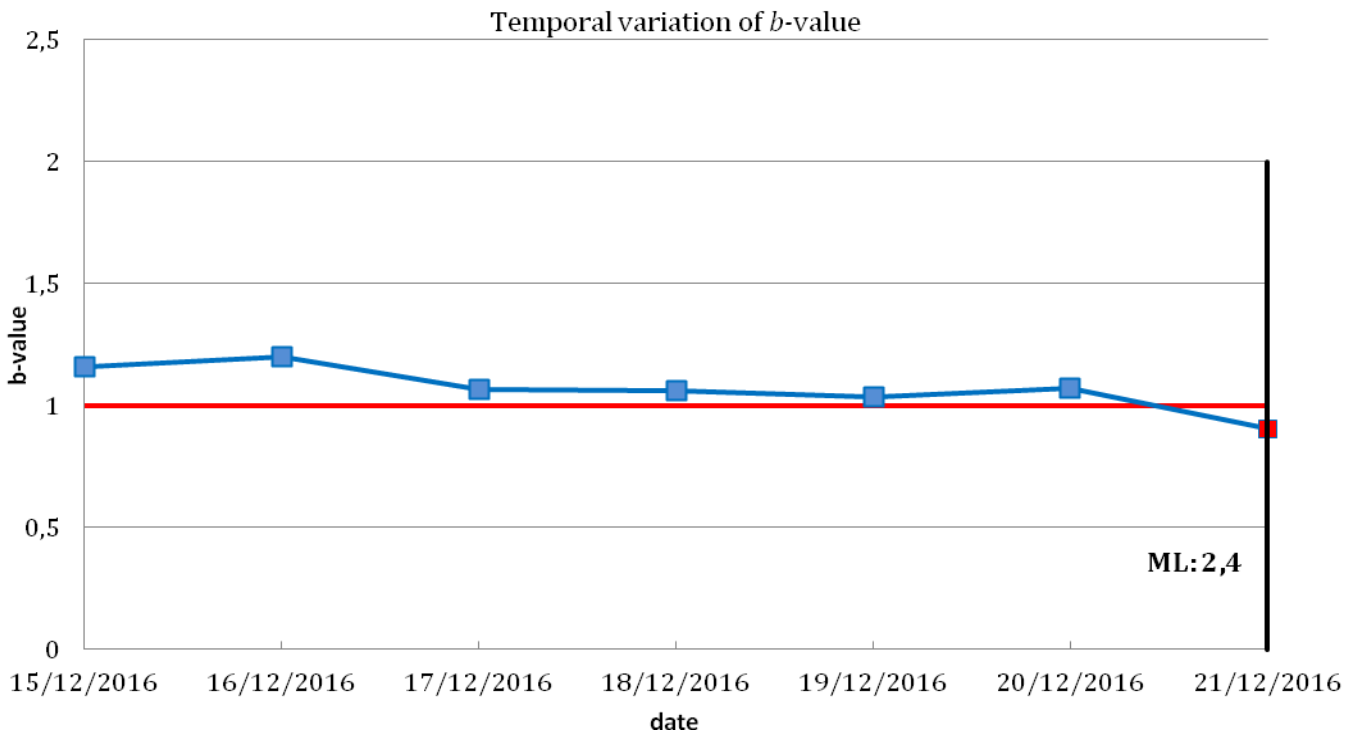


fig. 4.35: Temporal variation of b -value from December 15, 2016 to December 21, 2016.

44° seismic swarm, February 5, 2017 – earthquake M=2,5

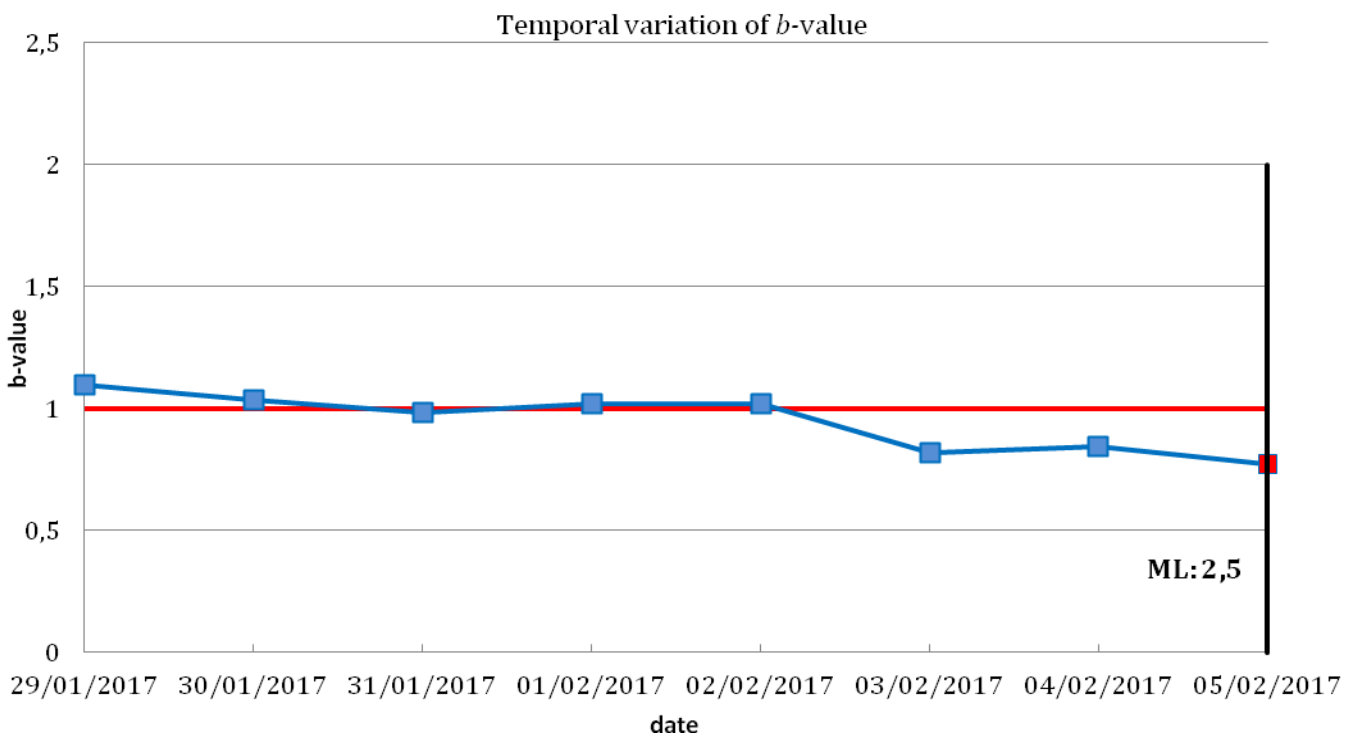


fig. 4.36: Temporal variation of b -value from January 29, 2017 to February 5, 2017.

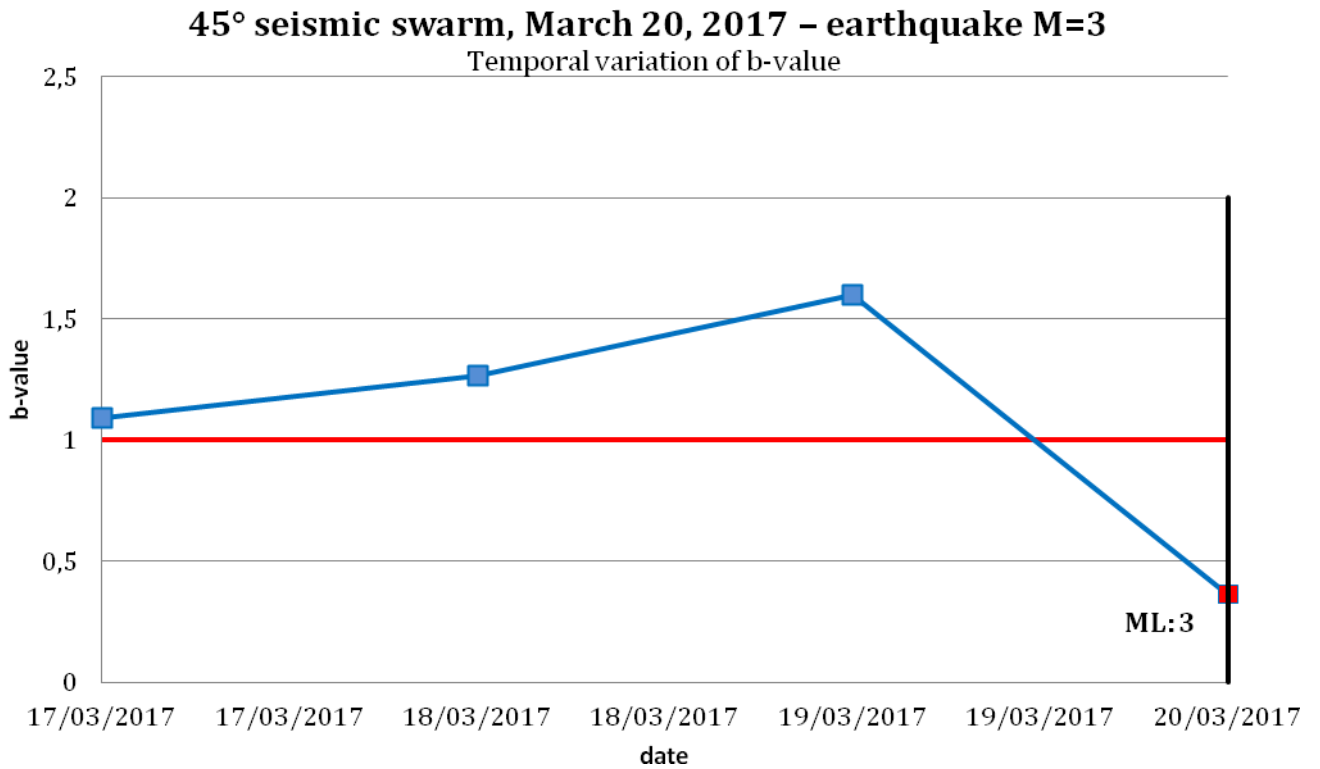


fig. 4.37: Temporal variation of *b*-value from March 17, 2017 to March 20, 2017.

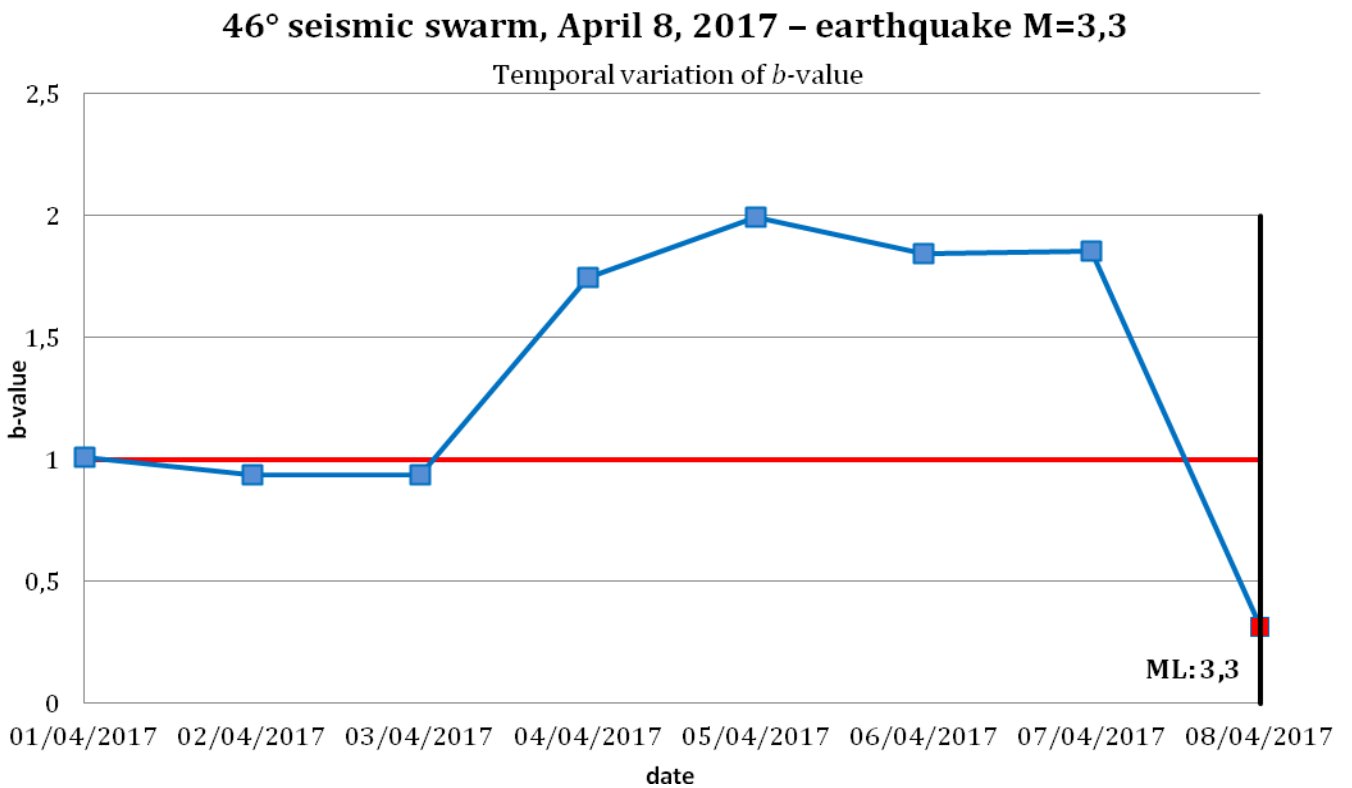


fig. 4.38: Temporal variation of *b*-value from April 1, 2017 to April 8, 2017.

17°-18°-19° seismic swarms, November 25, 2014; December 6, 2014; December 22, 2014-
earthquakes M=2,9, M=3,6, M=2,7
Temporal variation of b -value

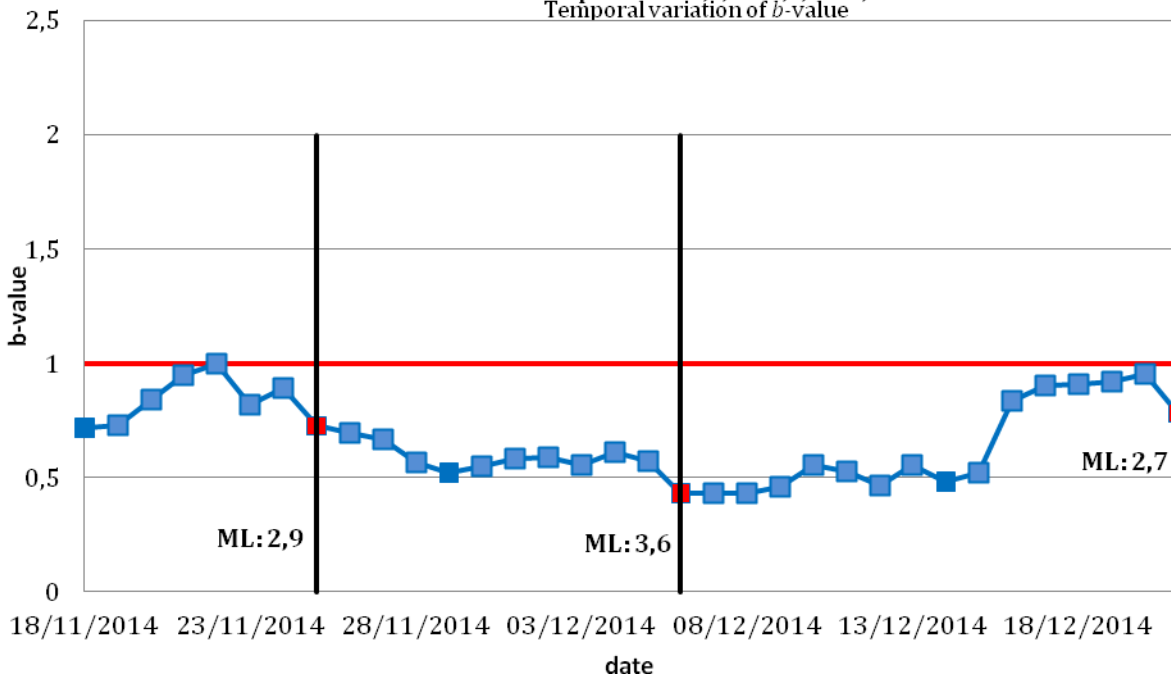


fig. 4.39: Temporal variation of b -value from November 18, 2014 to December 22, 2014.

The three vertical black lines are relative to the three seismic swarms with a respective local magnitude of ML=2,9 (November 25, 2014), ML=3,6 (December 6, 2014), ML=2,7 (December 22, 2014). b -value in these cases show a less precursive function because it is always under the critical state for the reasons just explained.

The diagrams until now analyzed are relative to the period comprised from June 2013 to June 2017. The following diagrams are always based on temporal variation of b -value as in the previous cases, but referred to the new semester (from June 2017 to December 2017). By the previous multi-modal analysis (Chapter 3), 4 seismic swarms were detected. From the calculation of b -value on the same earthquakes, 3 of 4 cases demonstrate the correct trend of the statistical seismic precursor (75% of the cases). In the cases in which b -value shows a less evident behaviour in terms of statistical seismic precursor we have a poor statistics or a seismic ratio too high (as just explained). However, even this last case led to a negative result, it can be transformed in a positive evaluation for fracto-emissions: statistics doesn't always work because it is in function of the number of the events spread over the number of days (that is the seismic ratio), fracto-emissions instead, are seem to be independent from the frequency of the events and so they seem to never lose their validity, as we can see from the analysis conducted for the total period of investigation. As a matter of the fact, even if the b -value relative to the seismic swarm of December 19, 2017 doesn't show an evident precursive behaviour, fracto-emissions, instead demonstrate their forecasting potentiality as reported in figs. 3.8-3.10.

The diagrams of temporal variation of b -value relative to the new semester are described below using the same conventions as for the previous ones.

49° seismic swarm, July 18, 2017 – earthquake M=2,9

Temporal variation of b -value

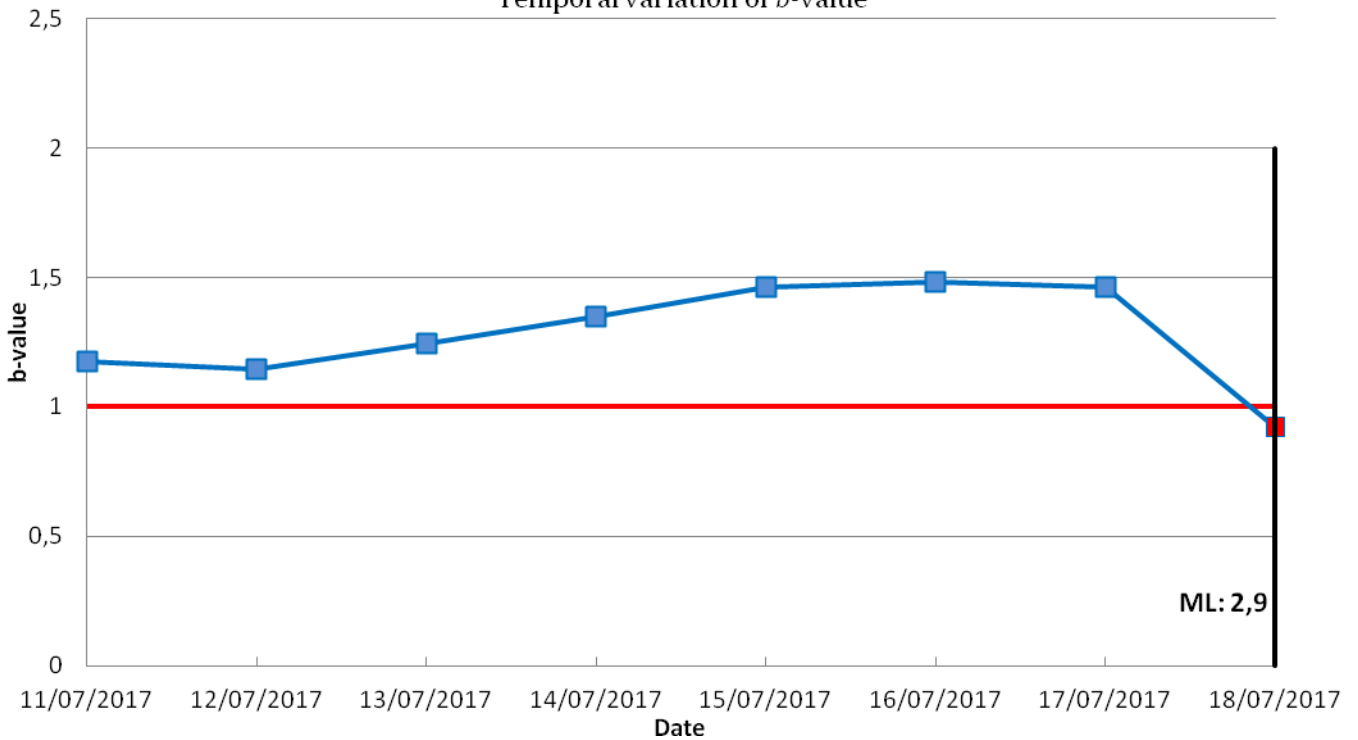


fig. 4.40: Temporal variation of b -value from July 11, 2017 to July 18, 2017

50° seismic swarm, September 10, 2017 – earthquake M=3,7

Temporal variation of b -value

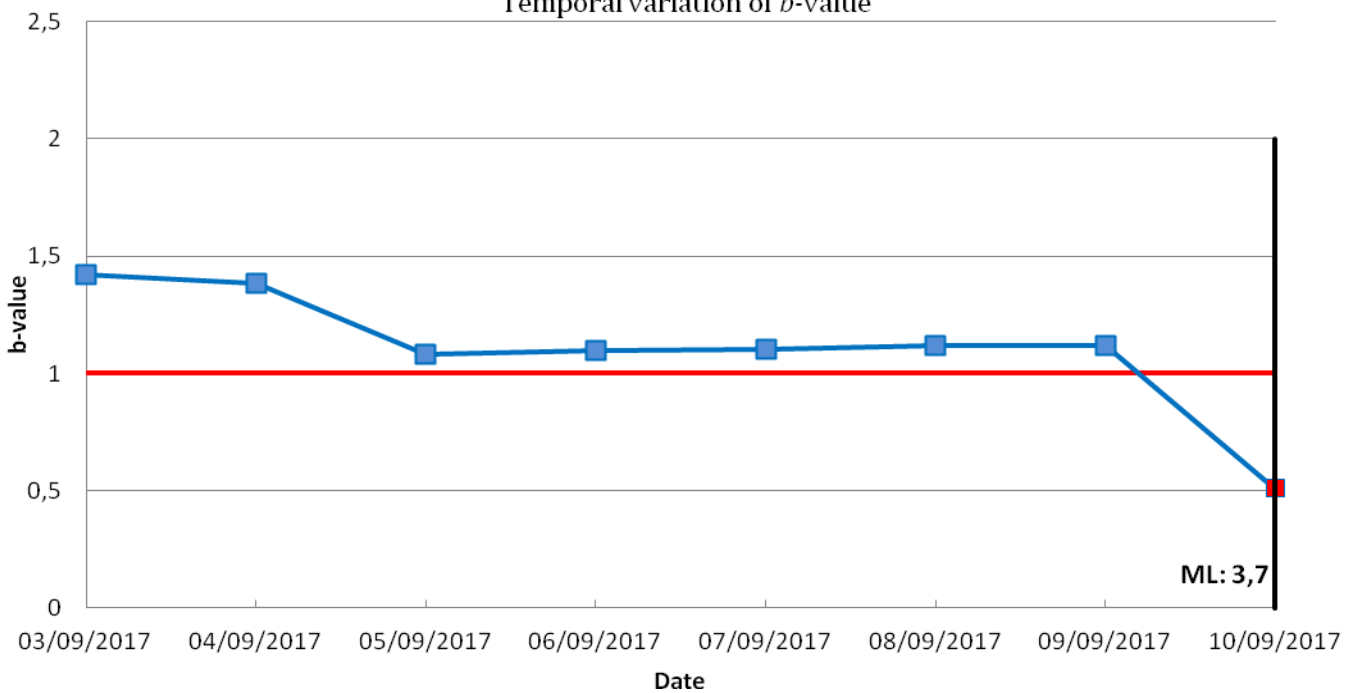


fig. 4.41: Temporal variation of b -value from September 3, 2017 to September 10, 2017

51° seismic swarm, October 27, 2017 – earthquake M=3,3

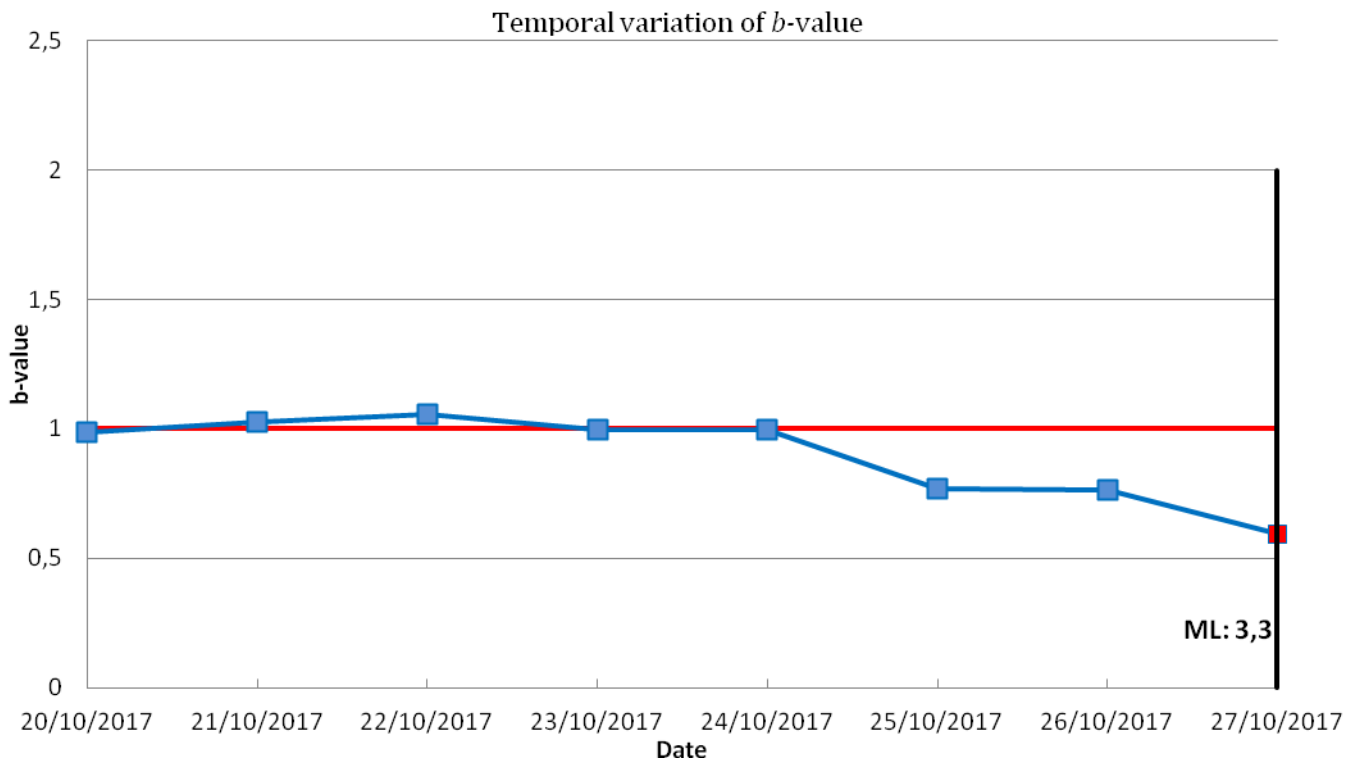


fig. 4.42: Temporal variation of b -value from October 20, 2017 to October 27, 2017

52° seismic swarm, December 19, 2017 – earthquake M=2,9

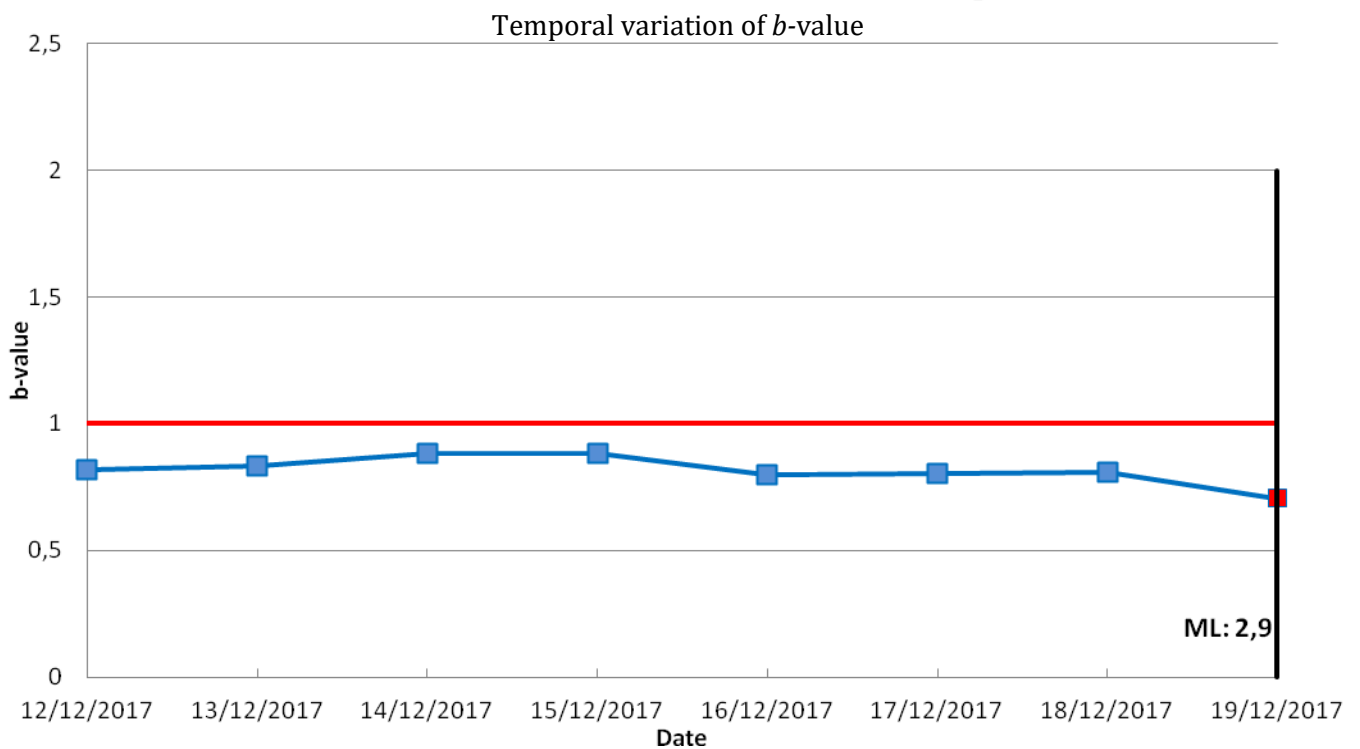


fig. 4.43: Temporal variation of b -value from December 12, 2017 to December 19, 2017

Concluding remarks

Pressure waves generated by the fracture phenomena that take place in a wide geographical area in the period before a seismic event occurrence, produce different kind of energy emissions (also known as fracto-emissions) characterized by a very specific frequency (from THz up to the simple Hz) in the form of acoustic, electromagnetic and neutron emissions (AE, EME, and NE). These fracto-emission signals can be considered as a very important tool in the field of earthquakes forecasting.

In this thesis, the recent experimental data acquired at the San Pietro-Prato Nuovo gypsum mine (Murisengo, Alessandria, Italy) in the period from July, 1st 2017 to December, 31 2017 have been discussed, and analyzed by a suitable multi-modal statistical approach. Multi-modal analysis is an iterative procedure that allows to obtain curves similar to Gaussians which best fit the discrete number of experimental data.

The analysis confirms the seismic forecasting potentiality of fracto-emissions (also in the case of low-magnitude earthquakes) as already observed during the preliminary experimental campaign carried out from July 2013 to June 2017.

In particular, by superimposing the multi-peaks distribution of earthquakes with the single ones coming from AE, EME and NE, a temporal shift can be seen. As a matter of the fact, the acoustic emissions happen about 1-2 days before the earthquake, the electromagnetic emissions anticipate the event of about 3-4 days while the neutron ones of about one week, reinforcing the idea of their use as a forecasting tool for earthquakes.

Important results have been also obtained for what concerns the correlation between seismic event occurrence and lunar phases. As a matter of fact, it is well known the important role of gravitational force exerted by the Moon and the Sun and the seismicity on Earth. In particular, it has been observed that main seismic events happen in correspondence or pretty close to the period of full and new Moon. In particular, the new experimental observation supports the previous studies and confirms the hypothesis according to which earthquakes can be triggered by the tides.

Besides fracto-emissions further experimental analysis on the changing in time of b -value has been performed (in the period from June 2013 to December 2017). Unlike the fracto-emissions, b -value is a statistical seismic precursor, coming from the well know frequency-magnitude Richter's law.

Typical values for this statistical precursor, related to its temporal and spatial variability, are comprised in the range from 1,5 to 1 (McGarr, 1984). Higher values for this parameter have been correlated with the occurrence of earthquakes with small magnitude spread over a wide geographical area, lower values are related to a concentration of earthquakes with higher magnitude localized along a fault. The real innovation about the use of b -value that is discussed in this thesis is its application also to low-magnitude earthquakes occurring in low-seismicity regions, since it has just been demonstrated valid for high-intensity earthquakes (Ouchi, T., Uekawa, T., 1986).

The analysis of b -value has been performed, considering the 52 seismic swarms observed at the gypsum mine in the period from July 2013 to December 2017. Starting from the computation of the Magnitude of Completeness, that is the magnitude below which calculations led to an incorrect result for the statistical parameter and choosing the best

temporal window of 15 days defined considering the seismicity of the monitored area, b -value has been derived from the slope of the regression line of the frequency-magnitude distribution, as largely discussed in Chapter 4. In particular, 36 cases over 52 seem to verify the precursory function of b -value: its value swings above the critical value of 1, decreasing rapidly about 2 days before the main event.

For this reason it could be compared with the Acoustic Emissions: AE peaks as b -value anticipate the seismic event with a similar delay-time.

On the other hand, the cases (16 over 52) in which b -value shows a less evident behaviour in terms of statistical seismic precursor are due to a poor statistics or to a meaningless seismic ratio (i.e. insufficient number of seismic events for a correct b -value estimation in the first case; a permanent critical state of the monitored regions in the second case).

In conclusion, the main results obtained in this thesis are that: (i) the fracto-emissions confirm their high potentiality as seismic precursors; (ii) the b -value statistical precursor provides very satisfactory results also when applied to low-magnitude earthquakes; (iii) the combined use of the two different seismic precursors (fracto-emissions and b -value) can provide important steps forward in the field of Civil Engineering and Seismology in terms of seismic risk prevention.

References

- Adams R.D., Seismological Observatory, Geophysics Division, Department of Scientific and Industrial Research, Wellington, New Zealand: The Haicheng, China, Earthquake of 4 February 1975; the first successfully predicted major Earthquake, *Earthquake Engineering & Structural Dynamics* Volume 4, Issue 5 July/September: 423–437, 1976.
- Aki, K. (1965): Maximum Likelihood estimate of b in the formula $\log N=a-bM$ and its confidence limits. *Bull. Earthquake Res Inst., Tokyo Univ.* 43, 237-239.
- Allen CR, Amand P, Richter CF, Nordquist JM (1965): Relation between seismicity and geological structure in the Southern California region. *Bull Seismol Soc Am* 55:752–797.
- Bahat D., Rabinovitch, A., and Frid, V.: *Tensile fracturing in rocks: Tectonofractographic and Electromagnetic Radiation Methods*, Springer Verlag, Berlin, 570 pp., 2005.
- Barone E.: "Fracto-emissions as seismic precursors: The lunar periodicity at Murisengo gypsum mine", Master thesis 2017.
- Batzel RE, Seaborg GT, (1951): Fission of medium weight elements, *Physical Review*, 82: 607-615.
- Bayrak Y., Yilmazturk A. and Ozturk S.; 2002: Lateral variations of the modal (a/b) values for the different regions of the world. *J. Geodyn.*, 34, 653-666.
- Bender B (1983): Maximum likelihood estimation of b -values for magnitude grouped data. *Bull Seismol Soc Am* 73:831–851.
- Bernardi, A., Fraser-Smith, A.C., McGill, P.R., Villard, O.G., 1991: ULF magnetic field measurements near the epicenter of the Ms 7.1 Loma Prieta earthquake, *Phys. Earth Planet. Int.* 68, 45–63.
- Borla O, Lacidogna G, Carpinteri A: Piezonuclear neutron emissions from earthquakes and volcanic eruptions. In Carpinteri A., Lacidogna G.,Manuello A. (eds): *Acoustic, Electromagnetic, Neutron Emissions from Fracture and Earthquakes*, pp. 135-151. Springer International Publishing Switzerland, 2015.
- Borla O.: *The Energy emissions as Fracture and Seismic Precursors Phd Thesis*, 2016.
- Bridgman PW, (1927): The breakdown of atoms at high pressures, *Physical Review*, 29: 188-191.
- Cadicheanu N., Ruymbeke M. van , and Zhu P.: Tidal triggering evidence of intermediate depth earthquakes in the Vrancea zone (Romania), *Natural Hazards and Earth System Science*, 2007, 7 (6), pp.733-740.
- Cardone F., Carpinteri A. and Lacidogna G. 2009b: Piezonuclear neutrons from fracturing of inert solids. *Phys. Lett. A* 373: 4158–4163.

Carpinteri A., Cardone F. and Lacidogna G.: Strain: Int. J. Exp. Mech. 45, 332 (2009a): Energy emissions from failure phenomena: mechanical, electromagnetic, nuclear.

Carpinteri A., Lacidogna G., Manuello A.: Acoustic, Electromagnetic, Neutron Emissions from Fracture and Earthquakes, Springer, 2015.

Carpinteri A., Manuello A., Veneziano D., Cook N.D. (2015b): "Piezonuclear fission reactions simulated by the lattice model", Journal of Condensed Matter Nuclear Science, Vol. 15, 149-161.

Carpinteri A., Borla O.: Fracto Emissions as Seismic Precursors: Engineering Fracture Mechanics Volume 177, 15 May 2017, Pages 239-250.

Carpinteri A., Borla O. (2018): Nanomechanics Instabilities and TeraHertz Vibrations: From Geochemical Evolution to Fracto-Emission Seismic Precursors. In: Starman L., Hay J. (eds) Micro and Nanomechanics, Volume 5. Conference Proceedings of the Society for Experimental Mechanics Series. Springer, Cham.

Cochran, E. S., J. E. Vidale, and S. Tanaka (2004): Earth tides can trigger shallow thrust fault earthquakes, Science, 306, 1164–1166, doi:10.1126/ science.1103961.

Cook ND, (2010): Models of the Atomic Nucleus, Springer, Dordrecht, 2nd Ed.

Davis, S. D. & Frohlich, C. (1991): Single-link cluster analysis of earthquake aftershock: decay laws and regional variations. J. Geophys. Res. 96, 6335-6350.

De Rubeis V., Dimitriu D., Papadimitriou E., and Tosi P.: "Recurrent Patterns in the Spatial Behaviour of Italian, Seismicity Revealed by the Fractal Approach", Geophys. Res. Lett. 20, 1911–1914 (1993).

De Rubeis V., Tosi P., and Vinciguerra S.: "Time Clustering of Seismicity in the Etna Region between 1874 and 1913", Geophys. Res. Lett. 21, 2331–2334 (1997).

Derjaguin BV, et al. (1989): Titanium fracture yields neutrons?, Nature, 34: 492.

Diebner K, (1962): Fusionsprozesse mit hilfe konvergenter stosswellen – einige aeltere und neuere versuche und ueberlegungen, Kerntechnik, 3: 89-93.

Ebel. J. E., Bonjer, K.-P. & Oncescu, M.C., 2000: Paleoseismicity: seismicity evidence for past large earthquakes, *Seism. Res. Lett.* 71, 283-294.

Eftaxias, K., Sgrigna, V., and Chelidze, T.: Mechanical and Electromagnetic Phenomena Accompanying Preseismic Deformation: from Laboratory to Geophysical Scale, Tectonophysics, 431, 1- 301, 2007.

Eftaxias, K., Athanasopoulou, L, Balasis, G., Kalimeri, M., Nikolopoulos, S., Contoyiannis, Y., Kopanas J., Antonopoulos G., and Nomicos, C. Unfolding the procedure of characterizing recorded ultra low frequency, kHz and MHz electromagnetic anomalies

prior to the L'Aquila earthquake as preseismic ones – Part 1. *Nat. Hazards Earth Syst. Sci.*, 9, 1953–1971, 2009.

Enescu B., Ito K., Radulian M., et al., *Pure Appl. Geophys.* 162, 249–271 (2005).

Fisher, R.A. (1950): *Contribution to Mathematical Statistics* (Wiley, New York).

Fraser-Smith, A.C., Bernardi, A., McGill, P.R., Ladd, M.E., Helliwell, R.A., Villard, O.G., 1990: Low-frequency magnetic field measurements near the epicenter of the Ms 7.1 Loma Prieta earthquake. *Geophys. Res. Lett.* 17, 1465–1468.

Frid V. Rabinovich A., Bahat D. (2003): Fracture induced electromagnetic radiation. *J. Phys D.* 36:1620-1628.

Fulmer CB, et al. (1967): Evidence for photofission of iron, *Phys. Rev. Lett.*, 19:522-523.

Fujii MF, et al. (2002): Neutron emission from fracture of piezoelectric materials in deuterium atmosphere, *Jpn. J. Appl. Phys.*, Pt.1, 41: 2115-2119.

Geilikman M.B., Gobuleva T. V., and Pisarenko V. F.: “Multifractal Patterns of Seismicity”, *Earth Planet. Sci. Lett.* 99, 127–132 (1990).

Godano C., Alonzo M. L., and Vilardo G.: “Multifractal Approach to Time Clustering of Earthquakes”, *Appl. Mt. Vesuvio Seismicity, Pure Appl. Geophys.* 149, 375–390 (1997).

Goltz C.: *Fractal and Chaotic Properties of Earthquakes* (Springer-Verlag, 1998).

Grassberger Peter, Procaccia Itamar: Measuring the strangeness of strange attractors, *Physica D: Nonlinear Phenomena*, Volume 9, Issues 1–2, 1983, Pages 189-208.

Hagelstein PL, Letts D, Cravens D, (2010): Terahertz difference frequency response of PdD in two-laser experiments, *J. Cond. Mat. Nucl. Sci.*, 3: 59.

Hagelstein PL, Chaudhary IU, (2015): Anomalies in fracture experiments and energy exchange between vibrations and nuclei , *Meccanica*, 50, 1189 – 1203.

Hainzl S., 2003: Self-organization of seismic swarms, *J. Geodyn*, 35, 157-172.

Han, Q., Wang, L., Xu, J., Carpinteri, A., Lacidogna, G., 2015: A robust method to estimate the b-value of the magnitude-frequency distribution of earthquakes. *Chaos. Solitons and Fractal* 81, pp. 103-110.

Hatzidimitriou P. M., Papadimitriou E. E., Mountrakis D. M., Papazachos B. C. (1985): The seismic parameter b of the frequency-magnitude relation and its association with the geological zones in the area of Greece. *Tectonophysics* 120:141–151.

Hayakawa, M. and Fujinawa, Y.: *Electromagnetic Phenomena Related to Earthquake Prediction*, Terrapub, Tokyo, 1994.

Hayakawa, M.: Atmospheric and Ionospheric Electromagnetic Phenomena Associated with Earthquakes, Terrapub, Tokyo, 1999.

Hayakawa, M. and Molchanov, O.: Seismo Electromagnetics, Terrapub, Tokyo, 2002.

Heaton, T. H.: Tidal triggering of earthquakes, *Geophys. J. R. Astron. Soc.*, 43, 307–326, 1975.

Heaton, T. H. (1982): Tidal triggering of earthquakes, *Bull. Seismol. Soc. Am.*, 72, 2181–2200.

Hirabayashi T., Ito K., and Yoshii T.: “Multifractal Analysis of Earthquakes”, *Pure Appl. Geophys.* 138, 591–610 (1992).

Holland R, Eernisse EP(1969): Design of resonant piezoelectric devices, Research Monograph 56, MIT Press, Cambridge.

Holtkamp, S. G., and M. R. Brudzinski (2011): Earthquake swarms in the circum-Pacific subduction zones, *Earth Planet. Sci. Lett.*, 305, 215–225.

Hutton, L. K. and Boore, D. M., 1987: The M_L scale in Southern California. *Bull. Seism. Soc. Am.*, 77 (6), pp. 2074-2094.

ISIDe Working Group (INGV) - Italian Seismological Instrumental and parametric database, disponibile al sito: <http://iside.rm.ingv.it/iside/standard/index.jsp>.

Iwata, Takaki & Katao, Hiroshi: Correlation between the phase of the moon and the occurrences of microearthquakes in the Tamba region through point-process modeling. *Geophysical Research Letters - GEOPHYS RES LETT.* 33. 10.1029/2005GL025510, 2006.

John, T. Burns: Cosmic Influences on Humans, Animals, and Plants: An Annotated Bibliography, Magill Bibliographies, pag. 147, 1997.

Kachakhidze M. K., Kereselidze Z. A., Kachakhidze N. K.: In connection with identification of VLF emissions before L’Aquila earthquake, *Nat. Hazards Earth Syst. Sci.*, 12, 1009–1015, 2012.

Kagan Y. Y. and Jackson D. D.: “Long-Term Earthquake Clustering”, *Geophys. J. Int.* 104, 117–133 (1991).

Kanamori H. Anderson D. L. , 1975: Theoretical basis of some empirical relations in seismology *Bull. seism. Soc. Am.*, 65,1073–1095.

Kanamori, H.: The nature of seismicity patterns before large earthquakes, Maurice Ewing Series Volume 4, Pages 1-19, 1981.

Kawabata A. (1973): Ultrasonic piezoelectric sensors and their application *J. Soc. Materials Science Japan* 22(232): 96-101.

Klotz, O.: Earthquakes, Phases of the Moon, Sub-Lunar and Sub-Solar Points, Journal of the Royal Astronomical Society of Canada, Vol. 8, p.273, 1914.

Lopez Casado C., Sanz de Galdano C., Delgado J. and Peinado M.A.; 1995: The b parameter in the Betic Cordillera, Rif and nearby sectors. Relations with the tectonics of the region. Tectonophysics, 248, 277-292.

Lucia U. and Carpinteri A. (2015): "GeV plasmons and spalling neutrons from crushing of iron-rich natural rocks", Chemical Physics Letters, 640: 112-114.

Mandelbrot B.B.: "How Long is the Coast of Britain? Statistical Self-Similarity and Fractional Dimension," Science 156, 636–638 (1967).

Mandelbrot B.B.: *The Fractal Geometry of Nature* (Freeman, San Francisco, 1992).

Maji AK, Sahu R. (1994): Acoustic emissions from reinforced concrete. Exper. Mech. 51:379-388.

McGarr A., 1984: Some application of seismic source mechanism studies to assessing underground hazard. In: N.C. Gay and E.H. Wainwright (Eds.), Proc. 1st Inter. Congress on Rockbursts and Seismicity in Mines. SAIM Johannesburg, pp. 199-208.

Metivier L., O. Viron C., Conrad P., Renault S., Diament M., and Patau G. (2009), Evidence of earthquake triggering by the solid earth tides, Earth Planet. Sci. Lett., 278, 370–375, doi:10.1016/j.epsl.2008.12.024.

Miroshnichenko M., Kuksenko V. (1980): Study of electromagnetic pulses in initiation of cracks in solid dielectrics. Sov Phys Solid State 22:895-896.

Mogi K. (1962): Magnitude-frequency relation for elastic shock accompanying fractures of various materials and some related problems in earthquakes. Bull Earthq Res Inst 40:831.

Mogi K. (1967): Earthquakes and fractures. Tectonophysics 5:35–55.

Mori Yasuhiho, Obata Yoshihiko and Sikula Josef: Acoustic and electromagnetic emission from crack created in rock sample under deformation, J. Acoustic Emission, 27 (2009), pp. 157-166.

Nuannin Paiboon (2006): The Potential of b -value Variations as Earthquake Precursors for Small and Large Events, Digital Comprehensive Summaries of Uppsala Dissertations from the Faculty of Science and Technology 183. 46 pp Uppsala ISSN 1651-6214.

Ogata, Y. (1983a): Likelihood analysis of point processes and its applications to seismological data, *Bull. Int. Stat. Inst.*, 50, Book 2, 943–961.

Ogata, Y. (1988): Statistical models for earthquake occurrences and residual analysis for point processes, *J. Am. Stat. Assoc.*, 83, 9–27.

- Ogata, Y, & Katsura, K. (1995): Analysis of temporal and spatial heterogeneity of magnitude frequency distribution inferred from earthquake catalogue. *Geophys. J. Int.* 113, 727-738.
- Ohtsu M. (1982): Theoretical treatment of acoustic emission and source mechanisms in concrete. *Mem. Fac. Eng.* 27:1-21.
- Ohtsu M. and Ono K. (1983): "Resonance Analysis of Piezoelectric Transducer Elements", *J. Acoustic Emission*, 2(4), 247-260.
- Ohtsu M (1994): New trends in non-destructive and in-place testing of concrete structures. Aguado A, Gettu R, Shah, SP (eds) *Proc. Concrete Technology: New Trends, Industrial Applications*. London, E&FN Spon.
- Ouchi, T., Uekawa, T., 1986: Statistical analysis of the spatial distribution of earthquakes-variation of the spatial distribution of earthquakes before and after large earthquakes, *Physics of the Earth and Planetary Interiors*, 44 (3), pp. 211-225.
- Ouyang C, Landis, EN, Shah, SP (1991): Damage assessment in concrete using quantitative acoustic emission. *J. Eng. Mech.* 117:2681-2697.
- O' Kneefe SG, Thief DV (1995): A mechanism for the production of electromagnetic radiation during fracture of brittle materials, *Phys Earth Planet Inter* 89:127-135.
- Pacheco J.F., Scholtz C.H., Sykes L.R., 1992: Changes in frequency-size relationship from small to large earthquakes, *Nature*, 355, pp. 71-73.
- Peitgen H. O., Jurgens H., and Saupe D., *Chaos and Fractals: New Frontiers of Science* (Springer-Verlag, 1992).
- Rabinovich A., Frid V., Bahat D. (2007): Surface oscillations. A possible source of fracture induced electromagnetic oscillations. *Tectonophysics* 431:15-21.
- Richter, C.F. 1958: *Elementary seismology*, W.H. Freeman and Co. San Francisco, USA.
- Rydelek, P. A., and I. S. Sacks (1989): Testing the completeness of earthquake catalogs and the hypothesis of self-similarity, *Nature*, 337, 251–253. 4, 7, 14, 15, 23, 24.
- Scholz C. H.: The frequency-magnitude relation of microfracturing in rock and its relation to earthquakes. *Bulletin of the Seismological Society of America* ; 58 (1): 399–415, 1968.
- Schorlemmer, D., A. Christophersen, A. Rovida, F. Mele, M. Stucchi, and W. Marzocchi (2010). An earthquake forecast experiment in Italy, *Ann. Geophys.* 53, 1–9.
- Shi Y, Bolt BA (1982): The standard error of the magnitude-frequency b-value. *Bull Seismol Soc Am* 72:1677–1687.

Smalley R. F., Chatelain J. L., Turcotte D. L., and Prevot R.: "A Fractal Approach to the Clustering of Earthquakes: Application to the Seismicity of the New Hebrides", *Bull. Seism. Soc. Am.* 77, 1368–1381 (1987).

Stroup, D. F., Bohnenstiehl D. R., Tolstoy M., Waldhauser F., and R. T. Weekly (2007): Pulse of the seafloor: Tidal triggering of microearthquakes at 9°50' N East Pacific Rise, *Geophys. Res. Lett.*, 34, L15301, doi:10.1029/2007GL030088.

Tanaka Sachiko, Ohtake Masakazu, Stato Haruo: Evidence for tidal triggering of earthquakes as revealed from statistical analysis of global data, *Journal of Geophysical Research*, Vol. 107, NO. B10, 2211, doi:10.1029/2001JB001577, 2002b.

Tanaka, S., Sato, H., Matsumura, S., and Ohtake, M.: Tidal triggering of earthquakes in the subducting Philippine Sea plate beneath the locked zone of the plate interface in the Tokai region, Japan, *Tectonophysics*, 417, 69–80, 2006.

Tolstoy, M., F. L. Vernon, J. A. Orcutt, and F. K. Wyatt (2002): The breathing of the seafloor: Tidal correlations of seismicity on Axial volcano, *Geology*, 30, 503 – 506, doi:10.1130/0091-7613(2002)0302.0.CO;2.

Tsapanos TM(1990): b-value of two tectonic parts in the Circum-Pasific belt. *Pure Appl Geophys* 134:229-242.

Tsuruoka, H., Ohtake, M., and Sato, H.: Statistical test of the tidal triggering of earthquakes: contribution of the ocean tide loading effect, *Geophys. J. Int.*, 122, 183–194, 1995.

Turcotte D. L.: "Fractal in Geology and Geophysics," *Pure Appl. Geophys.* 131, 171–196 (1989).

Turcotte D. L.: *Fractals and Chaos in Geology and Geophysics*, 2nd ed. (Cambridge University Press, 1997).

Turcotte D. L., Newman W. I., and Gabrielov A.: A Statistical Physics Approach to Earthquakes, GeoComplexity and the Physics of Earthquakes, in *Geophysical Monograph 120* (American Geophysical Union, 2000).

Ulomov V.I.: Ordering of geostructure and seismicity in seismoactive regions. Seismicity and seismic zoning of Northern Eurasia. Volume 1, Moscow, p.27-31, 1993.

Utsu T. (1965): A Method for determining the value of b in a formula $\log N = a - bM$ showing the magnitude-frequency relation for earthquakes. *Geophys Bull Hokkaido Univ* 13:99–103.

Utsu, T., Y. Ogata, and S. Matsu'ura: The centenary of the Omori formula for a decay law of aftershock activity, *J. Phys. Earth*, 43, 1–33, 1995.

Volodichev N.N., Kuzhevskij B.M., Nechaev O. Yu., Panasyuk M.I., Podorolsky A.N. and Shavri, P.I.: Sun-Moon-Earth connections: The neutron intensity splashes and seismic activity, *Astron. Vestnik* 34: 188-190 (2000).

Xuemin Zhang, Xuhui Shen, Jing Liu, Xinyan Ouyang. Ionospheric perturbations of electron density before the Wenchuan Earthquake. *International Journal of Remote Sensing* Vol. 31, No. 13, 10 July 3559–3569. 2010.

Wang J.-H. and Lee C. W.: “Multifractal Measures of Earthquakes in West Taiwan”, in *Bull. Inst. Earth Sci. (Academia Sinica, 1996)*, Vol. 16, pp. 131–145.

Widom A, Swain J, Srivastava YN, (2013): Neutron production from the fracture of piezoelectric rocks, *J. Phys. G: Nucl. Part. Phys.*, 40, 15006 : 1-8.

Widom A, Swain J, Srivastava YN, (2015): Photo-disintegration of the iron nucleus in fractured magnetite rocks with magnetostriction, *Meccanica*, 50, 1205-1216.

Wiemer Stefan and Wyss Max: Minimum Magnitude of Completeness in Earthquake Catalogs: Examples from Alaska, the Western United States and Japan, *Bulletin of the Seismological Society of America*, 90, 4, pp. 859–869, August 2000.

Wilcock, W. (2001): Tidal triggering of microearthquakes on the Juan de Fuca Ridge, *Geophys. Res. Lett.*, 28, 3999 – 4002, doi:10.1029/ 2001GL013370.

Wilcock, W. S. D. (2009): Tidal triggering of earthquakes in the northeast Pacific Ocean, *Geophys. J. Int.*, 179, 1055–1070, doi:10.1111/j.1365- 246X.2009.04319.x.

Wyss M., Sammis C.G. Nadeau R.M., Wiemer S. 2004: Fractal dimension and *b*-value on creeping and locked patches of the San Andreas near Parkfield, California. *Bull. Seismol. Soc. Am.* 94, 410-421.

Woessner, J, & Wiemer, S. (2005): Assessing the Quality of Earthquake Catalogues: Estimating the Magnitude of Completeness and Its Uncertainty, *Bull. Seismol. Soc. Am.*, doi:10.1785/0120040007,, 95, 684-698.

Yamada I., Masuda K., Mizutani H.: Electromagnetic and acoustic emission associated with the rock fracture *Physics of the Earth and Planetary Interiors*, Volume 57, Issues 1–2, October 1989, 157-168.

Yamashita, T., 1999: Pore creation due to fault slip in a fluid-permeated fault zone and its effect on seismicity: generation mechanism of earthquake swarm, *Pageoph*, 155, 625-647.